Cell Journal (Yakhteh)

Guide for Authors

Aims and Scope: The "Cell Journal (Yakhteh)" is a peer review and monthly English publication of Royan Institute of Iran. The aim of the journal is to disseminate information through publishing the most recent scientific research studies on exclusively Cellular, Molecular and other related topics. **Cell J**, has been certified by the Ministry of Culture and Islamic Guidance since 1999 and also accredited as a scientific and research journal by HBI (Health and Biomedical Information) Journal Accreditation Commission since 2000 which is an open access journal. **This journal holds the membership of the Committee on Publication Ethics (COPE).**

1. Types of articles

The articles in the field of Cellular and Molecular can be considered for publications in **Cell J.** These articles are as below:

A. Original articles

Original articles are scientific reports of the original research studies. The article consists of English Abstract (structured), Introduction, Materials and Methods, Results, Discussion, Conclusion, Acknowledgements, Author's Contributions, and References **(Up to 40).**

B. Review articles

Review articles are the articles written by well experienced authors and those who have excellence in the related fields. The corresponding author of the review article must be one of the authors of at least three published articles appearing in the references. The review article consists of English Abstract (unstructured), Introduction, Conclusion, Author's Contributions, and References **(Up to 70).**

C. Systematic Reviews

Systematic reviews are a type of literature review that collect and critically analyzes multiple research studies or papers. The Systematic reviews consist of English Abstract (unstructured), Introduction, Materials and Methods, Results, Discussion, Conclusion, Acknowledgements, Author's Contributions, and References **(Up to 70).**

D. Short communications

Short communications are articles containing new findings. Submissions should be brief reports of ongoing researches. The short communication consists of English Abstract (unstructured), the body of the manuscript (should not hold heading or subheading), Acknowledgements, Author's Contributions, and References **(Up to 30).**

E. Case reports

Case reports are short discussions of a case or case series with unique features not previously described which make an important teaching point or scientific observation. They may describe novel techniques or use equipment, or new information on diseases of importance. It consists of English Abstracts (Unstructured), Introduction, Case Report, Discussion, Acknowledgements, Author's Contributions, and References **(Up to 30).**

F. Editorial

Editorials are articles should be written in relevant and new data of journals' filed by either the editor in chief or the editorial board.

G. Imaging in biology

Images in biology should focus on a single case with an interesting illustration such as a photograph, histological specimen or investigation. Color images are welcomed. The text should be brief and informative.

H. Letter to the editors

Letter to the editors are in response to previously published **Cell J** articles, and may also include interesting cases that do not meet the requirement of being truly exceptional, as well as other brief technical or clinical notes of general interest.

I. Debate

Debates are articles which show a discussion of the positive and negative view of the author concerning all aspect of the issue relevant to scientific research.

2. Submission process

It is recommended to see the guidelines for reporting different kinds of manuscripts. This guide explains how to prepare the

manuscript for submission. Before submitting, we suggest authors to familiarize themselves with **Cell J** format and content by reading the journal via the website (www.celljournal.com). The corresponding author ensures that all authors are included in the author list and agree with its order, and they must be aware of the manuscript submission.

A. Author contributions statements

It is essential for authors to include a statement of responsibility in the manuscript that specifies the contribution of every one of them. This participation must include conception and design of the manuscript, data acquisition or data analysis and interpretation, drafting of the manuscript and/or revising it for critically important intellectual content, revision and final approval of the manuscript and statistical analysis, obtaining funding, administrative, technical, or material support, or supervision. Authors who do not meet the above criteria should be acknowledged in the **Acknowledgments section.**

B. Cover letter and copyright

Each manuscript should be accompanied by a cover letter, signed by all authors specifying the following statement: "The manuscript has been seen and approved by all authors and is not under active consideration for publication. It has neither been accepted for publication nor published in another journal fully or partially (except in abstract form). **Also, no manuscript would be accepted in case it has been pre-printed or submitted to other websites.** I hereby assign the copyright of the enclosed manuscript to **Cell J.**" Corresponding author must confirm the proof of the manuscript before online publishing. Also, it is needed to suggest three peer reviewers in the field of their manuscript.

C. Manuscript preparation

Authors whose first language is not English encouraged to consult a native English speaker in order to confirm his manuscripts to American or British (not a mixture) English usage and grammar. It is necessary to mention that we will check the plagiarism of your manuscript by iThenticate Software. The manuscript should be prepared in accordance with the "International Committee of Medical Journal Editors (ICMJE)". Please send your manuscript in two formats word and PDF (including: title, name of all the authors with their degree, abstract, full text, references, tables and figures) and also send tables and figures separately in the site. The abstract and text pages should have consecutive line numbers in the left margin beginning with the title page and continuing through the last page of the written text. Each abbreviation must be defined in the abstract and text when they are mentioned for the first time. Avoid using abbreviation in the title. Please use the international and standard abbreviations and symbols

It should be added that an essential step toward the integration and linking of scientific information reported in published literature is using standardized nomenclature in all fields of science and medicine. Species names must be italicized (*e.g., Homo sapiens*) and also the full genus and species written out in full, both in the title of the manuscript and at the first mention of an organism in a paper.

It is necessary to mention that genes, mutations, genotypes, and alleles must be indicated in italics. Please use the recommended name by consulting the appropriate genetic nomenclature database, e.g., HUGO for human genes. In another words; if it is a human gene, you must write all the letters in capital and italic (*e.g., OCT4, c-MYC*). If not, only write the first letter in capital and italic (*e.g., Oct4, c-Myc*). **In addition, protein designations are the same as the gene symbol but are not italicized.**

Of note, Cell J will only consider publishing genetic association study papers that are novel and statistically robust. Authors are advised to adhere to the recommendations outlined in the STREGA statement (http://www.strega-statement.org). The following criteria must be met for all submissions:

1. Hardy-Weinberg Equilibrium (HWE) calculations must be carried out and reported along with the P-values if applicable [see Namipashaki et al. 2015 (Cell J, Vol 17, N 2, Pages: 187-192) for a discussion].

2. Linkage disequilibrium (LD) structure between SNPs (if multiple SNPs are reported) must be presented.

3. Appropriate multiple testing correction (if multiple independent SNPs are reported) must be included.

Submissions that fail to meet the above criteria will be rejected before being sent out for review.

Each of the following manuscript components should begin in the following sequence:

Authors' names and order of them must be carefully considered (full name(s), highest awarded academic degree(s), email(s), and institutional affiliation(s) of all the authors in English. Also, you must send mobile number and full postal address of the corresponding author).

Changes to Authorship such as addition, deletion or rearrangement of author names must be made only before the manuscript has been accepted in the case of approving by the journal editor. In this case, the corresponding author must explain the reason of changing and confirm them (which has been signed by all authors of the manuscript). If the manuscript has already been published in an online issue, an erratum is needed.

Title is providing the full title of the research (do not use abbreviations in title).

Running title is providing a maximum of 7 words (no more than 50 characters).

Abstract must include Objective, Materials and Methods, Results, and Conclusion (no more than 300 words).

Keywords, three to five, must be supplied by the authors at the foot of the abstract chosen from the Medical Subject Heading (MeSH). Therefore; they must be specific and relevant to the paper.

The following components should be identified after the abstract:

Introduction: The Introduction should provide a brief background to the subject of the paper, explain the importance of the study, and state a precise study question or purpose.

Materials and Methods: It includes the exact methods or observations of experiments. If an apparatus is used, its manufacturer's name and address should be stipulated in parenthesis. If the method is established, give reference but if the method is new, give enough information so that another author can perform it. If a drug is used, its generic name, dose, and route of administration must be given. Standard units of measurements and chemical symbols of elements do not need to be defined.

Statistical analysis: Type of study and statistical methods should be mentioned and specified by any general computer program used.

Ethical considerations: Please state that informed consent was obtained from all human adult participants and from the parents or legal guardians of minors and include the name of the appropriate institutional review board that approved the project. It is necessary to indicate in the text that the maintenance and care of experimental animals complies with National Institutes of Health guidelines for the humane use of laboratory animals, or those of your Institute or agency.

Clinical trial registration: All of the Clinical Trials performing in Iran must be registered in Iranian Registry of Clinical Trials (www.irct.ir). The clinical trials performed abroad, could be considered for publication if they register in a registration site approved by WHO or www.clinicaltrials.gov. If you are reporting phase II or phase III randomized controlled trials, you must refer to the CONSORT Statement for recommendations to facilitate the complete and transparent reporting of trial findings. Reports that do not conform to the CONSORT guidelines may need to be revised before peer-reviewing.

Results: They must be presented in the form of text, tables, and figures. Take care that the text does not repeat data that are presented in tables and/or figures. Only emphasize and summarize the essential features of the main results. Tables and figures must be numbered consecutively as appeared in the text and should be organized in separate pages at the end of the manuscript while their location should be mentioned in the main text.

Tables and figures: If the result of your manuscript is too short, it is better to use the text instead of tables & figures. Tables should have a short descriptive heading above them and also any footnotes. Figure's caption should contain a brief title for the whole figure and continue with a short explanation of each part and also the symbols used (no more than 100 words). All figures must be prepared based on cell journal's guideline in color (no more than 6 Figures and Tables) and also in GIF or JPEG format.

Of Note: Please put the tables & figures of the result in the results section not any other section of the manuscript.

Supplementary materials would be published on the online version of the journal. This material is important to the understanding and interpretation of the report and should not repeat material within the print article. The amount of supplementary material should be limited. Supplementary material should be original and not previously published and will undergo editorial and peer review with the main manuscript. Also, they must be cited in the manuscript text in parentheses, in a similar way as when citing a figure or a table. Provide a caption for each supplementary material submitted.

Discussion: It should emphasize the present findings and the variations or similarities with other researches done by other researchers. The detailed results should not be repeated in the discussion again. It must emphasize the new and important aspects of the study.

Conclusion: It emphasizes the new and important aspects of the study. All conclusions are justified by the results of the study.

Acknowledgements: This part includes a statement thanking those who contributed substantially with work relevant to the study but does not have authorship criteria. It includes those who provided technical help, writing assistance and name of departments that provided only general support. You must mention financial support in the study. Otherwise; write this sentence "There is no financial support in this study".

Conflict of interest: Any conflict of interest (financial or otherwise) and sources of financial support must be listed in the Acknowledgements. It includes providers of supplies and services from a commercial organization. Any commercial affiliation must be disclosed, regardless of providing the funding or not.

Of Note: If you have already any patent related to the subject of your manuscript, or you are going to apply for such a patent, it must be mentioned in this part.

References: The references must be written based on the Vancouver style. Thus the references are cited numerically in the text and listed in the bibliography by the order of their appearance. The titles of journals must be abbreviated according to the style used in the list of Journals Indexed in PubMed. Write surname and initials of all authors when there are six or less. In the case of seven or more authors, the names of the first six authors followed by "et al." must be listed. You can download Endnote file for Journal references style: endnote file

The reference of information must be based on the following order:

Article:

Surname(s) and first letter of name &middle name(s) of author(s) .Manuscript title. Journal title (abbr).publication date (year); Volume & Issue: Page number.

Example: Manicardi GC, Bianchi PG, Pantano S, Azzoni P, Bizzaro D, Bianchi U, et al. Presence of endogenous nicks in DNA of ejaculated human spermatozoa and its relationship to chromomycin A3 accessibility. Biol Reprod. 1995; 52(4): 864-867.

Book:

Surname(s) and first letter of name & middle name(s) of author(s).Book title. Edition. Publication place: publisher name; publication date (year); Page number.

Example: Edelman CL, Mandle CL. Health promotion throughout the lifespan. 2nd ed. ST Louis: Mosby; 1998; 145-163.

Chapter of book:

Surname(s) and first letter of name & middle name(s) of author(s).Chapter title. In: Surname(s) and first letter of name & middle name(s) of editor(s), editors. Book title. Edition. Publication place: publisher name; publication date (year); Page number.

Example: Phillips SJ, Whisnant JP. Hypertension and stroke. In: Laragh JH, Brenner BM, editors. Hypertension: pathophysiology, diagnosis, and management. 2nd ed. New York: Raven Press; 1995; 465-478.

Abstract book:

Example: Amini rad O.The antioxidant effect of pomegranate juice on sperm parameters and fertility potential in mice. Cell J. 2008;10 Suppl 1:38.

Thesis:

Name of author. Thesis title. Degree. City name. University. Publication date (year).

Example: Eftekhari Yazdi P. Comparison of fragment removal and co-culture with Vero cell monolayers on development of human fragmented embryos. Presented for the Ph.D., Tehran. Tarbiyat Modarres University. 2004.

Internet references

Article:

Example: Jahanshahi A, Mirnajafi-Zadeh J, Javan M, Mohammad-Zadeh M, Rohani M. Effect of low-frequency stimulation on adenosineA1 and A2A receptors gene expression in dentate gyrus of perforant path kindled rats. Cell J. 2008; 10 (2): 87-92. Available from: http://www.celljournal.org. (20 Oct 2008).

Book:

Example: Anderson SC, Poulsen KB. Anderson's electronic atlas of hematology.[CD-ROM]. Philadelphia: Lippincott Williams & Wilkins; 2002.

D. Proofs are sent by email as PDF files and should be checked and returned within 72 hours of receipt. It is the authors' responsibility to check that all the text and data as contained in the page proofs are correct and suitable for publication. **We are requested to pay particular attention to author's names and affiliations as it is essential that these details be accurate when the article is published.**

E. Pay for publication: Publishing an article in **Cell J** requires Article Processing Charges (APC) that will be billed to the submitting author following the acceptance of an article for publication. For more information please see www.celljournal.org.

F. Ethics of scientific publication: Manuscripts that have been published elsewhere with the same intellectual material will refer to duplicate publication. If authors have used their own previously published work or work that is currently under review, as the basis for a submitted manuscript, they are required to cite the previous work and indicate how their submitted manuscript offers novel contributions beyond those of the previous work. Research and publication misconduct is considered a serious breach of ethics.

The Journal systematically employs iThenticate, plagiarism detection and prevention software designed to ensure the originality of written work before publication. Plagiarism of text from a previously published manuscript by the same or another author is a serious publication offence. Some parts of text may be used, only where the source of the quoted material is clearly acknowledged.

3. General information

A. You can send your manuscript via online submission system which is available on our website. If the manuscript is not prepared according to the format of **Cell J**, it will be returned to authors.

B. The order of article appearance in the Journal is not demonstrating the scientific characters of the authors.

C. Cell J has authority to accept or reject the manuscript.

D. The received manuscript will be evaluated by associate editor. **Cell J** uses a single-blind peer review system and if the manuscript suits the journal criteria, we select the reviewers. If three reviewers pass their judgments on the manuscript, it will be presented to the editorial board of **Cell J.** If the editorial board has a positive judgment about the manuscript, reviewers' comments will be presented to the corresponding author (the identification of the reviewers will not be revealed). The executive member of journal will contact the corresponding author directly within 3-4 weeks by email. If authors do not receive any reply from journal office after the specified time, they can contact journal office. Finally, executive manager will respond promptly to authors' request.

The Final Checklist

The authors must ensure that before submitting the manuscript for publication, they have to consider the following parts:

1. The first page of manuscript should contain title, name of the author/coauthors, their academic qualifications, designation & institutions they are affiliated with, mailing address for future correspondence, email address, phone, and fax number.

2. Text of manuscript and References prepared as stated in the "guide for authors" section.

3. Tables should be on a separate page. Figures must be sent in color and also in JPEG (Jpg) format.

4. Cover Letter should be uploaded with the signature of all authors.

5. An ethical committee letter should be inserted at the end of the cover letter.

The Editor-in-Chief: Ahmad Hosseini, Ph.D.

Cell Journal(Yakhteh)

P.O. Box: 16635-148, Iran

Tel/Fax: + 98-21-22510895

Emails: Celljournal@royaninstitute.org

info@celljournal.org

IN THE NAME OF GOD

ACECR

CC BY NC
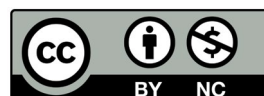
CONTENTS

Original Articles

● **Front page of Cell Journal_(Yakhteh): Figure 1.D, Page: 123**

Original Article

Protective Effect of Low Dose of Methamphetamine on The Amount of Extracellular Glutamine in Primary Fetal Human Astrocytes Induced by Amyloid Beta

Bita Soltanian, M.Sc.[1], Marzieh Dehghan Shasaltaneh, Ph.D.[2*], Gholamhossein Riazi, Ph.D.[3],

Nahid Masoudian, Ph.D.[1]

1. Department of Biology, College of Science, Damghan Branch, Islamic Azad University, Damghan, Iran
2. Department of Biology, Faculty of Science, University of Zanjan, Zanjan, Iran
3. Laboratory of Neuro-Organic Chemistry, Institute of Biochemistry and Biophysics (IBB), University of Tehran, Tehran, Iran

*Corresponding Address: Department of Biology, Faculty of Science, University of Zanjan, Zanjan, Iran
Email: dehghan@znu.ac.ir*

Abstract ————
Objective: Change in astrocytes is one of the first pathological symptoms of Alzheimer's disease (AD). Understanding the signaling pathways in astrocytes can be a great help in treating of AD. This study aimed to investigate signaling pathway relations between low dose of methamphetamine (METH), the apoptosis, cell cycle, and glutamine (Gln) pathways in the activated astrocyte.

Materials and Methods: In this experimental study, the activated astrocyte cells were exposed to a low dose of METH (12.5 µM) which was determined by Thiazolyl blue tetrazolium bromide (MTT) method. The groups were: group 1 cells with Aβ, group 2 cells with METH, group 3 cells with METH after 24 hours of adding Aβ (Aβ+METH, treated group), group 4 cells with Aβ after 24 hours of adding METH (METH+Aβ, prevention group), and group 5 as the control. The Gln was assayed by high-performance liquid chromatography (HPLC), and also the apoptosis, and cell cycle and *BAX, BCL-X* expression was evaluated.

Results: The amount of Gln was increased, and the value of late and early apoptosis was reduced in the treatment groups, and necrosis is decreased in the prevention group (group 4 compared to group 1). Moreover, it was revealed through cell cycle analysis that G2 in group 4 was reduced compared to group 1 and the expression of *BAX, BAX/BCL-X*, and *BCL-X* in group 3 and group 4, was decreased and increased, respectively compared to group 1.

Conclusion: These findings suggest that perhaps a non-toxic dosage of METH (low dose) can reduce the amount of apoptosis and *BAX* expression and increase the expression of *BCL-X*. Furthermore, the cells are arrested in the G2 phase and can raise the amount of extracellular glutamine, which has a protective role in neuron cells. These findings may provide a new perspective to design a new drug with less toxic results.

Keywords: Alzheimer's Disease, Astrocytes, Cell Cycle, Glutamine, Methamphetamine

Introduction

The presence of astrocytes is essential to keep up homeostasis in the brain. They are usually involved to maintain the nervous system and improve neurodegenerative diseases such as Alzheimer's disease (AD) (1). The important roles of astrocytes in the central nervous system (CNS) are: as follows establish homeostasis through regulation pH, recycling oxidized ascorbic acid, reserve lactate to neurons and ATP production, homeostasis of Ca^{2+}, production of glutathione, and osmolality adjustment (2). Astrocytes are actively involved in maintaining and protecting the CNS microenvironment in normal and pathophysiological position and participating in oxidative stress (3). Astrocytes produce glutamine (Gln) through glutamine synthetase (GS), Gln gain has a protective role in AD in response to injury or toxic substance (4). Astrocytes were activated and leads to hypertrophy and ramification process. Reactive astrocytes participated in inflammatory response and pathogenesis of AD (5).

Activation hypertrophy and ramification of astrocytes occurred after neurodegenerative diseases or traumatic brain injury. The GS is a specific astrocyte enzyme which could be converting glutamate (Glu) and ammonia to Gln. This enzyme was reduced in AD (6). In a senescence astrocyte, loss of synaptic plasticity, blood-brain barrier (BBB) dysfunction and Glu excitotoxicity were caused (7). Astrocytes can balance neuronal function by uptake of Glu and γ-aminobutyrate (GABA) and stimulates released from synapses. Glu is one of the neurotransmitter take part in memory and learning. Glutamate/aspartate transporter (GLAST) and Glutamate transporter-1 (GLT-1) absorbed Glu into astrocyte and GS converted Glu to Gln (8).

Oxidative stress acutely affects the activity of GS (9). Senile astrocyte capacity was reduced in neurodegenerative diseases (10). Accumulation of Gln in astrocytes leads to mitochondrial dysfunction and cell swelling. Ammonia detoxification due to the amidation of Glu to Gln (11). Neurons by Glu/Gln cycle absorb Gln and clear Glu from the synaptic cleft by astrocytes and convert it to glutamine. The stress response proteins

were reduced in a low concentration of Gln and cells will become hypersensitive to H_2O_2 and DNA damage (12).

Aβ deposition, chronic inflammation, hypoxia, ischemia and oxidative stress can directly reduce GS activity. Gln deficiency blocks mitochondrial energy production, DNA damage response, apoptosis, and autophagy (13). Aβ induces apoptosis in the cell cultures of neuron and the brain of transgenic mice; on the other hand, Aβ reduced expression of anti-apoptotic *BCL-X* significantly (14). Astrocytes are significant mediators in the neurotoxicity of AD and participated in neuronal death regulation induced by Aβ (15, 16).

METH is an incentive and major addiction in high repetitive doses in the world. It was used to treat attention deficit hyperactive disorder (ADHD), obesity, and narcolepsy (17). Recent evidence indicates that some herbal ingredients such as crocin, picrocrocin and safranal are neuroprotective (18). Moreover, low doses of METH (IV infusion with 0.5 mg/kg/h for 24 hours) can produce neuroprotection (19). Thus, it appears that METH under certain circumstances and correct dosage can produce a neuroprotective effect (4, 19, 20). It presents an interesting paradox of neuroprotection and neurotoxicity (21) effect of METH that needs further investigation *in vivo*. The appropriate (low) dose of METH was determined by the MTT method. Half-maximal inhibitory concentration (IC_{50}) was 25 μM, to evaluate the therapeutic effect of METH, we used a lower dose than IC_{50} (12.5 μM). Gln is an apoptosis suppressor and may be a protective effect on cells from stress (3). Also, Gln enriched-diet significantly enhances the expression of *BCL-X* (22). We intent to use astrocytes because the activation of astrocytes is one of the first findings in the brains of people who abused METH (23). Due to the findings of the anti-apoptotic effect of Gln in the past, we investigated a little dose of METH on astrocytes induction oxidative stress by exposure to Aβ (24) to understand the relationship between the amount of Gln in the supernatant of treated astrocyte, apoptosis, and expression of *BAX*, *BCL-X* genes. The novelty of the above research investigates the relationship between the effective dose of METH and the amount of Gln and the relationship of these pathways.

Materials and Methods

All animals used in the study were handled in accordance with the guidelines approved by the Ethics Committee of our University with approval ID: IR.IAU.DAMGHAN.REC.1398.005.

Preparation of Aβ1–42 peptide

In this experimental study, Aβ1-42 peptides are dissolved in some hexafluoro-2-propanol (HFIP, Sigma-920-66-1) to reach a final concentration of 1 mM (monomer). To evaporate the HFIP using a Speed Vac, the samples were stored at -20˚C until to use. For fibril formation, the large aggregates Aβ of the tube were directly dissolved in dH_2O and incubated at 37˚C for 72 hours.

Astrocytes culture and treatment

Primary fetal human astrocytes were isolated from the hypothalamus and cerebral cortex, which were previously isolated from hypothalamus and cerebral cortex of two human fetuses on gestational weeks 9-12 (gift from Bon Yakhteh Laboratory in Tehran) were cultured in DMEM with 10% heat-inactivated fetal bovine serum (FBS) and kanamycin (50 mg/mL the cells were incubated at 37˚C in 5% CO_2, 85-95% humidity. 200000-250000 cells were cultured in each well (25). According to the IC_{50}, after 24 hours, METH (donated by Tehran University) and Aβ were added to the well. METH was added to DMEM, containing 10% FBS, to reach the final concentration of 12.5 μM. METH remained in the vicinity of the cell for 24 hours. For treatment with Aβ, 10 μM of Aβ was kept at 37˚C for 72 hours (fibril formation) and then added to DMEM plus F12 without FBS (26). Cells were exposed to amyloid for 24 hours. All experiments have been performed according to the following procedures: group 1 cells with Aβ, group 2 cells with METH, group 3 cells with METH after 24 hours of adding Aβ (Aβ+METH, treated group), group 4 cells with Aβ after 24 hours of adding METH (METH+Aβ, prevention group) and group 5 as control.

Cell viability by MTT assay

Astrocytes were seeded in a 96-well plate (10000, 15000, and 20000 cells per well) with 5% FBS in DMEM, and exposed to various concentrations (0.8, 1.6, 3.12, 6.25, 12.5, 25, 50, and 100 μM) of METH for 24 hours, 48 hours, and 72 hours. Then, MTT [Sigma-Aldrich, USA, 5 mg/mL in phosphate-buffered saline (PBS, Jenabioscience, Germany)] was added. Dimethyl sulfoxide (DMSO, Sigma Aldrich, USA) was used to solubilize the crystals and the absorbance was measured at 570 nm (27).

Chromatographic system

The chromatographic conditions were used Waters 2795, fluorescence detector Waters474 and C18 column (250×4.6 mm, 10 μm) Empower software system and retention time (RT) condition. 0.4% tetrahydrofuran with 30 mmol/L potassium dihydrogen phosphate with pH=7.0 (adjust with 4 mol/L KOH) used as mobile phase A, and mobile phase B was acetonitrile 50%. All mobile phases were filtered by 0.22 μm filter and were degassed. The 340 nm and 455 nm wavelength respectively used as excitation and an emission wavelength. The volume was 10 μl. The gradient conditions were based on the previous study (28).

Standard solution

The standard solution was prepared similar to the sample in water, stored at -70˚C. The linearity range of the proposed method was 5 to 1000 μmol/L. The concentration of amino acid calculated by divided the area of sample to the area of internal standard. The correlation coefficients (r) were >0.99.

Sample preparation

For prepared 200 µl sample, 180 µL of high-performance liquid chromatography (HPLC) grade water was added to 20 µL sample. Then, 200 µl of methanol HPLC grade was added to precipitate protein. The samples were centrifuged for 5 minutes at 10,000 × g in RT. The supernatants were collect and mixed with derivatization reagent and incubated for 30 minutes before injection.

Apoptosis and necrosis assay

Annexin-V-FITC/PI immunostep kit (ANXVF-200T) was used to separate necrotic cells from apoptotic cells. Briefly, pre-treated astrocyte cells were harvested by trypsin and washed twice with PBS 0.01 M. After that, the cells centrifuge for 5 minutes at 2000 rpm, the cellular deposition was re-suspended in 500 µl of binding buffer; the density of cells must be 1×10^6 cell/ml. Following that, 5 µl Annexin, V-FITC, and 5 µl propidium iodide (PI) were added, respectively. Cells were incubated in the dark at 25˚C for 15 minutes and analyzed by flow cytometry (BD Biosciences, Franklin Lakes, NJ, USA).

Analysis of cell cycle

The pre-treated astrocyte cells were harvested by trypsin and washed twice with PBS after the cells centrifuge for 5 minutes at 2000 rpm, at 4˚C. The cells were resuspended in cold PBS (DNase- RNase-free Sigma) and stained with PI containing 1% Triton X-100 (v/v) (Sigma, USA). The solution was incubated at 20˚C for 30 minutes (preserved from light) and analyzed by flow cytometry (BD Biosciences, Franklin Lakes, NJ, USA) (29).

RNA extraction

According to the manufacturer's recommendation, total RNA of astrocyte culture was extracted by Roche RNA extraction kit (Roche 11828665001). By optical density (OD) at 260 nm, concentration of RNA samples was determined and by detecting 18S and 28S bands on agarose gel electrophoresis, the quality of RNA was confirmed. The RNA samples were incubated with DNase at room temperature for 15 minutes to remove residual DNA contamination.

cDNA synthesis

According to the manufacturer's protocol Thermo (K1621), cDNA was generated with oligo (dT) primers from the total RNA. Oligonucleotide primers *GAPDH* was used for housekeeping genes, and primer 3 was applied to design all primers. The primer of:

GAPDH-

F: 5´-GACCACTTTGTCAAGCTCATTTCC-3´
R: 5´-GTGAGGGTCTCTCTCTTCCTCTTG-3´ (168 bp)

BAX-

F: 5´-TGGAGCTGCAGAGGATGATTG-3´
R: 5´-GAAGTTGCCGTCAGAAAACATG-3´ (98 bp)

BCL-X-

F: 5´-CTGAATCGGAGATGGAGACC-3´
R: 5´-TGGGATGTCAGGTCACTGAA-3´ (211 bp) have been used.

Quantitative real-time polymerase chain reaction analysis

The *BCL-X* and *BAX* genes related to apoptosis were evaluated using the housekeeping gene (*GAPDH*). The primers were previously checked by conventional reverse transcription polymerase chain reaction (RT-PCR) and agarose gel (1.5%) electrophoresis. Quantitative PCR (Q-PCR) was performed using the Amplicon PCR Master Mix (A314406) and Qiagen Rotor-Gene Q system. All experiments were performed in triplicates. After an initial denaturation step of 3 minutes at 94˚C, 35 cycles of amplification were carried out. Each cycle included a denaturation step, 30 seconds at 94˚C; an annealing step, 30 seconds at 60˚C; and an elongation step, 45 seconds at 72˚C. The final elongation temperature was 72˚C for 5 minutes. The fold-change in gene expression was calculated using the melt curve method and was normalized to *GAPDH* then the relative gene expression levels were calculated with reference to the control (30).

Statistical analysis

SPSS v16 (Chicago, USA) and GraphPad Prism8 (San Diego, California, USA) were used for statistical analysis. Each of the treatment groups was compared with a group using sample t test in real-time PCR. $P<0.05$ was set as the level of significance. All error bars in the figures are based on the results of the mean ± standard deviation (SD). Each experiment was performed in triplicate.

Results

Viability of astrocyte in the presence of a different concentration of METH

MTT assay was used to determine the number of viable cells in exposure to METH. The cells were incubated with different concentrations of METH for 24, 48, and 72 hours. It was revealed the cell viability reduction (~ 10%) in the astrocytes within the limited concentrations of METH (0.8, 1.6, 3.1, 6.2, and 12.5 µM) for 24, 48, and 72 hours. Therefore, 12.5 µM concentration of METH was employed for further evaluation (Fig.1).

Glutamine analysis by HPLC

At the end of the treatment, the concentration of Gln in the supernatant of samples was assayed by HPLC. The concentration of Gln in group-3 (Aβ+METH) and group-4 (METH+Aβ) was amplified in comparison with group-1 (Aβ) as shown in (Fig.2).
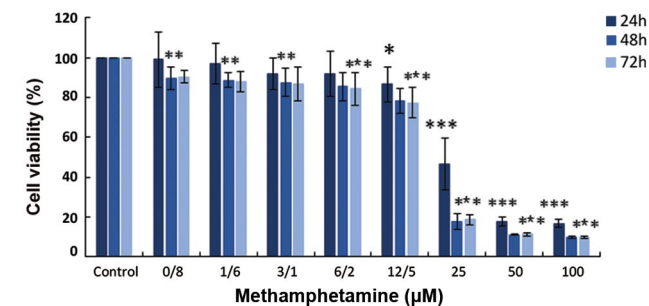
Fig.1: Effect of methamphetamine (METH) on astrocytes viability. The cells are treated with different concentrations (0.8-100 μM) of METH for 24 hours, 48 hours, 72 hours (n=3). Data values are expressed as % of control values. Significant change (*0.01<P<0.05, **0.01<P<0.001 and ***P<0.001) in comparison with control group). Concentration 12.5 μM of METH (*0.01<P<0.05), 25, 50, and 100 μM of METH (***P<0.001) in 24 hours. Concentration of (0.8, 1.6, 3.1 μM of METH (**0.01<P<0.001) and 6.2, 12.5, 25, 50 and 100 μM (***P<0.001) in 48 and 72 hours. The results show that 12.5 μM METH for 24 hours, 48 hours, and 72 hours has a 10% toxicity effect on astrocytes. The data presented as mean ± standard deviation (SD).
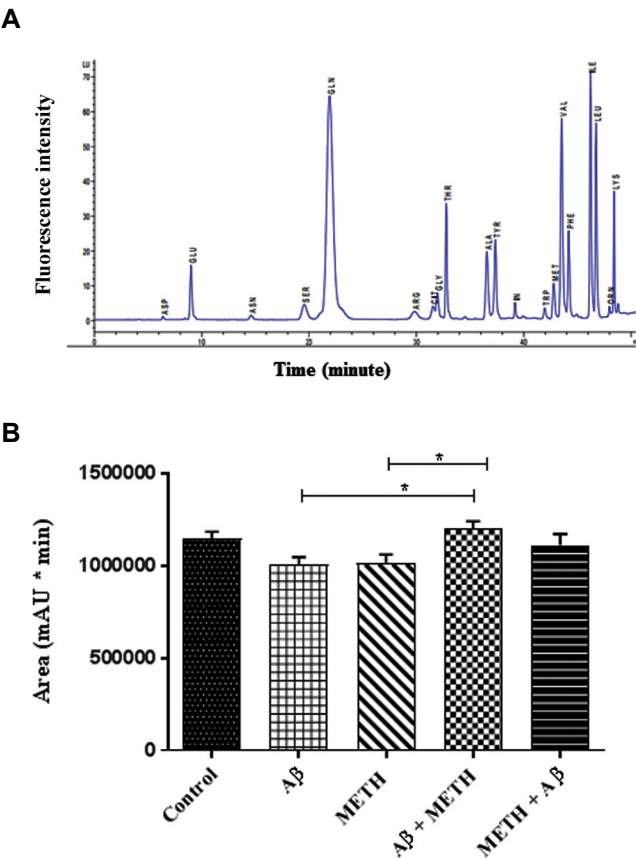
Fig.2: Glutamine analysis by HPLC. **A.** Glutamine analysis by HPLC. Group 1 (Aβ), group 2 (METH), group 3 (Aβ+METH), group 4 (METH+Aβ) and group 5 (control). The amount of glutamine in the supernatant of groups (Aβ+METH) and (METH+Aβ) was increased in comparison with a group (Aβ). **B.** The area of glutamine in astrocyte treated with a low dose of METH, The comparison between Aβ and (Aβ+METH) as well as METH and (Aβ+METH) was significant (*0.01<P<0.05). HPLC; High-performance liquid chromatography and METH; Methamphetamine.

Apoptosis and necrosis analysis

The flow cytometry method was adopted to determine the number of live cells, late apoptosis, early apoptosis, and necrosis. The percentage of early apoptosis decreased in

Aβ+METH (2.33%) and METH+Aβ (2.93%), compared to the Aβ group-1 (Aβ). Also, 91.5 and 90.3% of live cells arise in METH+Aβ and Aβ+METH groups compared to the Aβ group. The percentage of live cells rose in all treatments compared to Aβ. The amount of (early and late) apoptosis reduced in all groups in comparison to the Aβ group (Fig.3).
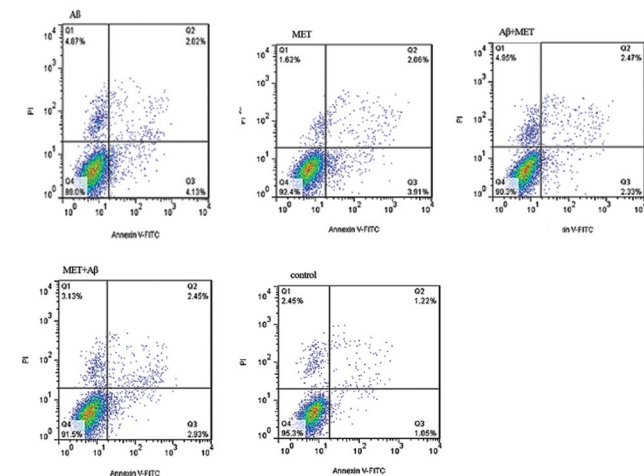
Fig.3: Evaluation of apoptosis in astrocytes in the presence of low dose of methamphetamine by flow cytometry. The control group shows the untreated astrocyte cells after 72 hours, (Aβ) group treated with 10 μM Aβ for 24 hours, (METH) group after astrocyte was treated with 12.5 μM METH for 24 hours, (Aβ+METH) group astrocyte which was treated for 24 hours with Aβ and then 24 hours with METH, (METH+Aβ) group that astrocyte was treated with METH for 24 hours and after that treated with Aβ for 24 hours, and the data was analyzed in both treated and untreated group. Q1; PI=Positive, Annexin V FITC negative (necrosis), Q2; PI=Positive, Annexin V FITC positive (late apoptosis), Q3; PI=Negative, Annexin V FITC positive (early apoptosis), Q4; PI=Negative, Annexin V FITC negative (live cell) (all tests were repeated twice), and METH; Methamphetamine.

Cell cycle analysis

Comparison of the results in different treatment groups showed that in group-1 (Aβ), the cells enter the S phase and arrest in G2 in comparison with the control group. In Aβ+METH group, astrocyte cells enter the S and G2 phases, G1 decreases, and the cells arrest in G2, compared to the Aβ group phase. In METH+Aβ group, the cells arrest in G2 and enter S compared to the Aβ group (Table 1, Fig.4).

Table 1: Cell cycle arrest in all groups, group 1 (Aβ), group 2 (METH), group 3 (Aβ+METH), group 4 METH+Aβ) and group-5 (control)

Groups	G1 (%)	S (%)	G2 (%)
Aβ	64.45	19.35	14.35
METH	63.92	21.71	11.8
Aβ+METH	44.07	29.76	22.64
METH+Aβ	66.44	13.43	13.05
Control	70.54	15.57	8.02

In group 3 and 4 the % of G2 w ere increased in comparison with group 5 control group. G1; Intermediate phase occupying the time between the end of cell division in mitosis, G2; Checkpoint prevents cells from entering mitosis, S; Stands for DNA synthesis, and METH; Methamphetamine.
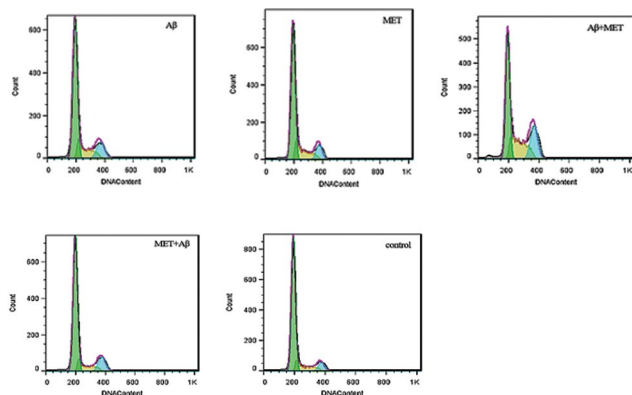
Fig.4: The effect of different treated METH on the cell cycle arrest group 1 (Aβ), group 2 (METH), group 3 (Aβ+METH), group 4 (METH+Aβ), and group-5 (control). G2 increases and G1 decreases in group-1. In group 4, G2 increases and G1 decreases, the amount of G2 decreases in group 3 and G1 increases, all groups compared to group-1 (all tests were repeated twice). METH; Methamphetamine.

Gene expressions *BAX* and *BCL-X*

Expressions of these genes were measured by RT-PCR in experimental groups. *BAX* expressions in group 3 (Aβ+METH) decreased significantly (P=0.035) despite an increase in *BCL-X* which was not significant compared to group 1 (Aβ). *BAX* in group 4 (METH+Aβ) decreased considerably (P=0.001) and *BCL-X* expression increased (P=0.048) compared to group 1 (Aβ). The ratio of *BAX/BCL-X* in group 3 (Aβ+METH) reduced about 0.432 fold (P=0.023) compared to group 1 (Aβ), while the ratio of *BAX/ BCL-X* in group 4 (METH+Aβ) decreased about 1.17 fold (P=0.047) compared to the same amount in group 1 (Aβ) (Fig.5A-F).
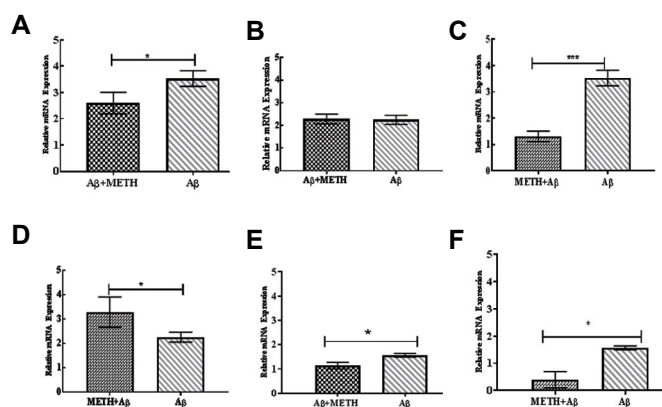
Fig.5: Real-time PCR analysis for *BAX* and *BCL-X* genes. The values put onto each graph represent the relative fold change calculated by calibrating the ΔΔCt data *BAX* and *BCL-X* gene expressions in several experiments. **A.** *BAX* in group 3 (Aβ+METH) and **B.** Group 4 (METH+Aβ) are decreased (P<0.001 and P<0.05, respectively). **C.** *BCL-X* in group 3 (Aβ+METH), **D.** Group 4 (METH+Aβ) are increased (P<0.001) and **E, F.** *BAX/BCL-X* in group 3, 4 are decreased in comparison with group 1 Aβ. Error bars indicate SEM. The significant level was define as *P≤0.05 and ***P<0.001. Group 1 (Aβ), group 2 (METH), group 3 (Aβ+METH), group 4 (METH+Aβ).

Discussion

We examined the hypothesis that astrocytes respond to a low dose of METH exposure by raising the amount of extracellular glutamine, as an indicator of neuroprotection, increase in extracellular Gln neurons. Our findings show that the amount of Gln increased in treatment with a low dose of METH in treated (Aβ+METH) and prevention (METH+Aβ) groups in comparison to the AD model or group 1 (Aβ). The cells in low concentrations of Gln are sensitive to stress oxidative and DNA damage. The value of proteins responding to stress was reduced as a result, and cells are more sensitive to the neurotoxic effects like Aβ. As well as Gln supplements have a neuroprotective effect on AD (12).

The Gln/Glu levels have been reduced in the AD brain, which confirmed our observations. One of the early signs of AD is a decrease in Gln levels (31). The present findings suggest that Gln in the AD model is lower than in the groups treated with METH. In previous studies, the neuroprotective effect of a low dose of METH was dependent on a PI3K/AKT pathway. Notably, the activation of the pathway PI3K/AKT suppresses apoptotic factors (32).

In our study, the effect of low concentration of METH on apoptosis of astrocyte cells in two treatment patterns was evaluated. Our results show that in group 3 and group 4, live cells were amplificated compared to activated astrocytes. Early and late apoptosis in all treatments were rebates, but the rate of necrosis was reduced only in the pretreatment position. Earlier research shows that mild stress can prevent the occurrence of larger ones. In this respect, researchers used METH with concentration 0-3 mM to provide mild stress and 6-hydroxydopamine (6-OHDA) as a potential source of toxic stress. The prior research has indicated that previous exposure to nontoxic concentrations of METH protected these cells against 6-OHDA toxicity, but higher concentrations of METH intensify it (33).

In our study, we explained two models for the treatment. In one group, there was astrocyte exposure with Aβ, and after 24 hours effective dose of METH (treatment group) was added. In another group, the cells were exposed to a little dose of METH, and then after 24 hours, Aβ was added (prevention group). In both models, we checked the therapeutic effects of METH on apoptosis and cell cycle in cell signaling pathways The apoptosis results in our study also show that the number of live cells was increased in the inhibition form (group 4) compared with the treatment form (group 3). It may be the effect of mild stress-induced by METH which can protect against the larger ones. The other effects of METH exposure were the up-regulate of the *BCL-2*. Exposure to low concentrations of METH causes many dopamine changes, alike decrease in their vulnerability to further oxidative stress (33).

Our findings show that the expression of *BCL-X* was enhanced in the prevention groups more than it did in the treatment form (group 4). Bile duct ligation (BDL)

in rodents can cause cognition deficits and treatment with Curcumin has a preventive and therapeutic role in memory impairment. Curcumin increased expression of the *BCL-X* and decreased the *BAX* gene expression level (34).

We observed that the expression level of *BAX* in both groups decreased through the representative data, but in the METH+Aβ group, the reduction was more than the Aβ+METH group. This finding may show that a slight increase in METH in the prevention mode may reduce *BAX* more efficiently than that in the treatment mode. As soon as neurons are born, they lose the capacity of division and differentiation. In stress conditions, like oxidative stress and DNA damage, and after neuronal differentiation, cell cycle modulators' expression increased (35). The cell cycle consists of four main phases: G1, S, G2, and M. Neurons remain in a G0 phase. G0 is a nondividing and nonreplicating phase, where cell division is initiated but not completed; it finally enters apoptosis. Before the neurons die, cell cycle abnormalities in AD may be arrested at the G2/M (36).

On the other hand, we analyzed the cell cycle in activated astrocytes treated with a low dose of METH. The results show that in prevention mode, G2 was reduced compared to AD, but increased in the treatment mode importantly, susceptible neurons before die may be arrested at the G2/M. Thus, the rate-limiting step before apoptosis of neurons might activate CDK1 at G2. Phosphorylation of tau during G2 is a direct link between the cell cycle and the cell death (37). Moreover, tau can be phosphorylated by CDK1 (38). Abnormally increased levels of tau phosphorylation cannot modulate G2 and prepare for mitosis. Initiators of the cell cycle can play major roles in treating AD and be regarded as a therapeutic target.

The previous study suggested insulin signaling impairment and glucose metabolism reduction in AD patients (39). In previous studies, low concentrations of METH (20 mM) on increasing glucose receptors have been investigated. METH exposure showed a dual effect on the uptake the glucose in astrocyte, in the concentration of 20 µM increases the uptake and in 200 µM inhibit the uptake of glucose (40). Perhaps the desired effect of low-dose of METH to improve the cognitive effects of AD was related to the increased glucose receptors, which requires further research. Thus, our findings provide a new perspective for understanding apoptosis's molecular mechanism, cell cycle, and Gln in reactive astrocytes.

To further confirm the protective effect of methamphetamine, more clinical trials are needed. Because of the lack of time and cost, we could not do it. It would have been better that method validation and system suitability was done for the HPLC method, that only assay standardization was performed.

Conclusion

Our results showed that since astrocytes are the most important supporter cells in the CNS, despite the effects of high-dose METH, low-dose of METH can reduce apoptosis rate induced by Aβ. It also affects the cell cycle and the cell arrested in the G2 phase. Therefore, an effective dosage of METH can increase the amount of extracellular glutamine, which has a protective role in neuron cells, as well as the amount of *BAX* and *BCL-X*, which respectively decreased and increased the expression of these genes. Although METH has the effects of addiction; on the other hand, due to the effects of the low dose of METH for the prevention and treatment of AD, a drug can be designed that has a protective effect but has no side effects as METH.

Acknowledgments

Authors' Contributions

B.S.; Performed all *in vitro* experiments, analyzed the data, and wrote the manuscript. M.D.S., G.H.R.; Contributed to concept and design, financial support, analyzed the data, and wrote the manuscript. N.M.; Analyzed the data and wrote the manuscript. All authors read and approved the final manuscript.

References

1. Sofroniew MV, Vinters HV. Astrocytes: biology and pathology. Acta Neuropathol. 2010; 119(1): 7-35.
2. Back A, Tupper KY, Bai T, Chiranand P, Goldenberg FD, Frank JI, et al. Ammonia-induced brain swelling and neurotoxicity in an organotypic slice model. Neurol Res. 2011; 33(10): 1100-1108.
3. Du J, Song D, Li Y, Liu J, Huang X, Li B, et al. Saikosaponin-D mitigates oxidation in SH-SY5Y cells stimulated by glutamate through activation of Nrf2 pathway: involvement of PI3K. Neurotox Res. 2022; 40(1): 230-240.
4. Rau TF, Kothiwal AS, Rova AR, Brooks DM, Rhoderick JF, Poulsen AJ, et al. Administration of low dose methamphetamine 12 h after a severe traumatic brain injury prevents neurological dysfunction and cognitive impairment in rats. Exp Neurol. 2014; 253: 31-40.
5. Liddelow SA, Barres BA. Reactive astrocytes: production, function, and therapeutic potential. Immunity. 2017; 46(6): 957-967.
6. Olabarria M, Noristani HN, Verkhratsky A, Rodríguez JJ. Age-dependent decrease in glutamine synthetase expression in the hippocampal astroglia of the triple transgenic Alzheimer's disease mouse model: mechanism for deficient glutamatergic transmission? Mol Neurodegener. 2011; 6: 55.
7. Han X, Zhang T, Liu H, Mi Y, Gou X. Astrocyte senescence and Alzheimer's disease: a review. Front Aging Neurosci. 2020; 12: 148.
8. Pajarillo E, Rizor A, Lee J, Aschner M, Lee E. The role of astrocytic glutamate transporters GLT-1 and GLAST in neurological disorders: Potential targets for neurotherapeutics. Neuropharmacology. 2019; 161: 107559.
9. Bellaver B, Souza DG, Souza DO, Quincozes-Santos A. Hippocampal astrocyte cultures from adult and aged rats reproduce changes in glial functionality observed in the aging brain. Mol Neurobiol. 2017; 54(4): 2969-2985.
10. Acosta C, Anderson HD, Anderson CM. Astrocyte dysfunction in Alzheimer disease. J Neurosci Res. 2017; 95(12): 2430-2447.
11. Howland DS, Liu J, She Y, Goad B, Maragakis NJ, Kim B, et al. Focal loss of the glutamate transporter EAAT2 in a transgenic rat model of SOD1 mutant-mediated amyotrophic lateral sclerosis (ALS). Proc Natl Acad Sci USA. 2002; 99(3): 1604-1609.
12. Chen J, Herrup K. Glutamine acts as a neuroprotectant against DNA damage, beta-amyloid and H2O2-induced stress. PLoS One. 2012; 7(3): e33177.
13. Borgan FR, Jauhar S, McCutcheon RA, Pepper FS, Rogdaki M, Lythgoe DJ, et al. Glutamate levels in the anterior cingulate cortex in un-medicated first episode psychosis: a proton magnetic reso-

110

nance spectroscopy study. Sci Rep. 2019; 9(1): 8685.

14. Yao M, Nguyen TV, Pike CJ. Beta-amyloid-induced neuronal apoptosis involves c-Jun N-terminal kinase-dependent downregulation of Bcl-w. J Neurosci. 2005; 25(5): 1149-1158.

15. Garwood CJ, Pooler AM, Atherton J, Hanger DP, Noble W. Astrocytes are important mediators of Aβ-induced neurotoxicity and tau phosphorylation in primary culture. Cell Death Dis. 2011; 2(6): e167.

16. Jana A, Pahan K. Fibrillar amyloid-beta-activated human astroglia kill primary human neurons via neutral sphingomyelinase: implications for Alzheimer's disease. J Neurosci. 2010; 30(38): 12676-12689.

17. Prakash MD, Tangalakis K, Antonipillai J, Stojanovska L, Nurgali K, Apostolopoulos V. Methamphetamine: effects on the brain, gut and immune system. Pharmacol Res. 2017; 120: 60-67.

18. Ghahghaei A, Bathaie SZ, Kheirkhah H, Bahraminejad E. The protective effect of crocin on the amyloid fibril formation of Aβ42 peptide in vitro. Cell Mol Biol Lett. 2013; 18(3): 328-339.

19. Rau T, Ziemniak J, Poulsen D. The neuroprotective potential of low-dose methamphetamine in preclinical models of stroke and traumatic brain injury. Prog Neuropsychopharmacol Biol Psychiatry. 2016; 64: 231-236.

20. Rau TF, Kothiwal AS, Rova AR, Brooks DM, Poulsen DJ. Treatment with low-dose methamphetamine improves behavioral and cognitive function after severe traumatic brain injury. J Trauma Acute Care Surg. 2012; 73(2 Suppl 1): S165-172.

21. Thrash B, Karuppagounder SS, Uthayathas S, Suppiramaniam V, Dhanasekaran M. Neurotoxic effects of methamphetamine. Neurochem Res. 2010; 35(1): 171-179.

22. Charbonneau JR, Furtak T, Lefebvre J, Gauthier ER. Bcl-xL expression interferes with the effects of L-glutamine supplementation on hybridoma cultures. Biotechnol Bioeng. 2003; 81(3): 279-290.

23. Miguel-Hidalgo JJ. The role of glial cells in drug abuse. Curr Drug Abuse Rev. 2009; 2(1): 76-82.

24. Matos M, Augusto E, Oliveira CR, Agostinho P. Amyloid-beta peptide decreases glutamate uptake in cultured astrocytes: involvement of oxidative stress and mitogen-activated protein kinase cascades. Neuroscience. 2008; 156(4): 898-910.

25. Sharif A, Prevot V. Isolation and culture of human astrocytes. Methods Mol Biol. 2012; 814: 137-151.

26. White JA, Manelli AM, Holmberg KH, Van Eldik LJ, Ladu MJ. Differential effects of oligomeric and fibrillar amyloid-beta 1-42 on astrocyte-mediated inflammation. Neurobiol Dis. 2005; 18(3): 459-465.

27. Bahuguna A, Khan I, Bajpai V K,Kang S C. MTT assay to evaluate the cytotoxic potential of a drug. Bangladesh Journal of Pharmacology. 2017; 12(2).

28. Shakibaie M, Vaezjalali M, Rafii-Tabar H, Sasanpour P. Phototherapy alters the oncogenic metabolic activity of breast cancer cells. Photodiagnosis Photodyn Ther. 2020; 30: 101695.

29. Riccardi C, Nicoletti I. Analysis of apoptosis by propidium iodide staining and flow cytometry. Nat Protoc. 2006; 1(3): 1458-1461.

30. Schmittgen TD, Livak KJ. Analyzing real-time PCR data by the comparative C(T) method. Nat Protoc. 2008; 3(6): 1101-1108.

31. Antuono PG, Jones JL, Wang Y, Li SJ. Decreased glutamate + glutamine in Alzheimer's disease detected in vivo with (1)H-MRS at 0.5 T. Neurology. 2001; 56(6): 737-742.

32. Rau TF, Kothiwal A, Zhang L, Ulatowski S, Jacobson S, Brooks DM, et al. Low dose methamphetamine mediates neuroprotection through a PI3K-AKT pathway. Neuropharmacology. 2011; 61(4): 677-686.

33. El Ayadi A, Zigmond MJ. Low concentrations of methamphetamine can protect dopaminergic cells against a larger oxidative stress injury: mechanistic study. PLoS One. 2011; 6(10): e24722.

34. Baghbaderani S, Hashemi M, Ebrahimi-Ghiri M, Zarrindast MR, Nasehi M, Entezari M. Curcumin prevents cognitive deficits in the bile duct ligated rats. Psychopharmacology (Berl). 2020; 237(12): 3529-3537.

35. Currais A, Hortobágyi T, Soriano S. The neuronal cell cycle as a mechanism of pathogenesis in Alzheimer's disease. Aging (Albany NY). 2009; 1(4): 363-371.

36. Bajić VP, Su B, Lee HG, Kudo W, Siedlak SL, Zivković L, et al. Mislocalization of CDK11/PITSLRE, a regulator of the G2/M phase of the cell cycle, in Alzheimer disease. Cell Mol Biol Lett. 2011; 16(3): 359-372.

37. Chen SD, Yang JL, Lin YC, Chao AC, Yang DI. Emerging roles of inhibitor of differentiation-1 in Alzheimer's disease: cell cycle reentry and beyond. Cells. 2020; 9(7): 1746.

38. Bennecib M, Gong CX, Grundke-Iqbal I, Iqbal K. Role of protein phosphatase-2A and -1 in the regulation of GSK-3, cdk5 and cdc2 and the phosphorylation of tau in rat forebrain. FEBS Lett. 2000; 485(1): 87-93.

39. Willette AA, Bendlin BB, Starks EJ, Birdsill AC, Johnson SC, Christian BT, et al. Association of insulin resistance with cerebral glucose uptake in late middle-aged adults at risk for alzheimer disease. JAMA Neurol. 2015; 72(9): 1013-1020.

40. Abdul Muneer PM, Alikunju S, Szlachetka AM, Haorah J. Methamphetamine inhibits the glucose uptake by human neurons and astrocytes: stabilization by acetyl-L-carnitine. PLoS One. 2011; 6(4): e19258.

Original Article

miR-205 Reverses MDR-1 Mediated Doxorubicin Resistance via *PTEN* in Human Liver Cancer HepG2 Cells

Mei Li, M.D.[1#], Zhubin Li, M.D.[1#], Juanrong Song, M.D.[1], Xu Li, M.D.[2], Pengtao Zhai, M.D.[1], Xudong Mu, M.D.[1],

Fakai Qiu, M.D.[1], Le Yao, M.D.[3*]

1. Department of Minimally Invasive Intervention, Shaanxi Provincial Cancer Hospital, Xi'an, Shaanxi, China
2. Department of Oncology, Shaanxi Provincial Cancer Hospital, Xi'an, Shaanxi, China
3. Department of Infectious Diseases, The First Hospital of Yulin, Yulin, Shaanxi, China

# These authors contributed equally to this work.

Corresponding Address: Department of Infectious Diseases, The First Hospital of Yulin, Yulin, Shaanxi, China
Email: sxsyaole@sina.com

Abstract

Objective: The aim of the recent study was to investigate the effects of *miR-205* on reversing Doxorubicin (DOX) resistance, as chemotherapeutic agents through up-regulation of *PTEN* in human liver cancer HepG2 cells.

Materials and Methods: In this experimental study, the drug resistance in liver cancer cells via drug efflux inhibition and enhancing apoptosis by the regulation of *PTEN* and multi-drug resistance/ P-glycoprotein (MDR/P-gp) expression was revealed. Using 3-(4,5-Dimethylthiazol-2-yl)-2,5-diphenyltetrazolium bromide (MTT) assay, effect of DOX on cell proliferation was evaluated after *miR-205* transfection in HepG2 and HepG2/DOX cells. Activity of P-gp on drug efflux was measured by the Rhodamine 123 (Rho-123) assay. *PTEN* mRNA expression levels were measured by quantitative reverse transcription polymerase chain reaction (qRT-PCR) and flow cytometry was used to measure the apoptotic ratio of HepG2/DOX cells.

Results: *miR-205* overexpression considerably inhibited the HepG2/DOX cells viability (P<0.05). qRT-PCR results revealed that *PTEN* is a pivotal regulator in PI3K/Akt/P-gp axis. Overexpression *miR-205* resulted in up-regulation *PTEN* and ultimately down-regulation of P-gp. This inhibits drug resistance, proliferation and induces apoptosis in HepG2/DOX cells (P<0.05). Whilst, treatment with 10 μM of special inhibitors, including LY294002 (PI3K) or PD098059 (MAPK), increased Rho 123-associated MFI, treatment with 10 μM of SF1670 (*PTEN*) almost abolished the effect of miR-205 overexpression (P<0.05). Finally, we found that *miR-205* was down-regulated in HepG2/DOX cells, and its overexpression led to enhancing apoptosis with re-sensitization of HepG2/DOX cell lines to DOX through *PTEN*/PI3K/Akt/MDR1 pathway.

Conclusion: These findings may introduce *miR-205* as a predictive biomarker and a potential treatment target for liver cancer therapy during MDR.

Keywords: Drug Resistance, Liver Cancer, *miR-205*, P-Glycoprotein, *PTEN*

Introduction

Liver cancer is one of the three most common causes of cancer-related mortality, all over the world. Considering high incidence of liver cancer, chemotherapy and prognosis of this malignancy are the primary focus of medical research (1). Although surgery and transplants applied as therapeutics for patients with early-stage of liver cancer, in many cases they are diagnosed when the disease has reached the stage beyond curative surgery (2). In this regard, cell lines that express differentiated hepatic functions have been used in liver studies, as an alternative to the cultured hepatocytes. HepG2 is a typical hepatoma cell line that survives well in various environments. Besides, it is widely applied for drug development and pharmaco-toxicological testing (3, 4).

Routinely, systemic chemotherapy serves a crucial role in the treatment of modalities for advanced liver cancer. Lamentably, systemic chemotherapy is usually inadequate because of the resistance of cancer cells to chemotherapeutic drugs, causing failure of this curative method (5). Doxorubicin (DOX) is a routinely anthracycline drugs applied as chemotherapeutic agents, particularly in patients with advanced or metastasis cancer, inducing apoptosis of these tumor cells. Mechanically, DOX represses topoisomerase II (Top II) and intercalates directly to DNA double-strand, finally resulting in the intervention of gene transcription (6, 7). Notwithstanding, DOX is extensively applied for treatment of cancers, drug-resistance largely restricted the clinical employment of DOX (8). In this case, resistance to a broad spectrum of chemotherapeutic agents in neoplasm is called multi-drug resistance (MDR) and it is the focal problem in chemotherapy (9-11). Many relevant mechanisms for MDR have been described and discussed, one of which overexpressed the plasma membrane drug efflux pumps P-glycoprotein (P-gp/ABCB1). It is encoded by *MDR1* gene and belongs to ATP-binding cassette (ABC). It is also involved in MDR (9, 12). Indeed, P-gp reduces the

intracellular accumulation of anti-cancer drugs including DOX to sub-therapeutic levels, thus decreasing or abolishing chemotherapy efficacy of this drug (13).

Among this, Akt/PKB is a pivotal element for protecting cells from undergoing programmed cell death. Thus, PKB-mediated survival-pathway is an attractive target for cancer chemotherapy. Loss of tumor suppressor gene "phosphate and tensin homolog deleted on chromosome 10" (*PTEN*) is common in cancer tumors, constitutively activating Akt (14). Phosphatase activity of *PTEN* is crucial in controlling the phosphatidylinositol-3 kinase (PI3K)/Akt signal transduction pathway. In this regard, down-regulation of *PTEN* in tumor cells may be associated with poor tumor prognosis and drug resistance (12). Indeed, inhibition of PI3K/Akt pathway can reverse MDR and sensitize tumor cells to these agents (12, 15).

Developing inhibitors of ABC transporters-based MDR is one of the solutions for MDR in carcinomas in the recent decades (16). However, with regard to the undesired side-effects and toxicity issues, these drugs are failed in the clinic (17). Therefore, combined therapy with some chemo-sensitizers agents is desirable to improve the anti-cancer effect to overcome DOX-resistance.

So far, several negative associations have identified between gene expression and MDR in human hepatoma cells (18). In the framework of modulate direct posttranscriptional regulation of gene expression, it is widely identified that microRNAs (miRNAs, also known as "miRs") are a class of short endogenous non-protein-coding single-stranded RNAs, which by binding to partially complementary sites within the 3′-untranslated region (3′-UTR) of target mRNAs, through Watson-Crick base pairing postulate, result in translational suppression or mRNA deadenylation and degradation (19). Growing evidence has illustrated that miRNAs have critical role in various biological processes such as cell survival, proliferation, differentiation, migration, invasion, sensitivity to chemotherapy and so on (20, 21). Recent studies have revealed that many specific miRNAs are capable of modulating MDR in cancers (22). miRNAs can function either as a promoter or suppressor to regulate MDR in cancers (23). Among this, *miR-205* is one of the best-studied conserved miRNAs, located in chromosome 1q32.2 and expressed in squamous epithelium-derived tissues as well as the mammary gland progenitor cells (24). *miR-205* targets *PTEN* and leucine-rich repeat protein phosphatase 2 to increase Akt pathway and drive malignant phenotypes in non-small cell lung (NSCL) tumors (25). Previously findings revealed that *miR-205* improves the chemosensitivity of breast cancer cells to TAC (docetaxel, doxorubicin plus cyclophosphamide) chemotherapy by repressing

both VEGFA and FGF2, leading to apoptosis (20). Therefore, better understanding the role of miRNA during MDR chemotherapy may provide new avenues for liver cancer diagnostic and treatment. In this study, miRNA targeting MDR-associated molecules has been illustrated, as potentially an effective factor in cancer therapy.

Overall, the aim of the recent study was to investigate the effects of *miR-205* on reversing DOX resistance, as chemotherapeutic agents through up-regulation of *PTEN* in human liver cancer HepG2 cells. For this purpose, we examined the pivotal role of *miR-205* on P-gp, as a member of ABC transporters through the *PTEN*/PI3K/Akt/MDR1/ABCB1/P-gp signaling pathway.

Materials and Methods

The multidrug resistance in liver cancer cells through drug efflux inhibition and apoptosis enhancement by the regulation of *PTEN* and MDR/P-gp expression was evaluated using 3-(4,5-Dimethylthiazol-2-yl)-2,5-diphenyltetrazolium bromide (MTT) assay. Effect of DOX on cell proliferation was tested after *miR-205* transfection in HepG2 and HepG2/DOX cells. P-gp activity on drug efflux was measured by Rhodamine 123 (Rho-123) assay. *PTEN* mRNA expression levels were measured by quantitative reverse transcription polymerase chain reaction (qRT-PCR) and flow cytometry was utilized to calculate the apoptotic ratio of HepG2/DOX cells.

This study was performed at the Shaanxi Provincial Cancer Hospital under Ethical Committee permission (SXNo.20190728).

Cell culture and cell transfection

In this experimental study, the human liver cancer cell line HepG2 and DOX-resistant cell line HepG2/DOX was obtained from National Cell Bank of China. All cells were cultured in DMEM basic medium with 0.33% sodium bicarbonate (Gibco, USA) supplemented with 10% heat-inactivated Fetal Bovine Serum (Gibco, USA), streptomycin (100 µg/ml), penicillin G (100 IU/ml; both from Sigma Aldrich, USA), and incubated at 37˚C in a humidified (vol/vol) atmosphere of 5% CO_2. HepG2/DOX cells were seeded and cultured in the presence of 0.5 µM of DOX or DOX-free medium for two weeks before investigations. Sequence of the miR-205 mimic was 5′-UCCUUCAUUCCACCGGAGUCUG-3′. Cells ($3×10^5$ cells/2 ml/well) were seeded in six-well microplates at 70% confluence. After 48 hours, the *miR-205* mimic or the negative control was transfected into the cells using Lipofectamine™ 2000 (Life Technologies, USA), at a final concentration of 50 nM, according to the manufacturer's protocols. In brief, the *miR-205* mimic or the negative control was mixed with 100 µl Lipofectamine 2000 in 12 ml culture medium and divided into per well of six-well microplates. Twenty-four hours after transfection, the

media was replaced with fresh medium and the cells were incubated for an additional 24 hours.

RNA extraction, cDNA synthesis and quantitative reverse transcription polymerase chain reaction

Briefly, 2×10^6 cells/2 ml/well was seeded onto six-well plates for 24 hours. According to the manufacturer's instructions, total RNA was extracted from the cells using a TRIzol® reagent (Invitrogen Life Technologies, USA). Complementary DNA (cDNA) was synthesized at 37°C for 15 minutes and 95°C for 10 minutes using Moloney Murine Leukemia Virus (MMLV) reverse transcriptase (Promega, USA). next, quantitative reverse transcription PCR (qRT-PCR) was performed using SYBR Premix Ex Taq (TaKaRa Bio, Japan) and specific primers in the Roche Light Cycler® 96 System (Roche, Germany). PCR amplification was performed as follow: 5 minutes of primary denaturation at 95°C, 40 cycles of 95°C for 45 seconds, 57°C for 30 seconds and 72°C for 60 seconds, followed by a final incubation at 72°C for 5 minutes. The applied primers include:

miR-205-

F: 5′-GCTCCTTCATTCCACCGG-3′
R: 5′-CAGTGCAGGGTCCGAGGT-3′

MDR-1-

F: 5′-CCCATCATTGCAATAGCAGG-3′
R: 5′-TGTTCAAACTTCTGCTCCTGA-3′

PTEN-

F: 5′-GGACGAACTGGTGTA-3′
R: 5′-CCTCTGACTGGGAATAG-3′

β-actin-

F: 5′-AAGCTGTGTTACGTGGCCCT-3′
R: 5′-GGGCAGCTCGTAGCTCTTCT-3′

All experiments were carried out in triplicates. Raw data were analyzed with the comparative Ct method using *β-actin* as an internal control gene.

Biological analysis by MTT assay

The effect of DOX on cell viability in liver cancer cell lines growth was evaluated by MTT assay. HepG2 and HepG2/DOX cells were seeded onto 96-well plates (1×10^4 cells/200 µl/well) and incubated overnight and transfected with *miR-205* at 37°C. Upon 24 hours incubation, both cell lines were treated with diverse concentrations of DOX for 48 hours. Subsequently, the cells were treated with 10% (5 mg/ml) 20 µl MTT (Sigma Aldrich, USA) was added to each well for another 4 hours. Next, 200 µl dimethyl sulfoxide (DMSO) was added to each well for dissolving formazan product. Optical density was measured at 490 nm using a Benchmark Plus microplate spectrometer (Bio-Rad laboratories, USA). The fold reversal (FR) of MDR was determined by dividing IC_{50} value of the cells treated with the indicated anticancer drug in the absence of a modulator by IC_{50} value of the cells treated with the same anticancer drug in the presence of a modulator. Absorbance values were normalized, allocating the value of the cells in medium without drug to 1.0 and the value of the no-cell control to 0.

Rho 123 efflux assay

To visualize the intracellular accumulation of P-gp and its level, the substrate (Rho 123) was applied. 1×10^6 cells/2 ml/well was seeded onto six-well plates. After 24 hours incubation, the cells were treated with serum-free medium containing 3.4 µM Rho 123 in the presence or absence of *miR-205* and they were incubated for 2 hours at 37°C. Verapamil was used as positive control for P-gp inhibition. The intracellular mean fluorescence intensity (MFI) associated with intracellular Rho 123 content was determined using FP-6200 fluorometer (Jasco Co., Japan).

Flow-cytometric analysis

Flow-cytometry was used to analyze the apoptotic rate of cells. The HepG2/DOX Cells (1.5×10^6 cells/2 ml/well) were seeded onto 6-well microplate after 70% confluence, incubated overnight and transfected with *miR-205* at 37°C. The cells were then centrifuged at $1500 \times g$ for 5 minutes at RT. The cell pellets were suspended in 10 µl of fluorescein isothiocyanate (FITC)-labeled Annexin V and propidium iodide (PI) solution for 10 minutes at dark in RT and then analyzed using a fluorescence-activated cell sorting (FACS) flowcytometer (BD LSR; Becton-Dickinson, USA) and Cell Quest software (Becton-Dickinson, USA).

Statistical data analysis

All experiments from at least three independent repeated tests were performed and analyzed using analysis of variance (ANOVA). Bonferroni's and Sidak's tests were used to ascertain the statically significant differences between the groups. Data analysis was performed with GraphPad Prism v6 software (USA) to examine significant differences. The results are expressed as the means ± standard deviation (SD), and $P < 0.05$ was considered statistically significant.

Results

Down-regulation of *miR-205* resulted in viability enhancement of HepG2/DOX cells in response to DOX compared to parental cells

To examine the possible role of *miR-205* in the HepG2/DOX cell, qRT-PCR analysis was firstly applied. The result of these investigations demonstrated that expression level of *miR-205* was higher in the HepG2 cells compared to the HepG2/DOX cells, following transfection of *miR-205* (Fig.1), which revealed that *miR-205* may be inversely correlated with DOX resistance in liver tumor cells. Next, we assessed the effect of DOX on cell viability using the MTT assay. As shown in (Fig.1), DOX (concentration range from 0.01 to 10 µM) revealed lower cytotoxicity towards the drug resistant cells compared to the parental cells causing enhancement of the viability of HepG2/DOX cell lines. The IC_{50} values for DOX were 0.21 µM in

HepG2 and 2.84 µM in HepG2/DOX cells, showing 13.52-fold resistance to DOX, compared to the HepG2 cells.

A

B
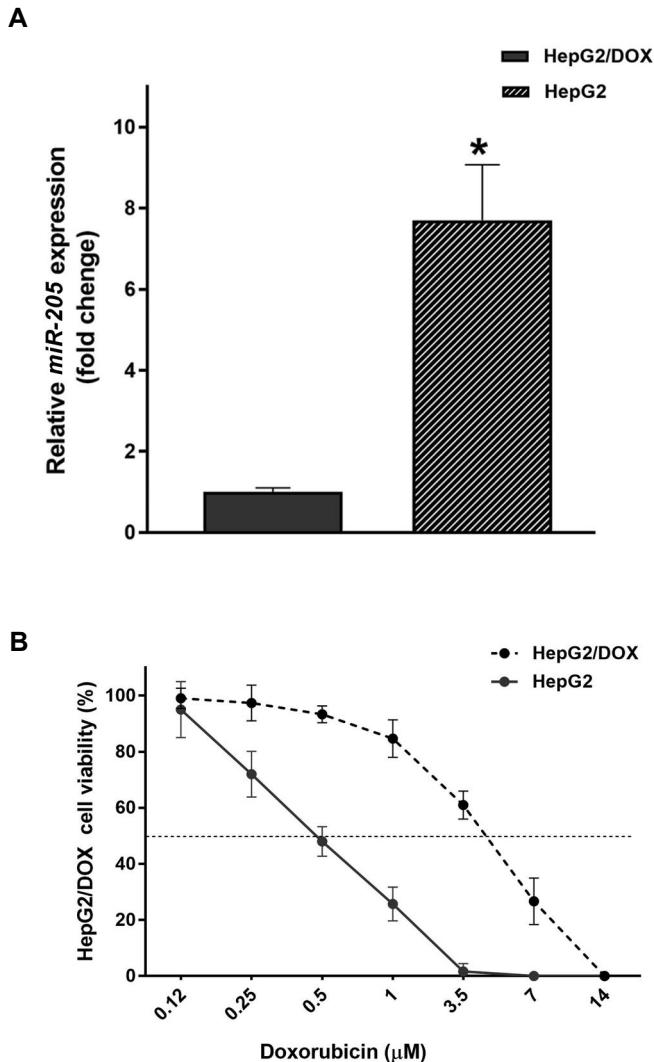
Fig.1: Expression levels of *miR-205* and sensitivity of HepG2 and HepG2/DOX cells to Doxorubicin (DOX). **A.** Expression levels of *miR-205* in HepG2 and HepG2/DOX cells. **B.** Cells were treated with versatile concentrations of DOX. After 48 hours of incubation, viability rates of the cells were measured using the 3-(4,5-Dimethylthiazol-2-yl)-2,5-diphenyltetrazolium bromide (MTT) assay. Each point represents the mean ± SD (n=3 independent experiments, *; P<0.05 compared to HepG2/DOX cells).

Overexpression of *miR-205* resulted in inhibiting viability and inducing apoptosis of HepG2/DOX cells

To ascertain the correlation between *miR-205* and HepG2/DOX cell lines, the effect of up-regulation of *miR-205* on the DOX-resistance cells was analyzed. The treated HepG2 cells with DOX and DOX+*miR-205* exhibited equal cytotoxicity (Fig.2A). In contrast, HepG2/DOX cells transfected with DOX+*miR-205* showed statically significant less survival rates than DOX group (Fig.2B). These results showed that overexpression of *miR-205* can sensitize the HepG2/DOX cells to DOX.

Flow-cytometric analysis was conducted to assess the impact of HepG2/DOX cells by Annexin V–FITC and PI staining, and apoptotic cells were detected 48 hours after *miR-205* transfection. The lower right quadrant indicates

pro-apoptotic cell rate. This revealed that combination of *miR-205* with DOX enhanced migration of the HepG2/DOX cells into apoptotic regions compared to the DOX group (Fig.2C).

A **B**

C
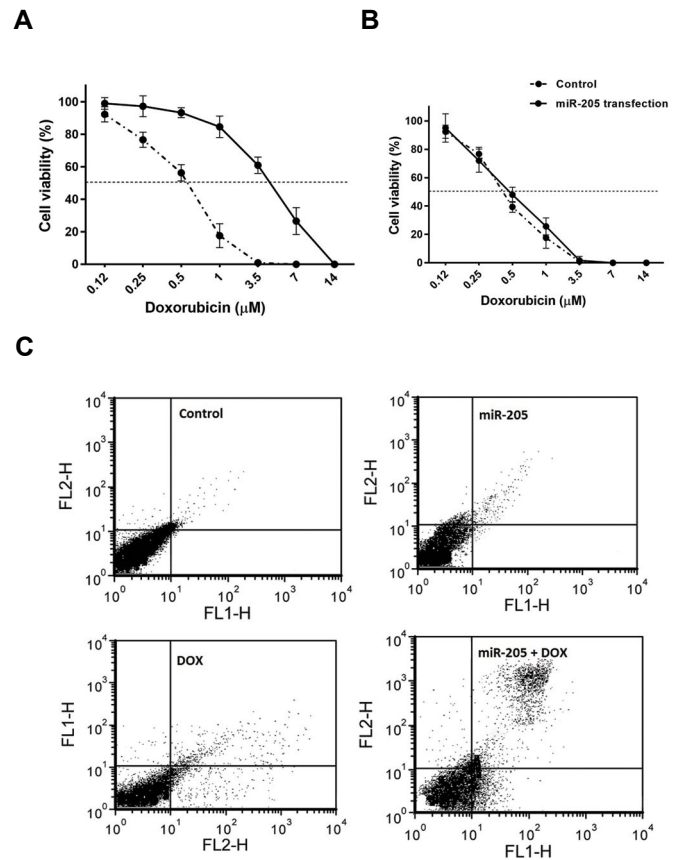
Fig.2: Effects of *miR-205* transfection on Doxorubicin (DOX) cytotoxicity and apoptotic analysis of HepG2/DOX cells. Upon culture for 48 hours after transfection with the *miR-205*, the **A.** HepG2/DOX cells and **B.** HepG2 cells were incubated with various concentrations of DOX for 48 hours and cell viability was defined by the 3-(4,5-Dimethylthiazol-2-yl)-2,5-diphenyltetrazolium bromide (MTT) assay. **C.** Then, cells were stained with Annexin V–FITC and PI 48 hours after transfection with *miR-205*. Control, *miR-205*, DOX 1 µM and *miR-205* plus DOX 1 µM. Each point represents mean ± SD (n=3 independent experiments, *; P<0.05 compared to control).

Overexpression of *miR-205* alleviated P-gp activity in HepG2 cell line

P-gp activity was determined using intracellular Rho 123 accumulation assay. Verapamil was used as a positive control agent. Figure 3 obviously demonstrates that *miR-205* enhanced Rho 123 accumulation in the HepG2/DOX cells after 2 hours, while the HepG2 cells did not show such enhancement when transfected with *miR-205*. Indeed, transfection of *miR-205* in the HepG2/DOX cells with the Rho 123 resulted in enhancement in the MFI (P<0.05). This effect is comparable with that observed in the HepG2/DOX cell lines treated with verapamil. Nevertheless, no accumulation of substrate was recognized in parental HepG2 cells over the same period. Therefore, it was proposed that activity of P-gp was inhibited via *miR-205* in HepG2/DOX cells.
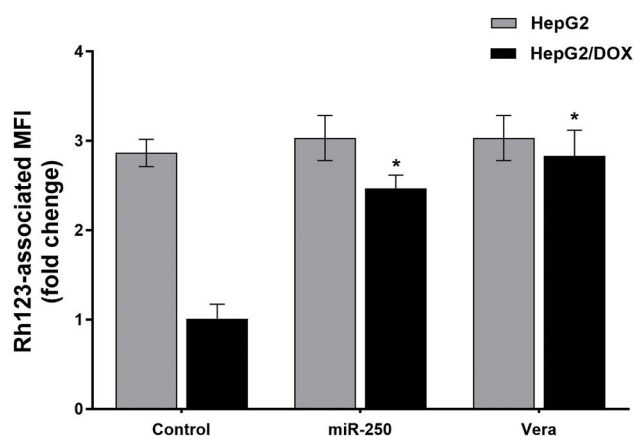
Fig.3: Effect of *miR-205* on the intracellular accumulation of Rho 123. Upon culture for 48 hours after treatment, the cells were incubated with 5 μM of Rho 123 in the presence or absence of *miR-205* and 10 μM of verapamil for 2 hours and then, Rho 123-associated mean fluorescence intensity (MFI) was measured. Each point depicts the mean ± SD from four tests. *; P<0.05 compared to control.

Overexpression of *miR-205* reversed resistance through down-regulation of MDR-1 in HepG2 cell line

Herein, we extended our work to a HepG2/DOX cell to evaluate whether the observed effects were cancer cell type-specific or they might be more generally applicable. PCR analyses showed while the HepG2/DOX cells expressed significant amounts of MDR-1, no MDR-1 was detectable in the parental HepG2 cells. These data robustly showed that the HepG2/DOX cell line was phenotypically MDR and this MDR phenotype was correlated to up-regulation of P-gp (Fig.4). We found out that *miR-205* down-regulated P-gp in the mRNA levels in HepG2/DOX cells. This can describe the elevated intracellular accumulation of DOX and cytotoxicity in the *miR-205*-treated HepG2/DOX cells.

Inhibition of *PTEN* abolished *miR-205* effects on DOX-mediated resistance in HepG2 cell line

We speculated that *miR-205* may play crucial role in the inhibition of MDR-1 expression by down-regulating PI3K/Akt signaling pathway activity. Therefore, to further scrutinize the fundamental molecular mechanisms, we investigated the MDR-reversing effect of *miR-205* in the presence of special inhibitors of *PTEN* (SF1670) and PI3K (LY294002). As shown in Table 1, compared to the control group, DOX cytotoxicity was heightened in the *miR-205*-treated group. The IC$_{50}$ values (μM) were diminished from 2.84 ± 0.37 to 0.32 ± 0.09, 0.29 ± 0.08, 0.38 ± 0.08, and 1.99 ± 0.31 in control (DOX), *miR-205*+DOX, *miR-205*+LY294002 10 μM+DOX, *miR-205*+SF1670 10 μM+DOX, respectively. However, *miR-205* effect was significantly attenuated by SF1670 treatment. In addition, results revealed that FR in *miR-205*+SF1670 10 μM+DOX was significantly different from *miR-205*+DOX. After transfection with *miR-205*, cultured for 48 hours. The effect of SF1670 and LY294002 on the *miR-205*-induced intracellular Rho 123 related MFI accumulation was observed in HepG2/DOX cells. Indeed, treatment with

10 μM LY294002 enhanced Rho 123-correlated MFI and treatment with 10 μM SF1670 almost abrogated the action of *miR-205* overexpression (Fig.5A).

Table 1: Cytotoxicity effect of DOX and reversing MDR in HepG2/DOX cells role of miR-205 and co-exposure with LY294002 and SF1670 as selective inhibitors

Treatment	HepG2/DOX	
	IC$_{50}$ (μM)	FR
Control (DOX)	4.54 ± 0.57	-
miR-205+DOX	0.52 ± 0.8^a	8.65
miR-205+LY294002 10 μM+DOX	$0.49 \pm 0.08^{a, b}$	9.26
miR-205+SF1670 10 μM+DOX	3.69 ± 0.31	1.23

MTT reduction activity was used to determine cell viability. Each value represents the mean ± SD of three independent tests. The fold reversal (FR) of MDR was distinguished by dividing the IC$_{50}$ of control to IC$_{50}$ of each test. Statically significant different from control at [a]; P<0.05, No significant difference from miR-205+DOX group [b]; P>0.05.
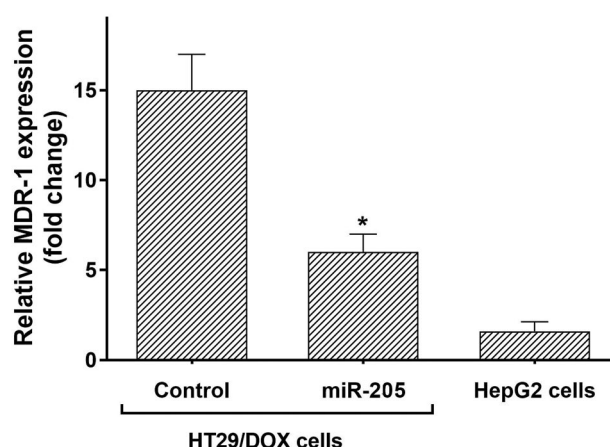
Fig.4: Effect of *miR-205* on the MDR-1 expression in HepG2 and HepG2/DOX cells. *miR-205* down-regulated MDR-1 in HepG2/DOX cells. Each point represents the mean ± SD from four experiments (n=3, *; P<0.05 compared to control).

In this regard, our findings clearly demonstrated that *miR-205* in HepG2/DOX cells, 48 hours after transfection, attenuated *MDR-1* mRNA. Besides, SF1670 suppressed the effects of *miR-205* (Fig.5B, C). Further examinations showed that in the presence of 10 μM SF1670, eliminated *miR-205* effects on P-gp expression was noted. However, no similar effect with 10 μM ofLY294002 was noticed. Overall, these results illustrated that *miR-205*-induced down-regulation of P-gp was correlated as *PTEN*-dependence in HepG2/DOX cells.

Up-regulation of *PTEN* by *miR-205* overexpression resulted in down-regulation of MDR-1 in HepG2 cell line

PTEN induces cell death and MDR reversal effect by suppression of PI3K/Akt pathway. Finally, this

mechanism resulted in the down-regulation of P-gp and enhancement of drug accumulation in cells. In order to investigate correlation between *miR-205* and *PTEN*, *PTEN* expression was assessed in HepG2/DOX cell lines (Fig.5C).

A

B

C
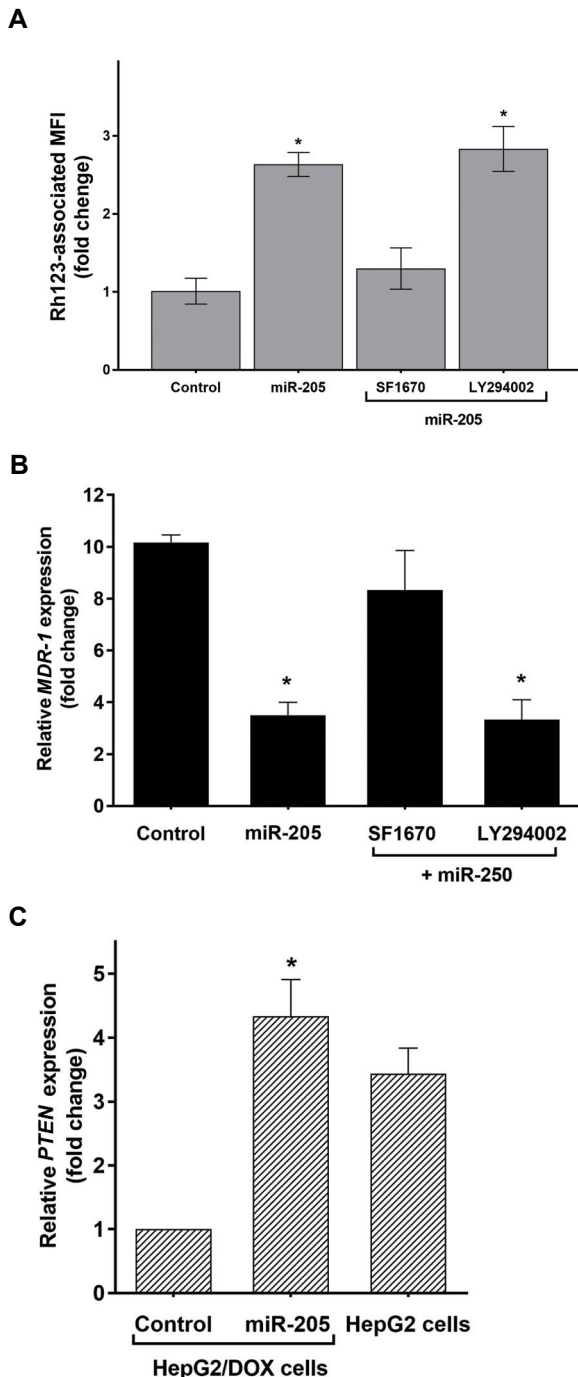
Fig.5: *PTEN* inhibition abolished *miR-205* effects on MDR. **A.** Intracellular Rho 123 accumulation in HepG2/DOX cells was affected by *miR-205* and specific inhibitors. Treatment with 10 µM LY294002 increased Rho 123-associated MFI and treatment with 10 µM SF1670 almost abolished the effect of miR-205 overexpression. **B.** *MDR-1* mRNA in HepG2/DOX cells 48 hours after transfection. SF1670 suppress the effects of *miR-205*. **C.** *miR-205* up-regulated *PTEN* levels in HepG2/DOX cells. The data represent mean ± SD (n=3, *; $P<0.05$ compared to non-transfected HepG2/DOX cells).

Discussion

Herein, we showed that *miR-205* overexpression considerably inhibited drug resistance, viability and proliferation of HepG2/DOX cells. Furthermore, our data revealed that significant down-regulation of P-gp expression with *PTEN,* was through *miR-205,* which inhibits MDR in HepG2/DOX cells. In fact, *miR-205* re-sensitized human liver cancer HepG2/DOX cells to DOX by targeting *PTEN*/PI3K/Akt/MDR1/P-gp signal transduction pathway.

Cancer resistance to chemotherapeutic agents led to the manifested MDR due to the overexpression of ABC transporters, including P-gp. It is a crucial unresolved impede that hinders the chemotherapy of liver cancer. Hence, it is crucial to identify unique strategies to enhance the effectiveness of DOX for curative purposes. Recent researches have revealed that miRNAs play a key role in the MDR of liver cancers and they could modulate MDR by regulating P-gp (22, 26). In this regard, many miRNAs have been found to regulate drug resistant genes including *ABCG2*, *Bcl-2*, *MDR1* and *PTEN* (27).

MicroRNAs have emerged as pivotal regulators of cellular pathways, which result in altered gene expressions (28). *miR-205* is correlated with cancer development (29), as an epithelial-specific miRNA and it has been demonstrated to modulate chemo-sensitivity and chemo-resistance in a diverse population of cancer cells through behaving as tumor suppressor (ts-miRNAs) or oncogenes (onco-miRNAs) depending on the function and mechanism of their targets (30, 31). *miR-205* conducts conflicting functions in human cancers (32). In this regard, Bhatnagar and colleagues (33) demonstrated that in prostate cancer cell lines *miR-31* and *miR-205* are down-regulated leading to the resistance to chemotherapy-induced apoptosis of these cells. Additionally, Chaudhary and co-workers (34) demonstrated that *miR-205* overexpression re-sensitized gemcitabine (GEM)-resistant pancreatic cancer cells to GEM. Thus, it acts as a tumor suppressor. Shao and colleagues (31) revealed that *miR-205-5p* expression was down-regulated in all hepatic cancer cell line, whilst *miR-205-5p* expression was up-regulated by 5-fluorouracil (5-Fu) treatment in Bel-7402 (Bel) cells. With referring to the previous studies, our data revealed that *miR-205* was significantly down-regulated in HepG2/DOX cells, compared to the parental HepG2 liver cancer cells. Indeed, overexpression of *miR-205* in HepG2/DOX cells restored DOX sensitivity and significantly declined viability of HepG2/DOX cells. Indeed, we sought to clarify whether or not combination of *miR-205* with DOX enhanced apoptosis of HepG2/DOX cells compared to HepG2 cells. In this regard, we received desirable response from these DOX-resistant cells. In fact, DOX was particularly concentrated in the nuclei when it combined use with *miR-205* or verapamil. On the other hand, DOX accumulation in the cytoplasm happens when it administrated as a single drug in HepG2/DOX cells. In addition, *miR-205* could improve the drug-transport function of MDR1 assessed

by Rho 123. This showed that *miR-205* had the capability to improve DOX-mediated apoptosis.

Evidence revealed that *PTEN* negatively regulates cell cycle progression and cell survival by dephosphorylating PIP3 to PIP2 followed by inhibition of the Akt/PKB pathway (35). Inhibiting the PI3K/Akt axis with a specific inhibitor (LY294002) or Akt siRNA could retrieve drug sensitivity with down-regulating expression of P-gp and MRP1. Although the accurate mechanisms that underlie the role of PI3K/Akt pathway activation remain unclear. These results clearly revealed that the PI3K/Akt pathway played a major role in the pathogenesis of MDR (36). So far, several studies have showed that *PTEN* is a direct target of *miR-205*. In this regard, a study was conducted on two different cell lines of human ovarian cancer. They demonstrated that inhibition of *miR-205-5p* in C13K cells led to overexpression of *PTEN* and following decrease in its downstream targets including p-AKT. This was resulted in cisplatin sensitiveness in these cells. In contrast, overexpression of *miR-205-5p* in OV2008 cells led to down-regulation of *PTEN* and following enhancement of p-AKT level, which resulted in cisplatin resistance (37). To validate whether *PTEN* was direct targets of *miR-205*, we demonstrated for the first time a positive regulation of *PTEN* exert by *miR-205* in liver cancer HepG2 cells. Moreover, we showed that *PTEN* expression was significantly lower in HepG2/DOX cells. In fact, *miR-205* led to overexpression of *PTEN* in HepG2/DOX cell lines. Furthermore, FR results revealed when *PTEN* is inhibited compared to the other groups, *miR-205* could not reverse MDR in HepG2/DOX cells. Furthermore, to confirm the participation of *PTEN* or *PI3K* in this pathway and to elucidate its fundamental molecular mechanism, we investigated the MDR-reversing effect of *miR-205*. The investigation was performed in the presence of special inhibitors for *PTEN* (SF1670) and PI3K (LY294002). Desirable results of this investigation illustrated crucial role of *miR-205* involvement in this pathway.

MDR reversal is significantly important in the progress of cancer treatment (38). Recently, novel therapeutic approaches focused on affected miRNAs in modulating MDR by modifying the expression of ABC transporters including P-gp in cancer cells (39). Studies revealed that up-regulation of P-gp in tumors can be either intrinsic or acquired following chemotherapy depending on the tissue of origin (13). It is reported that many anti-cancer drugs, such as DOX and paclitaxel, are substrates of P-gp (40). Up-regulation of P-gp in tumor cells elevated drug resistance, meaning that inhibiting the P-gp was shown to reverse drug resistance. These indicate defined the classical MDR associated role of P-gp. In this regard, Zheng et al. (40) demonstrated that *miR-34a* overexpression significantly enhanced the lethal effect of DOX on HepG2 cells by down-regulating MDR1/P-gp. To our knowledge, there is no similar study about the role of *miR-205* on P-gp expression in liver cancer cells, until recently. In this regard, we illustrated that *miR-205* is able to hinder the efflux of Rho 123 in HepG2/DOX cell

lines. Furthermore, transfection of *miR-205* in HepG2/DOX cells with the Rho 123 resulted in enhancement of the MFI. In fact, our data showed that transfecting resistant cells with *miR-205* could reverse MDR by increasing *PTEN* expression, inhibiting the P-gp activity and enhancing the intracellular accumulation of DOX, in HepG2/DOX cells. Additionally, verapamil, a known P-gp inhibitor, enhanced the Rho 123 accumulation in HepG2/DOX cells, as a positive control for validation of our results. With this perspective, the results showed that *miR-205* significantly diminished activity of mRNA/protein expression levels of P-gp in HepG2/DOX cell lines. Furthermore, inhibition of P-gp with a specific inhibitor significantly enhanced the growth inhibition rate of the HepG2/DOX cell lines rather than the control group. Hence, *miR-205* re-sensitized HepG2/DOX cells to DOX.

Conclusion

The results of this study revealed that *miR-205* had a key role in improving drug resistance in liver cancer cells via inhibiting drug efflux and enhancing apoptosis via up-regulation of *PTEN* and down-regulation of MDR1/P-gp expression. The data obtained from this study revealed that transfection of *miR-205* in HepG2/DOX cells along with DOX could inhibit MDR, cell proliferation and promoted apoptosis. These are through the regulation in *miR-205*/*PTEN*/PI3K/Akt/MDR1/P-gp pathway and attenuated expression of P-gp. Notwithstanding, these results may provide an axillary step to reach into the potential role of *miR-205* in the progression of therapeutic target for liver cancer treatment during MDR.

Acknowledgments

Authors' Contributions

Z.L., M.L.; Participated in study design and performance of experiments. J.S., X.L.; Contributed extensively in interpretation of the data and conclusion. X.M.; Prepared materials and solutions. P.Z., F.Q., L.Y.; Performed revision and statistical analysis, L.Y; Designed the study. All authors performed editing and approved the final version of this paper for submission.

References

1. Chai Z, Yin X, Chen J, Shi J, Sun J, Liu C, et al. MicroRNA-101 modulates cisplatin chemoresistance in liver cancer cells via the DNA-PKcs signaling pathway. Oncol Lett. 2019; 18(4): 3655-3663.
2. Pan C, Wang X, Shi K, Zheng Y, Li J, Chen Y, et al. MiR-122 reverses the doxorubicin-resistance in hepatocellular carcinoma cells through regulating the tumor metabolism. PLoS One. 2016; 11(5): e0152090.
3. Donato MT, Tolosa L, Gomez-Lechon MJ. Culture and functional characterization of human hepatoma HepG2 cells. Methods Mol Biol. 2015; 1250: 77-93.
4. Harjumäki R, Nugroho RWN, Zhang X, Lou YR, Yliperttula M, Valle-Delgado JJ, et al. Quantified forces between HepG2 hepato-

carcinoma and WA07 pluripotent stem cells with natural biomaterials correlate with in vitro cell behavior. Sci Rep. 2019; 9(1): 7354.

5. Ikeda M, Morizane C, Ueno M, Okusaka T, Ishii H, Furuse J. Chemotherapy for hepatocellular carcinoma: current status and future perspectives. Jpn J Clin Oncol. 2017; 48(2): 103-114.

6. Lage H, Aki-Sener E, Yalcin I. High antineoplastic activity of new heterocyclic compounds in cancer cells with resistance against classical DNA topoisomerase II-targeting drugs. Int J Cancer. 2006; 119(1): 213-220.

7. Nitiss JL. Targeting DNA topoisomerase II in cancer chemotherapy. Nat Rev Cancer. 2009; 9(5): 338-350.

8. Xu F, Wang F, Yang T, Sheng Y, Zhong T, Chen Y. Differential drug resistance acquisition to doxorubicin and paclitaxel in breast cancer cells. Cancer Cell Int. 2014; 14(1): 142.

9. Katayama K, Noguchi K, Sugimoto Y. Regulations of P-glycoprotein/ABCB1/MDR1 in human cancer cells. New J Sci. 2014; 2014.

10. Yousefi B, Samadi N, Baradaran B, Rameshknia V, Shafiei-Irannejad V, Majidinia M, et al. Differential effects of peroxisome proliferator-activated receptor agonists on doxorubicin-resistant human myelogenous leukemia (K562/DOX) cells. Cell Mol Biol (Noisy-le-grand). 2015; 61(8): 118-122.

11. Zhang J, Gu Y, Chen B. Mechanisms of drug resistance in acute myeloid leukemia. Onco Targets Ther. 2019; 12: 1937-1945.

12. Yousefi B, Azimi A, Majidinia M, Shafiei-Irannejad V, Badalzadeh R, Baradaran B, et al. Balaglitazone reverses P-glycoprotein-mediated multidrug resistance via upregulation of PTEN in a PPARγ-dependent manner in leukemia cells. Tumour Biol. 2017; 39(10): 1010428317716501.

13. Nanayakkara AK, Follit CA, Chen G, Williams NS, Vogel PD, Wise JG. Targeted inhibitors of P-glycoprotein increase chemotherapeutic-induced mortality of multidrug resistant tumor cells. Sci Rep. 2018; 8(1): 967.

14. Oki E, Baba H, Tokunaga E, Nakamura T, Ueda N, Futatsugi M, et al. Akt phosphorylation associates with LOH of PTEN and leads to chemoresistance for gastric cancer. Int J Cancer. 2005; 117(3): 376-380.

15. Yousefi B, Samadi N, Ahmadi Y. Akt and p53R2, partners that dictate the progression and invasiveness of cancer. DNA Repair (Amst). 2014; 22: 24-29.

16. Joshi P, Vishwakarma RA, Bharate SB. Natural alkaloids as P-gp inhibitors for multidrug resistance reversal in cancer. Eur J Med Chem. 2017; 138: 273-292.

17. Longley DB, Johnston PG. Molecular mechanisms of drug resistance. J Pathol. 2005; 205(2): 275-292.

18. Wang J, Chan JYW, Fong CC, Tzang CH, Fung KP, Yang M. Transcriptional analysis of doxorubicin-induced cytotoxicity and resistance in human hepatocellular carcinoma cell lines. Liver Int. 2009; 29(9): 1338-1347.

19. Janssen HL, Reesink HW, Lawitz EJ, Zeuzem S, Rodriguez-Torres M, Patel K, et al. Treatment of HCV Infection by Targeting MicroRNA. N Engl J Med. 2013; 368(18): 1685-1694.

20. Hu Y, Qiu Y, Yagüe E, Ji W, Liu J, Zhang J. miRNA-205 targets VEGFA and FGF2 and regulates resistance to chemotherapeutics in breast cancer. Cell Death Dis. 2016; 7(6): e2291.

21. Li J, Hu K, Gong G, Zhu D, Wang Y, Liu H, et al. Upregulation of MiR-205 transcriptionally suppresses SMAD4 and PTEN and contributes to human ovarian cancer progression. Sci Rep. 2017; 7: 41330.

22. Zhao Y, Chen J, Wei W, Qi X, Li C, Ren J. The dual-inhibitory effect of miR-338-5p on the multidrug resistance and cell growth of hepatocellular carcinoma. Signal Transduct Target Ther. 2018; 3: 3.

23. Berindan-Neagoe I, Monroig PdC, Pasculli B, Calin GA. MicroRNAome genome: a treasure for cancer diagnosis and therapy. CA Cancer J Clin. 2014; 64(5): 311-336.

24. Ma C, Shi X, Guo W, Feng F, Wang G. miR-205-5p downregulation decreases gemcitabine sensitivity of breast cancer cells via ERp29 upregulation. Exp Ther Med. 2019; 18(5): 3525-3533.

25. Zhu L, Liu R, Zhang W, Qian S, Wang JH. MicroRNA-205 regulates ubiquitin specific peptidase 7 protein expression in hepatocellular carcinoma cells. Mol Med Rep. 2015; 12(3): 4652-4656.

26. El-Serag HB. Hepatocellular carcinoma. N Engl J Med. 2011; 365(12): 1118-1127.

27. To KKW. MicroRNA: a prognostic biomarker and a possible druggable target for circumventing multidrug resistance in cancer chemotherapy. J Biomed Sci. 2013; 20(1): 99.

28. Nordby Y, Richardsen E, Ness N, Donnem T, Patel HRH, Busund LT, et al. High miR-205 expression in normal epithelium is associated with biochemical failure-an argument for epithelial crosstalk in prostate cancer? Sci Rep. 2017; 7(1): 16308.

29. Cai J, Fang L, Huang Y, Li R, Yuan J, Yang Y, et al. miR-205 targets PTEN and PHLPP2 to augment AKT signaling and drive malignant phenotypes in non-small cell lung cancer. Cancer Res. 2013; 73(17): 5402-5415.

30. Hezova R, Kovarikova A, Srovnal J, Zemanova M, Harustiak T, Ehrmann J, et al. MiR-205 functions as a tumor suppressor in adenocarcinoma and an oncogene in squamous cell carcinoma of esophagus. Tumour Biol. 2016; 37(6): 8007-8018.

31. Shao P, Qu WK, Wang CY, Tian Y, Ye ML, Sun DG, et al. MicroRNA-205-5p regulates the chemotherapeutic resistance of hepatocellular carcinoma cells by targeting PTEN/JNK/ANXA3 pathway. Am J Transl Res. 2017; 9(9): 4300-4307.

32. Bai J, Zhu X, Ma J, Wang W. miR-205 regulates A549 cells proliferation by targeting PTEN. Int J Clin Exp Pathol. 2015; 8(2): 1175-1183.

33. Bhatnagar N, Li X, Padi SKR, Zhang Q, Tang MS, Guo B. Downregulation of miR-205 and miR-31 confers resistance to chemotherapy-induced apoptosis in prostate cancer cells. Cell Death Dis. 2010; 1(12): e105.

34. Chaudhary AK, Mondal G, Kumar V, Kattel K, Mahato RI. Chemosensitization and inhibition of pancreatic cancer stem cell proliferation by overexpression of microRNA-205. Cancer Lett. 2017; 402: 1-8.

35. Qu C, Liang Z, Huang J, Zhao R, Su C, Wang S, et al. MiR-205 determines the radioresistance of human nasopharyngeal carcinoma by directly targeting PTEN. Cell Cycle. 2012; 11(4): 785-796.

36. Chen JR, Jia XH, Wang H, Yi YJ, Wang JY, Li YJ. Timosaponin A-III reverses multi-drug resistance in human chronic myelogenous leukemia K562/ADM cells via downregulation of MDR1 and MRP1 expression by inhibiting PI3K/Akt signaling pathway. Int J Oncol. 2016; 48(5): 2063-2070.

37. Shi X, Xiao L, Mao X, He J, Ding Y, Huang J, et al. miR-205-5p mediated downregulation of PTEN contributes to cisplatin resistance in C13K human ovarian cancer cells. Front Genet. 2018; 9: 555.

38. Sun W, Ma Y, Chen P, Wang D. MicroRNA-10a silencing reverses cisplatin resistance in the A549/cisplatin human lung cancer cell line via the transforming growth factor-beta/Smad2/STAT3/STAT5 pathway. Mol Med Rep. 2015; 11(5): 3854-3859.

39. Haenisch S, Werk AN, Cascorbi I. MicroRNAs and their relevance to ABC transporters. Br J Clin Pharmacol. 2014; 77(4): 587-596.

40. Zheng SZ, Sun P, Wang JP, Liu Y, Gong W, Liu J. MiR-34a overexpression enhances the inhibitory effect of doxorubicin on HepG2 cells. World J Gastroenterol. 2019; 25(22): 2752-2762.

Mouse Degenerating Optic Axons Survived by Human Embryonic Stem Cell-Derived Neural Progenitor Cells

Shiva Nemati, Ph.D.[1], Zahra Seiedrazizadeh, M.Sc.[1], Susan Simorgh, M.Sc.[1], Mahdi Hesaraki, M.Sc.[1], Sahar Kiani, Ph.D.[1],

Mohammad Javan, Ph.D.[1, 2], Farzad Pakdel, M.D.[3], Leila Satarian, Ph.D.[1*]

1. Department of Stem Cells and Developmental Biology, Cell Science Research Center, Royan Institute for Stem Cell Biology and Technology, ACECR, Tehran, Iran
2. Department of Physiology, Faculty of Medical Sciences, Tarbiat Modares University, Tehran, Iran
3. Ophthalmic Research Center, Tehran University of Medical Sciences, Tehran, Iran

*Corresponding Address: P.O.Box: 16635-148, Department of Stem Cells and Developmental Biology, Cell Science Research Center, Royan Institute for Stem Cell Biology and Technology, ACECR, Tehran, Iran
Email: l.satarian@royan-rc.ac.ir

Abstract

Objective: Any damage to the optic nerve can potentially lead to degeneration of non-regenerating axons and ultimately death of retinal ganglion cells (RGCs) that in most cases, are not curable by surgery or medication. Neuroprotective functions of different types of stem cells in the nervous system have been evaluated in many studies investigating the effectiveness of these cells in various retinal disease models. Neural progenitor cells (NPCs) secrete an assortment of trophic factors that are vital to the protection of the visual system. We aimed to assess the therapeutic potentials of NPCs in an ONC mouse model.

Materials and Methods: In this experimental study, NPCs were produced using noggin and retinoic acid from human embryonic stem cells (hESCs). Fifty mice were divided into the following three groups: i. Intact, ii. Vehicle [optic nerve crush+Hank's balanced salt solution (HBSS)], and iii. Treatment (optic nerve crush+NPCs). The visual behavior of the mice was examined using the Visual Cliff test, and in terms of RGC numbers, they were assessed by Brn3a immunostaining and retrograde tracing using DiI injection.

Results: Intravenous injection of 50,000 NPCs through visual cliff did not produce any visual improvement. However, our data suggest that the RGCs protection was more than two-times in NPCs compared to the vehicle group as examined by Brn3a staining and retrograde tracing.

Conclusion: Our study indicated that intravenous injection of NPCs could protect RGCs probably mediated by trophic factors. Due to this ability and good manufacturing practices (GMP) grade production feasibility, NPCs may be used for optic nerve protection.

Keywords: Human Embryonic Stem Cells, Optic Nerve Injury, Visual Cliff

Introduction

Nearly 0.5-5 percent of vehicular accidents lead to optic nerve crush (ONC) injuries; serious damages that could lead to cell degradation and eventual vision loss, due to the limitations in retinal ganglion cells (RGCs) regeneration (1).

Currently available medical interventions involving administration of neuroprotective medications such as corticosteroids to reduce inflammation, or surgery to remove pressure, have yielded little therapeutic success (2). Therefore, a large number of injured individuals-mostly of young ages-suffer from blindness (3). Nevertheless, it is anticipated that stem cells, which have the potential to cure neurological disorders, may help in overcoming this issue (4).

The following therapeutic methods are currently employed for neuropathological conditions: protecting the damaged cells, preventing further degeneration, and replacing the degenerated cells with cell transplants. RGC axons transfer the signals induced by visual stimuli in the eye to the brain's targets. Since RGC axons are very long and possess complex pathways, it does not seem logical to replace the degenerated cells with cell transplants. However, protecting the degenerating RGCs might be a promising approach.

Due to the protective and regenerative properties of stem cells, various types of these cells, including adult, embryonic and induced pluripotent stem cells at different levels of differentiation, have been studied in a variety of retinal disease models (5).

NPCs are located in the adult brain or derivatives from pluripotent stem cells. In the adult brain, they are found in two defined areas named subventricular zone (SVZ), which is around the ventricles of cerebral cortex, and subgranular zone (SGZ), located in the hippocampus. These parts of the brain are in charge of generating new neural cells. An injury or disease leading to neuronal loss and inflammation in the adult CNS will activate the NPCs by increasing their proliferation and migration rates. Studies have demonstrated that NPCs act mostly through

two main regenerative approaches: cell replacement and bystander effects (6).

In general, according to previous observations, conditioned medium properties and low integration of NPCs in retina, have led to the production of only a few regenerated axons from integrated cells. Application of NPCs is currently regarded as a more promising strategy for protecting the degenerating RGCs, due to their ability to secrete valuable neurotrophic factors (6).

Nonetheless, very few studies have examined the beneficial effects of NPC transplantation in the context of RGCs and photoreceptor cell defects in different eye diseases (7). Notably, these studies shared the fact that NPCs could protect the remaining RGCs and photoreceptors. However, functional replacement seems to be rare particularly in the case of RGCs that have long-distance innervating axons compared to the short-distance targeting axons of photoreceptors.

In this study, we aimed to assess the therapeutic potentials of NPCs in an ONC mouse model. We induced differentiation of human embryonic stem cells (hESCs) into NPCs, and subsequently injected them into tail veins of the ONC mice, in which ONC was induced two days prior to the injections. The purpose of this experiment was to determine the effects of NPCs on optic nerve function and probable long-term protection by evaluating RGC survival. Potential improvements of the NPC-conditioned medium led to secretion of some trophic factors including CNTF, bFGF and IGF1 (6). In this study, we hypothesized that intravenous (IV) injection of hESC-NPCs compared to its conditioned medium can improve functional recovery in ONC mice by paracrine effects, more efficiently.

Materials and Methods

Culture of hESC and Neuronal differentiation

In this experimental study, the hESC (Royan H6 line, passage 20) colonies were expanded and passaged according to the report by Mollamohammadi et al. (8). To generate expandable NPCs, hESCs were maintained and differentiated under serum and feeder-free conditions. The hESCs were induced to generate NPCs in two steps (6). The adherent colony culture of hESCs was treated with Noggin (R&D, 1967-NG, 100 ng/ml, USA) for six days (1) and the treatment was followed in the same medium with an increased concentration (250 ng/ml) of Noggin along with retinoic acid (Sigma-Aldrich, R2625, USA) for an additional six days. After appearance of the rosette structures, to reduce the contamination by other cells, they were manually picked up under phase-contrast microscopy and re-plated on poly-l-ornithine (Sigma-Aldrich, P4707, USA)/laminin (Sigma-Aldrich, L2020, USA) at a 1:15 volume/volume concentration. These structures were plated in NPC expansion medium containing DMEM F12, Knock out serum replacement (KSR) 5%, basic fibroblast growth factor (bFGF, Royan Biotech, Iran, 100 ng/ml) and epidermal growth factor (EGF, Sigma-Aldrich, USA, E9644, 20 ng/ml). After one week, the outgrowing colony

like cells were dissociated into single cells by 0.008% trypsin in 2 mM EDTA solution (Invitrogen, USA, 25300) and transferred to poly-l-ornithine (1:6)/laminin (1:1000) coated plates containing fresh NPCs expansion medium. The neural progenitor cells were passaged every 5-7 days at a ratios of 1:2 or 1:3 and remained proliferative with a highly homogenous morphology. For spontaneous differentiation, hNPCs received half the volume medium changes every 4 days in the absence of growth factors for 30 days.

Immunostaining

Immunofluorescence analysis was done according to standard protocols. In brief, we started with sample fixation in 4% paraformaldehyde (PFA, Sigma-Aldrich, USA, P6148) for 20 minutes at room temperature (RT), then, permeabilization using 0.1% Triton X-100 for 10 minutes. The samples were then incubated in blocking solution (10% secondary antibodies host serum) for 1 hour at RT, followed by an overnight incubation with primary antibodies at 4°C. Next, the cells were washed in phosphate buffered saline (BSA) and incubated with secondary antibodies for 45 minutes in an incubator at 37°C temperature. Table S1 (See Supplementary Online Information at www.celljournal.org) lists the primary and secondary antibodies used in this work. As negative control we incubated the cells with secondary antibodies only after the permeabilization step. Nuclei were stained by incubating the samples in 4, 6-diamidino-2-phenylindole (DAPI, Sigma-Aldrich, USA, D9542, 5 μg/ml) or propidium iodide (Abcam, UK, ab14083) in PBS for 3 minutes at RT. The analysis was done under a fluorescent microscope (Olympus, Japan, IX71).

RNA isolation and polymerase chain reaction

Determining hNPCs identity was done by relative gene expression analysis versus undifferentiated hESCs. For this purpose, total mRNA was isolated from NPCs at passage 10, and from undifferentiated hESCs in triplicates by RNase Plus Universal Mini Kit (Qiagen, Germany, 73404). RNA purity and concentration were assessed by a UV/Visible Spectrophotometer (WPA, Biowave II). Then, the first-strand of cDNA was synthesized by 2 μg of total RNA by the Revert Aid First-strand cDNA Synthesis Kit and random hexamer primer (Fermentase, USA, k1632) in 20 μl reaction mixture, according to the manufacturer's instructions. Quantitative real-time RT-PCR was done in 20 μl PCR reaction containing 12.5 ng of synthesized cDNA in 2 μl and 10 μl 2x Power SYBR Green Master Mix (Applied Biosystems, USA) and 1 μl of 5 pmole forward and reverse primers. Reactions were run in a Rotor-Gene 6000 (Corbett Life Science, Australia). All qRT-PCR experiments were performed using three technical and three independent biological replicates. The amount of mRNA was normalized against *GAPDH* mRNA and compared using the ΔΔCt method. Primer sequences are presented in Table S2 (See Supplementary Online Information at www.celljournal.org).

Induction of optic nerve crush in mice

Male mice (C57BL/J6), at around 8-10 weeks of age, were kept on a 12 hours day/night cycle with free access to food and water. All animal trials were done in compliance with institutional guidelines and the ARVO statement for the use of animals in ophthalmic and vision research and Royan Institute ethic committee (IR.ACECR.ROYAN. REC.1397.251). The mice were anesthetized using a 1:4 mixture of xylazine/ketamine intraperitoneally (i.p). ONC was induced using fine forceps (tweezers #5B forceps, World Precision Instruments) according to the protocol in our pervious study (9). In summary, using an operating microscope (Olympus, Japan) left optic nerve (for behavioral test group left and right) was grasped approximately 1 mm from the globe for 5 seconds. Antibiotic ointments mixed of Gentamicin (Daroupakhsh, Iran) and tetracycline (Daroupakhsh, Iran) were administered for post-operative infection control. After ONC, the animals were randomly divided into the vehicle or hESC-NPCs groups.

Cell transplantation

C57BL/J6 mice were divided in defined groups as follows: i. Intact, ii. Vehicle, and iii. NPCs group. Unlike the vehicle and the hESC-NPCs groups, no injuries were made in the intact group (i.e., healthy mice), which comprised of mice of the same age as the ones in the other two groups. For determining the protective effects of intravenous injection of hESC-NPCs on the crushed nerve of the mice, the animals were held and fed under optimal conditions within 60 days from induction of the injury. On days 2, 4, and 6 after causing the injury, 200 µl of HBSS was injected to the tail vein of each mouse of the vehicle group (9) while the mice in the hESC-NPCs group received 50,000 cells in the same manner. We evaluated different doses of 100,000 and 50,000 cells and observed a higher survival rate after IV injection of 50,000 NPCs (data not shown). On day 60 after injury induction, the animals underwent behavioral tests and then, the murine retinas were isolated and subjected to various tests in order to determine the protective effects of the injected cells.

Visual behavioral test

The visual cliff test was used to analyze depth perception and the fear of crossing the deep side of the platform in mice; this method shows the relationship between the eye and the visual cortex. The mice individually underwent the test in a box while being recorded on video for 120 seconds. The videos were then analyzed by two condition-blinded persons. The test was done for at least 8 mice in each group 60 days after the crush. The box was designed according to a previous study (10). To begin the test, the mice first entered the shallow area, and then the time spent to cross the border to the deep area was considered as the latency time. Also, the mean time spent on staying in shallow area was measured and compared among the groups.

Examination of retrograde tracing

Retrograde tracing was used to determine RGC axonal integrity rate after the crush and treatment. In this experiment we had four mice in each group. For this purpose, according to the Paxinos atlas, on a stereotaxic device, a hole was made in each mouse skull over the superior colliculus (SC), and 2 µl of 2% DiI was injected into each SC. After 7 days, the animals were euthanized and their retinas were extracted after perfusion with saline and 4% PFA. The retina was then placed on a microscope slide and photographed under an IX51 Olympus fluorescence microscope.

Comparing neuron survival between groups

After 60 days of optic nerve crush, at least 6 mice from each group were sacrificed and the eyes were fixed in 4% PFA overnight. Then, the cornea and lens were cut out and the retinas were separated to perform immunostaining to detect the transcription factor Brn3a, which is a marker of RGC nuclei in the eye. Twelve images were taken of six retinas from each retina quadrants. The photos were then examined manually and the number of RGCs was compared among the groups.

Statistical analysis

GraphPad Prism (version 8, USA) was used to test the differences in behavioral and whole mount tests. Values plotted in visual test and the whole mount data are presented as mean ± SD. ***P<0.001; One way ANOVA and the Tukey's post hoc tests were used for more confirmation.

Results

Generation and characterization of hESC- NPCs

Generation of NPCs from hESC and related cell morphologies are detailed in Figure 1A. We selected increasing Noggin concentrations during the first 2 weeks of differentiation by adding RA during days 7-12 of the study Around day 12, hESC-NPCs showed typical morphology of defined clusters as columnar cells with rosette structures. The rosette structures were detectable under phase-contrast microscope. Afterward, they were manually picked up and re-plated (considered passage 0) on poly-L-ornithin/laminin-coated plates for expansion. Fortunately, NPCs were passaged every 5-7 days and they had uniform spindle-like morphology (Fig.1A, cell morphology at passage 15).

NPCs were characterized for cellular and molecular key markers at passage 10-15 and were used in the current study. The NPCs expressed neural progenitor markers including NESTIN, PAX6, OTX2, N-Cadherin, SOX1 and SOX 2 at both gene and protein levels (Fig.1B, C), which confirmed their differentiation potency toward various neural cell subtypes. Moreover, upregulation of *OTX2* gene against *OLIG2* and *HOXB2* confirmed our NPC population rostral identity and their potency

to differentiate toward retinal lineage. Finally, our spontaneous differentiation analysis confirmed their neuronal (TUJ1, MAP2 and NF) and glial (GFAP) differentiating potencies (Fig.1D).
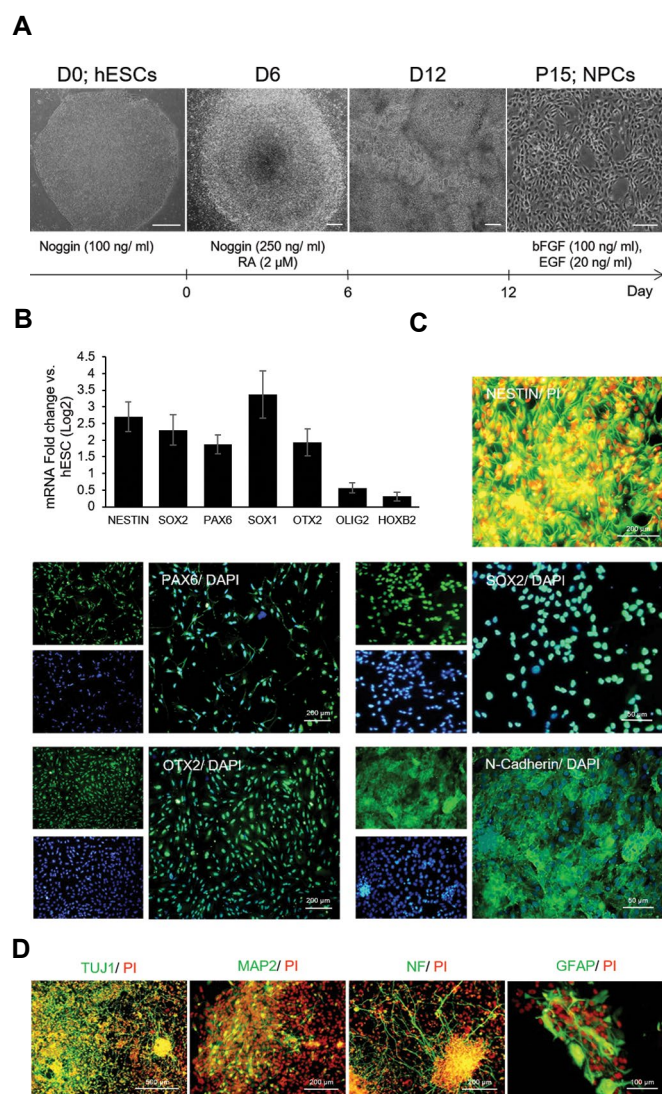
Fig.1: Characterization of hESC-NPCs. **A.** Timeline and phase-contrast images of the differentiation protocol used for generating NPCs from hESCs (scale bar: 200 μm). **B.** NPCs gene expression as assessed by qPCR. **C.** Fluorescent microscopic images of hESC-NPCs at passage 10-15 after immunostaining for NESTIN, N-Cadherin, PAX6, OTX2 and SOX2 as neural progenitor markers. Nuclei were counterstained with DAPI (blue) or PI (red). **D.** Fluorescent microscopic images of NPCs immunostaining after 30 days of spontaneous differentiation for TUJ1, MAP2, and NF as mature neural and GFAP as glial markers. Nuclei were counterstained with PI (red). hESCs; Human embryonic stem cells, NPCs; Neural progenitor cells, qPCR; Quantitative polymerase chain reaction, and PI; Propidium iodide.

NPC intravenous injection does not improve animal visual behavior

Figure 2A shows a schematic timeline of the present work. We injected 50,000 NPCs/200 μl HBSS intravenously via tail vein, 2, 4, and 6 days after the crush.

Mice were evaluated by visual cliff test for optic nerve regeneration. In this test, the time that was spent by the mice to cross the border between the shallow (safe area) and the deep (latency time) ends, was measured during two-minute periods. Considering the animals' fear of heights, latency time for the mice with healthy vision was longer. Our data showed that on day 60 post-injury, the average latency time for intact, vehicle and NPCs groups were 33.0 ± 6.13, 7.8 ± 3.5 and 14.5 ± 4.5 s, respectively (Fig.2B).

Total time in the safe area had the same trend in all groups, but the mice in the intact group stayed for a longer period of time in the shallow area compared to the vehicle and NPCs groups. Visual Cliff data were analyzed by one way ANOVA and showed no significant increase in latency time and time spent in the shallow area in animals that had received NPCs compared to the vehicle group, after two months.
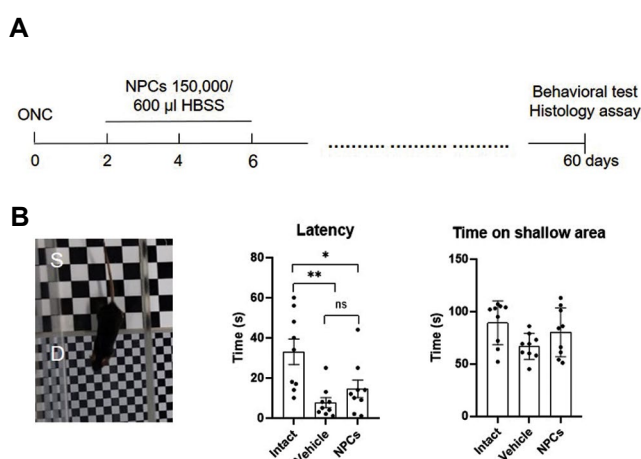
Fig.2: Study timeline and behavioral test. **A.** Schematic timeline of the intravenous injection of cells or HBSS (optic nerve crush time was considered day 0). **B.** Visual behavioral test was done 60 days after induction of the crush. Mouse in the visual cliff box (view from the top) with passing of the border between shallow (S) and deep area (D), Visual behavioral test was done on day 60 with non-significant difference of decision time between NPCs and Vehicle group, n=9 for each group. Values plotted are mean ± SD; unpaired t test. HBSS; Hanks' balanced salt solution and NPCs; Neural progenitor cells.

NPCs improved neuroprotection in the retina

Compared to the vehicle groups, significantly higher RGC nuclei concentrations were found in the NPCs group as shown by immunofluorescent staining. After extracting the whole retinas, the RGCs were detected by labeling the transcription factor Brn3a, which is a marker specifically used to stain RGC nuclei (Fig.3A). Average cell count of the whole retinas on day 60 per each group was as follows: Intact group: 688.68; Vehicle group: 158.66; and NPCs group: 404.74. Data were analyzed by GraphPad Prism using one-way ANOVA and Tukey's multiple comparisons test. Based on data obtained from counting the nuclei stained with Brn3a, the NPCs group showed a significant improvement compared to the vehicle group ($P<0.0001$, Fig.3B).

A

B
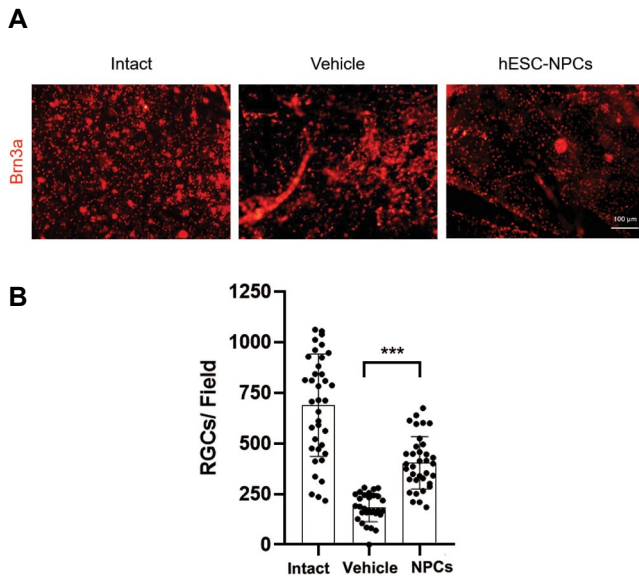
Fig.3: Survival rate in hESC-NPCs group compared to the vehicle and intact on day 60 post crush. **A.** Whole mount retinas stained with Brn3a against RGCs nuclei (scale bar: 100 µm). **B.** Average numbers of viable RGCs counted in 30-38 fields of four retinas from each of the intact, vehicle and NPCs groups. Data are presented as mean ± SD. hESCs; Human embryonic stem cells, NPCs; Neural progenitor cells, RGCs: Retinal ganglion cells, and ***; P<0.001, unpaired t test.

Retrograde tracing showed extensive neuroprotection

Retrograde tracing test was used to inspect the healthy RGC axons that deliver signals from the brain to the retina. For this purpose, DiI was injected in the SC of the mouse brain and was tracked in RGC bodies at 5 to 7 days post-injection. Photographs taken from at least four eyes in each group, were compared qualitatively. The results indicated a significant higher axon survival rate in the NPCs group compared to the vehicle group (Fig.4).
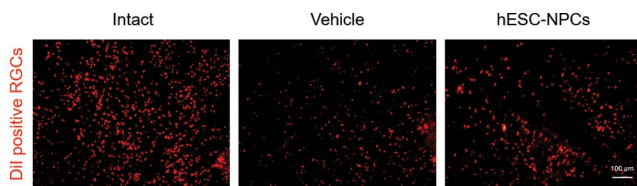
Fig.4: Retrograde tracing in the hESC-NPCs group compared to the vehicle and intact groups on day 60 after Crush. Retrograde tracing using DiI showed more RGC intact axons in the whole mount retinas of the NPCs-treated group compared to the vehicle group, n=4 for each group (scale bar: 100 µm). hESCs; Human embryonic stem cells, NPCs; Neural progenitor cells, and RGCs: Retinal ganglion cells.

Discussion

Optic nerve damage, caused by vehicular accidents or diseases, leads to degeneration RGCs, which have a very limited regeneration rate in mammals. This will ultimately cause permanent impaired vision or even blindness. Anti-inflammatory medicines such as corticosteroids as well as surgical interventions have been proven effective in delaying disease progression and removing the pressure from the nerve, but these solutions have limited outcomes. Thus, researches have been looking for novel approaches like using different stem cells.

Over the recent years, stem cells have created new hope for curing neurodegenerative diseases. Due to their protective and regenerative potentials, various types of stem cells such as the NPCs are being used; NPCs are adult stem cells in the central nervous system that can nowadays be derived from pluripotent stem cells.

Studies have shown that transplanted NPCs are able to migrate to the injury site, and after homing, they can apply this bystander effect through multiple displays including secretion of neurotrophic cytokine (e.g. NGF, VEGF, GDNF, NT-3, BDNF, etc.) that are vital for neural protection and can stimulate endogenous repair potentials of the residing progenitors (11, 12).

However, in the case of the trauma-induced neurodegenerative conditions occurring near a deleterious inflammatory environment, such as spinal cord or optic nerve crush injuries, or conditions that are due to a combination of genetic and environmental factors [e.g. Alzheimer's (13), Huntington's (14), and ischemic brain injury (15)], a simple replacement of the lost cells does not seem to be enough. Indeed, a potentially successful approach to treat such conditions should provide a multidimensional cross-talk between immune cells, neural progenitors and damaged mature neurons. Therefore, NPCs via exerting bystander effects, are still retained as a fascinating choice for cell transplantation in CNS diseases. In addition, it was demonstrated that NPCs can exert immunological properties by expressing various surface molecules, such as TLRs, chemokine receptors, integrins and specific cell adhesion molecules (11). However, the underlying cellular and molecular mechanisms are not completely understood at this time. Nonetheless, the results of clinical and preclinical studies on NPC transplantation in different neurodegenerative diseases (16) indicates that direct integration and replacement of the transplanted cells have insignificant (or even zero) impact on observed functional recovery, thus making the bystander effect hypothesis stronger regarding the NPC transplantation approach.

According to previous studies, after direct intravitreal injection of neurotrophic factors such as Ciliary neurotrophic factor, NT3 and VEGF, prevention of cell degeneration after the injury was observed in damaged RGCs (17). Based on the literature, trophic factors help RGCs to survive, but their use is limited due to high costs and the invasive nature of repeated injections. Secreted neurotrophic factors such as PDGF and BDNF are important for RGC protection (18, 19). NPCs secrete neurotrophic factors that improve the lesion microenvironment, thereby providing an appropriate condition for the repair (20).

Numerous studies have confirmed the positive effects of NPCs on regeneration of peripheral and central

124

nervous tissues (13). Also, NPCs have been proven effective in protecting neurons and the neural tissue in neurodegenerative diseases such as Parkinson's, stroke and spinal cord injury. Although the complete mechanism of this effect remains unknown, it is assumed to be a secondary event, which is dependent on neurotrophic factors such as IGF, NGF, CNTF, BDNF and FGF2 (12).

To date, only a few studies have investigated the potential effects of human pluripotent stem cell-derived NPCs on optic nerve regeneration. Banin et al., by subretinal or intravitreal transplantation of hESC-neural precursors in rat eyes, successfully showed the potential of these cells for retinal differentiation (21). Underlying mechanisms of cell therapy in the retina are still unclear. In addition, considering the complexity of retinal structure, we hypothesized that RGC regeneration is possible in the presence of NPC trophic factors. Therefore, continuous secretion of trophic factors by the NPCs injected systemically was considered for this study. Here, we showed that IV injected hESC-derived NPCs were beneficial for RGC survival without a loss of efficacy. Some studies on neural stem cell transplantation in neurological diseases, similarly suggested the function of neurotrophic factors as an underlying mechanism for neural regeneration (22, 23).

Our study showed that hESCs efficiently differentiated into neural progenitors using the Noggin protein as BMP- antagonist, and retinoic acid (RA) as a morphogen. The hNPCs expressed SOX1 and 2, NESTIN, PAX6, OTX2, and N-cadherin, and showed neural subtype differentiation potencies *in vitro*. Furthermore, NPCs had high expression levels of PAX6 and OTX2 markers of anterior brain and retinal differentiating linage cells (24, 25). According to our previous study, lower passages of NPCs derived from pluripotent stem cells, could express transcription factors that mostly confirmed the forebrain and rostral identity (26).

Since our NPCs had a rostral identity, they seemed to be suitable therapeutic candidates for degenerated RGCs. Moreover, we could claim that due to our NPC line homogeny along with less commitments toward a specific neural cell types, they have the capacity for homing properly, integrating in the injured optic nerve and releasing appropriate neurotrophic factors *in vivo* (27). Subsequently, they could change the inflammatory site toward noninvasive environment (in the site of injury), which will cause sufficient improvement as observed in the current study.

In the present animal study, C57 mice were used to provide an optic nerve damage model and on days 2, 4 and 6 each mouse received 50,000 ESC-derived NPCs over a 6-day period. We selected this cell therapy regimen since trophic factors are gradually secreted by NPCs. For selecting the hESC-NPCs dosage, our pilot study showed that triple IV injections of 50,000 cells is safe and appropriate.

To do this, at least 8 animals were tested in each group and the results, which were indicative of a cognitive behavior (i.e., the animal's fear of height), showed that different crossing times in the NPCs and vehicle groups carried no significant relationship; thus, we concluded that no behavioral improvement was achieved.

We found that NPCs significantly increased the survivability of RGCs compared to the vehicle controls. The significant neuroprotection offered by hESC-NPCs was confirmed by retrograde tracing test. This was performed through the injection of DiI into the SC in the brain. DiI entered RGCs and moved towards the cell body through the axons (28). Our results confirmed higher concentrations of DiI-stained RGCs in the NPCs group compared to the vehicle group.

Conclusion

These findings created new potentials for treating optic nerve damage using ESCs-derived NPCs. Further investigations should be carried out to help find a proper treatment for optic nerve damage. Taken together, human ES-NPCs promoted neuroprotection of RGC in ONC mice. The ease of transplantation without any side effects makes hES-NPCs an acceptable therapy for RGCs degeneration. Clearly, in translating these findings to the clinical applications, factors such as cell dosage and immune-related issues remain to be unraveled.

Acknowledgments

Authors' Contributions

Sh.N.; Data collection, analysis, interpretation, and manuscript writing. Z.S., S.S., M.H.; Collection and/ or assembly of data, data analysis and interpretation, and manuscript writing. S.K., F.P.; Data analysis and interpretation, and manuscript writing. M.J., L.S.; Conducting experiments, conception and design, data analysis and interpretation, administrative and financial support. L.S.; Manuscript proof. All authors read and approved the final manuscript.

References

1. Steinsapir KD, Seiff SR, Goldberg RA. Traumatic optic neuropathy: where do we stand? Ophthalmic Plast Reconstr Surg. 2002; 18(3): 232-234.
2. Zuo KJ, Shi JB, Wen WP, Chen HX, Zhang XM, Xu G. Transnasal endoscopic optic nerve decompression for traumatic optic neuropathy: analysis of 155 cases. Zhonghua Yi Xue Za Zhi. 2009; 89(6): 389-392.
3. Selhorst JB, Chen Y. The optic nerve. Semin Neurol. 2009; 29(1): 29-35.
4. Zwart I, Hill AJ, Al-Allaf F, Shah M, Girdlestone J, Sanusi AB, et al. Umbilical cord blood mesenchymal stromal cells are neuroprotec-

tive and promote regeneration in a rat optic tract model. Exp Neurol. 2009; 216(2): 439-448.

5. Aoki H, Hara A, Niwa M, Motohashi T, Suzuki T, Kunisada T. Transplantation of cells from eye-like structures differentiated from embryonic stem cells in vitro and in vivo regeneration of retinal ganglion-like cells. Graefes Arch Clin Exp Ophthalmol. 2008; 246(2): 255-265.

6. Satarian L, Javan M, Kiani S, Hajikaram M, Mirnajafi-Zadeh J, Baharvand H. Engrafted human induced pluripotent stem cell-derived anterior specified neural progenitors protect the rat crushed optic nerve. PLoS One. 2013; 8(8): e71855.

7. Mead B, Berry M, Logan A, Scott RA, Leadbeater W, Scheven BA. Stem cell treatment of degenerative eye disease. Stem Cell Res. 2015; 14(3): 243-257.

8. Mollamohammadi S, Taei A, Pakzad M, Totonchi M, Seifinejad A, Masoudi N, et al. A simple and efficient cryopreservation method for feeder-free dissociated human induced pluripotent stem cells and human embryonic stem cells. Hum Reprod. 2009; 24(10): 2468-2476.

9. Seyedrazizadeh SZ, Poosti S, Nazari A, Alikhani M, Shekari F, Pakdel F, et al. Extracellular vesicles derived from human ES-MSCs protect retinal ganglion cells and preserve retinal function in a rodent model of optic nerve injury. Stem Cell Res Ther. 2020; 11(1): 203.

10. de Lima S, Koriyama Y, Kurimoto T, Oliveira JT, Yin Y, Li Y, et al. Full-length axon regeneration in the adult mouse optic nerve and partial recovery of simple visual behaviors. Proc Natl Acad Sci USA. 2012; 109(23): 9149-9154.

11. Kokaia Z, Martino G, Schwartz M, Lindvall O. Cross-talk between neural stem cells and immune cells: the key to better brain repair? Nat Neurosci. 2012; 15(8): 1078-1087.

12. Drago D, Cossetti C, Iraci N, Gaude E, Musco G, Bachi A, et al. The stem cell secretome and its role in brain repair. Biochimie. 2013; 95(12): 2271-2285.

13. Blurton-Jones M, Kitazawa M, Martinez-Coria H, Castello NA, Müller FJ, Loring JF, et al. Neural stem cells improve cognition via BDNF in a transgenic model of alzheimer disease. Proc Natl Acad Sci USA. 2009; 106(32): 13594-13599.

14. Kerkis I, Haddad MS, Valverde CW, Glosman S. Neural and mesenchymal stem cells in animal models of huntington's disease: past experiences and future challenges. Stem Cell Res Ther. 2015; 6: 232.

15. Abe K. Therapeutic potential of neurotrophic factors and neural stem cells against ischemic brain injury. J Cereb Blood Flow Metab. 2000; 20(10): 1393-1408.

16. De Feo D, Merlini A, Laterza C, Martino G. Neural stem cell transplantation in central nervous system disorders: from cell replacement to neuroprotection. Curr Opin Neurol. 2012; 25(3): 322-33.

17. Leaver SG, Cui Q, Plant GW, Arulpragasam A, Hisheh S, Verhaagen J, et al. AAV-mediated expression of CNTF promotes long-term survival and regeneration of adult rat retinal ganglion cells. Gene Ther. 2006; 13(18): 1328-1341.

18. Johnson TV, DeKorver NW, Levasseur VA, Osborne A, Tassoni A, Lorber B, et al. Identification of retinal ganglion cell neuroprotection conferred by platelet-derived growth factor through analysis of the mesenchymal stem cell secretome. Brain. 2014; 137(Pt 2): 503-519.

19. Sahu A, Foulsham W, Amouzegar A, Mittal SK, Chauhan SK. The therapeutic application of mesenchymal stem cells at the ocular surface. Ocul Surf. 2019; 17(2): 198-207.

20. Tang Y, Yu P, Cheng L. Current progress in the derivation and therapeutic application of neural stem cells. Cell Death Dis. 2017; 8(10): e3108.

21. Banin E, Obolensky A, Idelson M, Hemo I, Reinhardtz E, Pikarsky E, et al. Retinal incorporation and differentiation of neural precursors derived from human embryonic stem cells. Stem Cells. 2006; 24(2): 246-257.

22. Xu L, Yan J, Chen D, Welsh AM, Hazel T, Johe K, et al. Human neural stem cell grafts ameliorate motor neuron disease in SOD-1 transgenic rats. Transplantation. 2006; 82(7): 865-875.

23. Tan J, Zheng X, Zhang S, Yang Y, Wang X, Yu X, et al. Response of the sensorimotor cortex of cerebral palsy rats receiving transplantation of vascular endothelial growth factor 165-transfected neural stem cells. Neural Regen Res. 2014; 9(19): 1763-1769.

24. Salehi H, Karbalaie K, Salamian A, Kiani A, Razavi S, Nasr-Esfahani MH, et al. Differentiation of human ES cell-derived neural progenitors to neuronal cells with regional specific identity by co-culturing of notochord and somite. Stem Cell Res. 2012; 8(1): 120-133.

25. Shaham O, Menuchin Y, Farhy C, Ashery-Padan R. Pax6: a multi-level regulator of ocular development. Prog Retin Eye Res. 2012; 31(5): 351-376.

26. Mu X, Klein WH. A gene regulatory hierarchy for retinal ganglion cell specification and differentiation. Semin Cell Dev Biol. 2004; 15(1): 115-123.

27. Gamm DM, Wang S, Lu B, Girman S, Holmes T, Bischoff N, et al. Protection of visual functions by human neural progenitors in a rat model of retinal disease. PLoS One. 2007; 2(3): e338.

28. Liang YX, Yang J, Yuan TF, So KF. Uptake of retrograde tracers by intact optic nerve axons: a new way to label retinal ganglion cells. PLoS One. 2015; 10(6): e0128718.

Characterization of The Retinal Progenitor Cells Generated Using Co-Culture Systems

Sara Momenzadeh, M.Sc.[1, 2], Fereshteh Karamali, Ph.D.[2], Atefeh Atefi, M.Sc.[2], Mohammad Hossein Nasr-Esfahani, Ph.D.[2*]

1. Higher Education Jahad University of Isfahan Province, Isfahan, Iran
2. Department of Cellular Biotechnology, Cell Science Research Center, Royan Institute for Biotechnology, ACECR, Isfahan, Iran

*Corresponding Address: P.O.Box: 8159358686, Department of Cellular Biotechnology, Cell Science Research Center, Royan Institute for Biotechnology, ACECR, Isfahan, Iran
Email: mh.nasr-esfahani@royaninstitute.org

Abstract

Objective: Degeneration of the photoreceptors due to retinal disorders can affect vision, and even lead to blindness. Recently therapeutic progress in retinal degeneration, using human embryonic stem cells (hESCs), has been facing technical challenges, demanding the development of simple and standardized protocols. In addition to the designing of the protocols, characterization of the obtained cells is highly required for confirming the reliability of the applied methods for future medical applications. Previously, we showed that human stem cells from apical papilla (SCAP) have stromal cell-derived inducing activity (SDIA).

Materials and Methods: In this experimental study, we developed an efficient retinal differentiation protocol, based on the co-culture of confluent hESCs and SCAP in the absence of exogenous molecules, such as activators or inhibitors of molecular signaling pathways. This experimental procedure resulted in the generation of self-forming neural retina (NR)-like structures containing retinal progenitor cells (RPCs) within 4 weeks.

Results: We have focused on the characterization of the derived RPCs, as a crucial step towards further verification of the efficiency of our previously suggested protocol. The differentiated cells expressed eye-field markers, PAX6, RAX, LHX2, and SIX3, and also generated neurospheres by a floating culture system for one week.

Conclusion: We have reported that the treatment of hESC-derived RPCs by the Notch pathway-inhibitor induced the generation of photoreceptor precursor cells (PPCs). The presented method demonstrates the fact that a co-culture of hESCs and SCAP without exogenous molecules provides an efficient approach to produce RPCs for the treatment of retinal disease, and act as an *in vitro* model for the development of human retina.

Keywords: Co-Culture, Human Embryonic Stem Cell, Photoreceptors, Progenitor Cell

Introduction

Rod and Cone photoreceptors convert electrical signals into electrical messages, initiating the visual transduction cascade, which sends visual information to the brain. Recent advances in cell therapy have opened a window of hope for patients who have visual impairments or blindness. To obtain an expandable source of cells for transplantation, *in vitro* differentiation of human pluripotent stem cells (hPSCs) into retinal cells has been studied (1-4). During eye development, mesenchymal cells play a critical role through the secretion of morphogens and interaction with epithelial cells (5). This reciprocal interaction results in the determination of both cell type fates. The released bioactive factors, some of which are packed as extracellular vesicles, have a different role during eye development. They include the factors triggering signaling pathways affecting cell survival, proliferation, differentiation, anti-apoptotic pathways, and immune modulation (6). This phenomenon, which is called stromal cell-derived inducing activity (SDIA), has been well studied in mesenchymal cells such as PA6 and MS5 (7, 8), as well as dental stem cells (DSCs) (9). Human DSCs, which are originated from cranial neural crest cells, are considered as multipotent cells with rapid proliferation rate and mesenchymal characteristics (10, 11). DSCs are isolated from different regions of the tooth and are named accordingly; such stem cells are stem cells from apical papilla (SCAP) (12), dental pulp stem cells (DPSCs) (13), stem cells from human exfoliated deciduous teeth (SHED) (14), and periodontal ligament stem cells periodontal ligament stem cells (PDLSCs) (15). Secreted proteins from DSCs could affect different biological phenomena (16, 17).

To induce differentiation of hESCs, we selected the co-culture system according to previous *in vivo* studies on cells involved in eye field development (5). In a co-culture system, multiple cell types were cultured directly or indirectly with each other and the cell fates were affected by the secreted factors in each culture. Although, during the direct co-culture system, physical contact is also provided (18).

Our previous study showed that SCAP could induce differentiation of hPSCs to retinal fate via secretion of Wnt pathway inhibitors (9). As an indicator for the accuracy of our previous approach for generating

RPCs, in this experimental research, we have mainly focused on the biological methods which were used in characterization of the differentiated cells. Therefore, the suggested approach in this study may have preclinical and therapeutic applications in the future.

Materials and Methods

Cell culture

In this experimental study, the hESC line RH6 and the SCAPs were maintained as previously described by Baharvand et al. (19) and Karamali et al. (9), respectively. Briefly, RH6 was passaged enzymatically and re-plated on matrigel-coated dishes (1:30, Sigma, St. Lois, MO in DMEM/F12, Gibco Life Technologies, UK) in the presence of 20% knockout serum replacement (KSR, Gibco Life Technologies, UK). SCAPs were kept in DMEM medium (Sigma, St. Lois, MO, USA) supplemented with 10% fetal bovine serum (FBS, Gibco Life Technologies, UK). All experimental cell cultures were done according to the research Ethics standards of the Royan Institute Committee (IR.ACECR.ROYAN.REC.1396.100).

Co-culture of hESCs with SCAP

SCAPs were used as inducing stromal cells to design a co-culture system. At first, SCAPs were inactivated with 10 μM Mitomycin C (Sigma, St. Lois, MO, USA) for 2 hours. then, they were cultured at a density of 5×10^4 /cm^2 in DMEM medium supplemented with 10% FBS. Subsequently, the mechanically isolated RH6, as mentioned above, were cultured on top of the SCAP cell layer at a density of 100 colonies/SCAP (Fig.1). The cells were maintained at 37°C, 5% CO$_2$ and refreshed the medium twice a week.

Culture and maintenance of hESC-derived RPCs

Four weeks after the start of the co-culture, tube-like neural structures were isolated mechanically using glass pipettes, dissociated by accutase (Millipore, Temecula, California, USA), and re-plated on matrigel-coated dishes (Sigma, St. Lois, MO, USA). The cells were allowed to expand in DMEM/F12: neurobasal (Gibco Life Technologies, UK) supplemented with 5% KSR (Sigma, St. Lois, MO, USA), basic fibroblast growth factor (bFGF, 20 ng/ml, Royan Biotech, Iran), epidermal growth factor (EGF, 20 ng/ml, Royan Biotech, Iran), L-ascorbic acid (200 μM, Sigma, St. Lois, MO, USA) and Y27632 (10 μM, Sigma, St. Lois, MO). The RPCs from the first three passages were used for further analysis.

Differentiation of RPCs to PPCs

To assess the potential of RPCs to differentiate into photoreceptors, the attached RPCs were washed with PBS$^-$, dissociated into single cells using accutase and plated on matrigel-coated dishes at a density of around 10^5/cm^2. The photoreceptor differentiation medium containing DMEM/F12: neurobasal supplemented by N2 (2%, Gibco Life

Technologies, UK), B27 (1%, Gibco Life Technologies, UK), and 5% KSR was applied. One day later, notch inhibitor DAPT (Sigma, St. Lois, MO, USA) was added at the final concentration of 10 μM for two additional weeks (20).
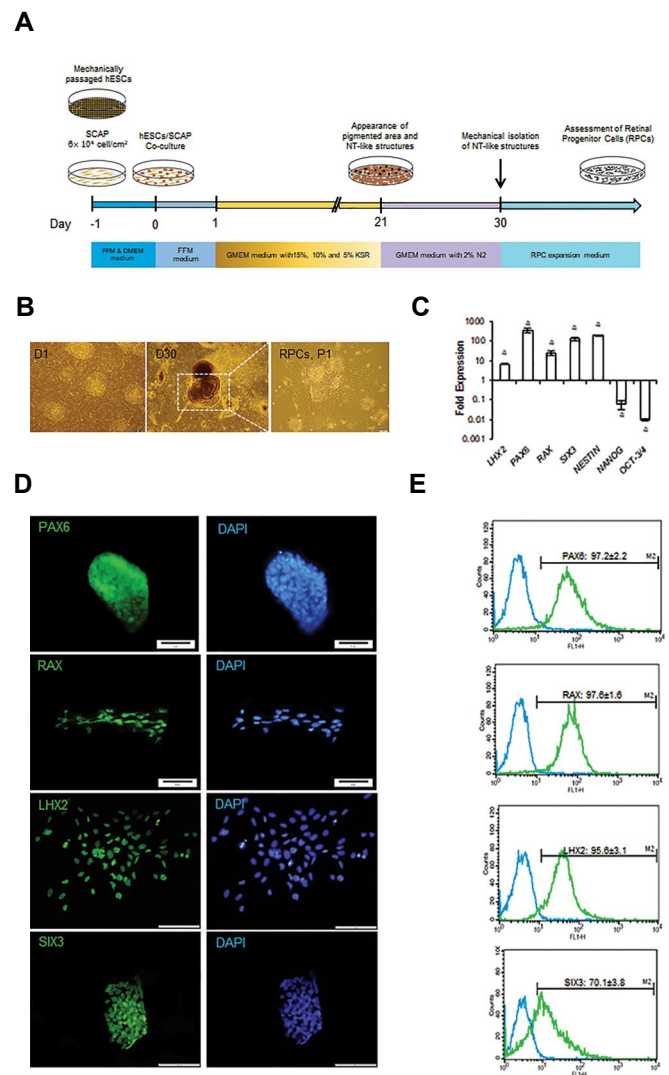
Fig.1: Eye field differentiation of hESCs by SDIA. **A.** Schematic diagram showing stages of the differentiation protocol. **B.** Phase contrast images of differentiated hESCs on SCAP. Left: hESC colonies on SCAP one day after co-culture. Middle: neural-tube like structures on day 21 (white rectangle). Right: isolated and cultured neural tube like structures (passage 1) (scale bars: 100 μm). **C.** RT-qPCR analysis of eye field transcription factors *LHX2, PAX6, RAX, SIX3,* and *NESTIN* as well as pluripotency markers *NANOG* and *OCT4* in RPCs at passage 4 (P4). Data were normalized to hESC at D0, which is present as one-fold and therefore, folds increase or decrease were relative to hESC at D0. Data are presented as mean ± SEM of three independent replicates (one-way ANOVA was used to examine statistical differences, a; P≤0.05. **D.** Immunofluorescence staining of the RPCs at P4 for PAX6, RAX, LHX2, and SIX3 (scale bars: 100 μm). **E.** Flow cytometry analysis of eye field markers LHX2, PAX6, RAX, and SIX3 in RPCs at P4. hESCs; Human embryonic stem cells, SDIA; Stromal cell-derived inducing activity, SCAP; Stem cells from apical papilla, qRT-PCR; Quantitative reverse transcription polymerase chain reaction, and RPCs; Retinal progenitor cells.

Neurosphere generation

To generate neurosphere from hESC-RPC, single

cells were cultured in suspension on 1% agar coated dishes at a density of 10-15 cells/µl using DMEM/F12 containing: neurobasal, N2 (Gibco Life Technologies, UK), B27 (Gibco Life Technologies, UK), bFGF (20 ng/ml), EGF (20 ng/ml) and KSR (5%) was added. One week later, the images of neurospheres provided by inverted microscopy (Olympus, Center Valley, PA, USA) equipped with an Olympus DP70 camera were employed for analyzing their size using the ImageJ software (version 1.6.0, NIH).

Immunofluorescence analysis

For the analysis of the intracellular markers, after fixation of the cells by paraformaldehyde 4%, the cells were permeabilized by 0.4% Triton 100-X for 30 minutes at room temperature. For cytoplasmic markers, 0.2% Triton was used. Next, the fixed and permeabilized cells were incubated with primary antibodies [goat anti-SIX3 (1:300, Santa Cruz Biotechnology, Santa Cruz, CA, USA), rabbit anti-PAX6 (1:300, Santa Cruz Biotechnology, Santa Cruz, CA, USA), rabbit anti- RAX (1:300, Santa Cruz Biotechnology, Santa Cruz, CA, USA), mouse anti-LHX2 (1:300, Santa Cruz Biotechnology, Santa Cruz, CA, USA), CRX (1:300, Santa Cruz Biotechnology, Santa Cruz, CA, USA), rabbit anti-short-wavelength-selective (S)-Opsin (1:50, Abcam, Cambridge, MA, USA), rhodopsin (1:300, Santa Cruz Biotechnology, Santa Cruz, CA, USA), recoverin (1:300, Santa Cruz Biotechnology, Santa Cruz, CA, USA)]. Subsequently, secondary antibodies [goat anti-mouse IgG-FITC (1:50, Sigma, St. Lois, MO) and goat anti-rabbit IgG-FITC (1:50, Sigma, St. Lois, MO) secondary] were used. The expression of specific markers was then evaluated by a fluorescence microscope (Olympus, Center Valley, PA, USA) equipped with an Olympus DP70 camera. Further characterization of the hESC-RPCs was performed via flow cytometry. The single cells were stained with specific markers mentioned earlier and the results were quantified using a FACS Calibur flow cytometer (BD Biosciences, San Diego, CA, USA) and CellQuest software.

Real-time polymerase chain reaction analysis

To extract total RNA, Trizol reagent was used. Reverse transcription was done using the Takara cDNA synthesis kit (TaKaRa, Japan) and quantitative reverse transcription polymerase chain reaction (qRT-PCR) was performed in triplicate. The results were normalized to *GAPDH*, and $\triangle\triangle$Ct method was selected to calculate the relative expression of the experimental genes in comparison to the control groups. The sequences of the primers used are shown in Table 1.

Statistical analysis

All data were collected from three independent experiments and analyzed using GraphPad Prism software (V.7, GraphPad Software, Inc., San Diego, CA) with Student's t test. The data were presented for evaluation as means ± SEM and the statistical significance were achieved when P<0.05.

Table 1: Primers used for gene expression analysis by quantitative reverse transcription polymerase chain reaction

Genes	Primer sequence (5´-3´)	Accession no.
OCT3/4	F: TCTATTTGGGAAGGTATTCAGC	NM_001173531.1
	R: ATTGTTGTCAGCTTCCTCCA	
NANOG	F: CAGCTACAAACAGGTGAAGAC	NM_024865.2
	R: TGGTGGTAGGAAGAGTAAAGG	
NESTIN	F: TTCCCTCCGCATCCCGTCAG	NM_006617.1
	R: GCCGTCACCTCCATTAGC	
LHX2	F: TAGCATCTACTGCAAGGAAGAC	NM_004789.3
	R: GTGATAAACCAAGTCCCGAG	
PAX6	F: TTGCTGGAGGATGATGAC	NM_000280.3
	R: CTATGCTGATTGGTGATGG	
RAX	F: CAACTGGCTACTGTCTGTC	NM_013435.2
	R: CTTATTCCATCTTTCCCACCT	
SIX3	F: TCCTCCTCTTCCTTCTCC	NM_005413.3
	R: GTTGTTGATAGTTTGCGGTT	
CRX	F: AAGCCAGGAAGAGTGACAA	NM_000554.4
	R: GGAAGAGGAGGACAGATAAGG	
S-OPSIN	F: GATGAATCCGACACATGCAG	NM_001708.2
	R: CTGTTGCAAACAGGCCAATA	
RHODOPSIN	F: TCATCATGGTCATCGCTTTC	NM_000539.3
	R: CATGAAGATGGGACCGAAGT	
RECOVERIN	F: TAACGGGACCATCAGCAAG	NM_002903.2
	R: CCTCGGGAGTGATCATTTTG	

Results

Generation of RPCs from hESCs and SCAP in a co-culture system

To achieve neural retinal cells from hESCs, we developed an easy and effective co-culture method. At first, hESCs were cultured according to the timeline proposed in Figures 1A and B (left). Three days after co-culture, boundaries of the colonies started to change morphologically and exhibited rosette-like structures between 2 to 3 weeks, and subsequently, neural tubes were appeared (Fig.1A, B).

Expansion and culture of RPCs

To obtain a homogenous population of RPCs, we cultured

the mechanically-isolated tube-like structures on matrigel-coated dishes, providing a suitable condition for RPCs to attach. Previous reports have shown that the presumptive eye field is defined by a group of transcription factors (eye field transcription factors; EFTFs), including *RAX*, *PAX6*, *SIX3,* and *LHX2* (21). After neural tube cell expansion, the expression of EFTFs was assessed at both RNA and protein levels in the attached RPCs (Fig.1C-E). The RT-qPCR our analysis showed a significant reduction in the expression of stemness factors including OCT4 and NANOG and a significant increase in RPC-specific factors (Fig.1C) compared to undifferentiated cells. Immunostaining assessment of eye field markers in hESC-RPC revealed the expression of RPC markers (Fig.1D). Quantitative flow cytometric analysis confirmed that the cells expressed PAX6 (97.2 ± 2.2%), RAX (97.6 ± 1.6%), LHX2 (95.6 ± 3.1%) and SIX3 (70.1 ± 3.8%) (Fig.1E). These data have demonstrated that a large fraction of hESC-derived RPCs were kept in the progenitor state at least for three passages in retinal culture medium. But after the third passage, the morphology of the cells began to change, thus we did not assess these cells after the third passage.

Generation of PPCs

The RPCs were dissociated into single cells, and subsequently, they were cultured on matrigel-coated dishes in the presence of Notch inhibitor DAPT. Three days later, some cells displayed neurite processes. While, these morphological changes did not observe in DMSO group (Fig.2A). CRX, as a cone and rod homeobox gene, has been considered to direct cells for differentiation towards photoreceptors via accelerating chromatin remodeling (22). Therefore, increased expression of CRX as it is shown in Figure 2B and C, committed the RPCs to differentiate into PPCs. Two weeks later, evaluation of differentiation markers showed that DAPT-treated cells expressed S-OPSIN (a mature cone marker) and RHODOPSIN (a rod marker) (Fig.2C). Additionally, we analyzed the expression levels of the genes associated with photoreceptor maturation by qRT-PCR. These results showed a significant increase in the levels of *CRX* (the first PPC marker), *S-OPSIN*, *RHODOPSIN*, and *RECOVERIN* one week after DAPT treatment (Fig.2B).

Generation of neurospheres

Figure 3A illustrates schematic of RPC culture to form neurospheres and its preparation for further analysis. As depicted in Figures 3B and C, RPCs were able to produce neurospheres and increase in size in a time dependent manner during one week. We further showed that these neurospheres express Nestin as a common neural progenitor marker and PCNA as a proliferating cell marker, which confirmed the identity of neurospheres induced by RPCs (Fig.3D).
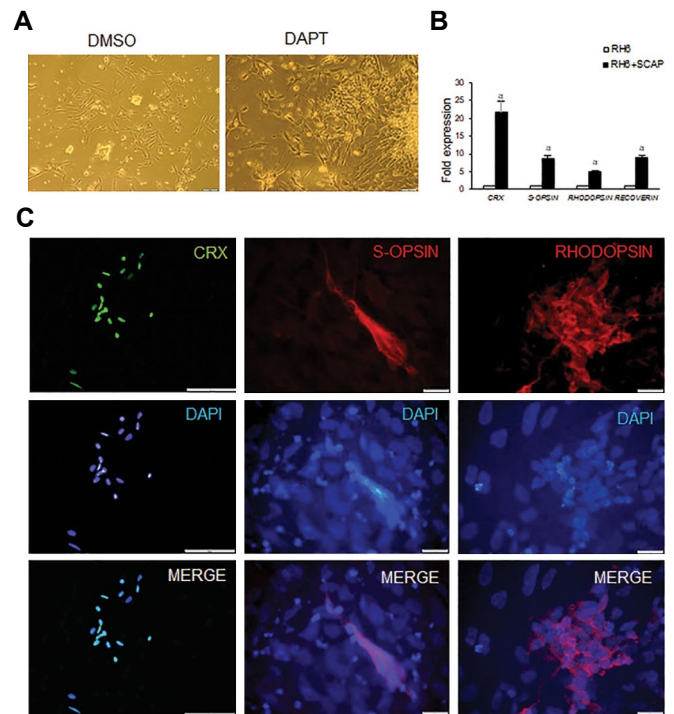
Fig.2: *In vitro* acceleration of mature photoreceptor-like cells generation from human ESC-derived RPCs by Notch inhibition. **A.** Morphological changes of RPCs after treatment of the cells with DAPT and DMSO as the solvent. **B.** qRT-PCR analysis of *CRX, S-OPSIN, RHODOPSIN* and, *RECOVERIN* markers in RPCs at P4. After calculating the relative expression to *GAPDH*, the data were normalized to cells treated with DMSO at D42 which considered as one-fold change. **C.** Immunofluorescence staining of RPCs at P4 for CRX, S-OPSIN, RHODOPSIN (scale bars: 100 μm). ESC; Embryonic stem cell, RPCs; Retinal progenitor cells, DAPT; (N-[(3,5-difluorophenyl)acetyl]-L-alanyl-2-phenyl]glycine-1,1-dimethylethyl), DMSO; Dimethyl sulfoxide, and qRT-PCR; Quantitative reverse transcription polymerase chain reaction.
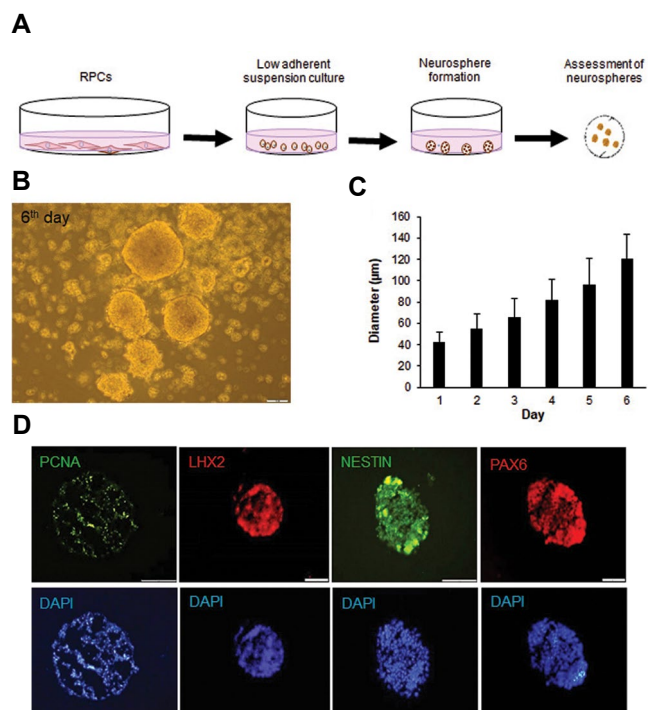
Fig.3: *In vitro* generation of neurospheres from human ESC derived RPCs. **A.** Schematic diagram showing stages of the neurosphere generation protocol. **B.** Sphere formation of RPCs after six days and **C.** Diameter changes over days one to six. **D.** Immunofluorescence analysis of cryo-sectioned RPCs at passage 4 (P4) for LHX2, PAX6, NESTIN, and PCNA (scale bars: 100 μm). ESC; Embryonic stem cell and RPCs; Retinal progenitor cells.

Discussion

In this study, we generated RPCs from hESCs via a co-culture system that induces both differentiation of hESCs into PPCs and formation of neurospheres. Therefore, inconsistent with previous studies (9, 16), it is speculated that SCAP secret various factors that participate in the induction of differentiation of hESCs toward RPCs. These RPCs from our co-culture systems were characterized and the identity of the cells was confirmed using PAX6, RAX, LHX2 and SIX 3 expression at both the RNA and the protein levels. Besides, according to our knowledge, for the first time we have shown that these RPCs, like other neural precursor cells, can produce neurospheres. The proliferative capacity of the cells into neurospheres was proven by the expression of PCNA as a proliferative marker, as well as the increase in the sizes of the neurospheres over time. The differentiated cells also expressed Nestin as a neural progenitor marker in addition to the retinal neural progenitor markers PAX6 and RAX. To our knowledge, there is no report on the derivation of RPC neurospheres from hESCs. It is important to note that the only report on the human retinal neurospheres is by Gamm et al., who obtained neurospheres from prenatal retinal tissue (23).

In order to efficiently differentiate hESCs into RPCS, researchers have introduced different recombinant proteins and/or small molecules to inhibit Wnt and BMP signaling pathways (24-26). In this study, we achieved the same goal by eliminating extrinsic factors. These founding might highlight future clinical applications of the introduced procedure. In this regard, Reichman et al. (27) stated that introducing a simple retinal differentiation method without the formation of embryoid bodies and/or exogenous molecules is widely applicable to future research.

Our results showed a high percentage of cells expressing eye field markers following a decrease in the expression of stem cell markers *OCT4* and *NANOG*. The efficiency of our findings is likely modulated in part by the presence of IGF and DKK (Wnt inhibitors) and Noggin (BMP inhibitor) expressed by SCAP or DPSCs (9, 28), which are commonly added as exogenous factors in most studies of anterior neural differentiation (4, 9, 24-26).

After mechanical isolation of the neural tube like structures, over 90% of the cells expressed specific markers of RPCs including PAX6, RAX, and LHX2, thereby indicating that these isolated neural tubes, in addition to the anterior neural identity, revealed neural retinal specification.

As previous studies have demonstrated, RPCs are committed to form a photoreceptor lineage that due to the increased expression levels of CRX, the cone and rod homeobox transcription factor (20). Nelson et al. (29) were the first researchers who demonstrated that exposure to the secretase inhibitor, DAPT, at an early RPC culture stage, induces differentiation into various retinal cell types. DAPT treatment also increases the number of CRX photoreceptor precursor and ganglion cells. One of the important safety concerns regarding the transplantation of hESC derivatives is their tumorigenicity. In this regard, the use of a notch inhibitor during differentiation of RPCs to PPCs induces RPCs to exit from the cell cycle and thus reduces their ability to form tumors. The hESC-derived RPCs induced by DAPT showed extended cytoplasmic neurite-like processes (30). However, this treatment was sufficient to enhance the expression of the photoreceptor precursor markers such as S-opsin, CRX, recoverin and rhodopsin (31). The RPCs derived in this study are appropriate candidates for disease modeling and photoreceptor cell replacement therapy (5, 27, 32-37).

Conclusion

The simple and efficient protocol described in this study is highly suitable for the production of a high-percentage hESC-derived RPC culture as a potential source for cell replacement studies in preclinical animal models.

Authors' Contributions

S.M., F.K., M.H.N.-E.; Contributed to conception and design. S.M., F.K.; Contributed to all experimental work, data and statistical analysis, and interpretation of data. M.H.N.-E.; Was responsible for overall supervision. S.M.; Drafted the manuscript, which was revised by F.K., and M.H.N.-E. All authors read and approved the final manuscript.

References

1. Barber AC, Hippert C, Duran Y, West EL, Bainbridge JW, Warre-Cornish K, et al. Repair of the degenerate retina by photoreceptor transplantation. Proc Natl Acad Sci USA. 2013; 110(1): 354-359.
2. Luo J, Baranov P, Patel S, Ouyang H, Quach J, Wu F, et al. Human retinal progenitor cell transplantation preserves vision. J Biol Chem. 2014; 289(10): 6362-6371.
3. Pearson RA, Barber AC, Rizzi M, Hippert C, Xue T, West EL, et al. Restoration of vision after transplantation of photoreceptors. Nature. 2012; 485(7396): 99-103.
4. Lamba DA, Gust J, Reh TA. Transplantation of human embryonic stem cell-derived photoreceptors restores some visual function in Crx-deficient mice. Cell Stem Cell. 2009; 4(1): 73-79.
5. Cvekl A, Tamm ER. Anterior eye development and ocular mesenchyme: new insights from mouse models and human diseases. Bioessays. 2004; 26(4): 374-386.
6. Pittenger MF, Discher DE, Péault BM, Phinney DG, Hare JM, Caplan AI. Mesenchymal stem cell perspective: cell biology to clinical progress. NPJ Regen Med. 2019; 4: 22.
7. Kawasaki H, Mizuseki K, Nishikawa S, Kaneko S, Kuwana Y, Nakanishi S, et al. Induction of midbrain dopaminergic neurons from ES cells by stromal cell-derived inducing activity. Neuron. 2000; 28(1): 31-40.
8. Schwartz CM, Spivak CE, Baker SC, McDaniel TK, Loring JF, Nguyen C, et al. NTera2: a model system to study dopaminergic

differentiation of human embryonic stem cells. Stem Cells Dev. 2005; 14(5): 517-534.

9. Karamali F, Esfahani MN, Taleahmad S, Satarian L, Baharvand H. Stem cells from apical papilla promote differentiation of human pluripotent stem cells towards retinal cells. Differentiation. 2018; 101: 8-15.

10. Thesleff I, Nieminen P. Tooth morphogenesis and cell differentiation. Curr Opin Cell Biol. 1996; 8(6): 844-850.

11. Tucker A, Sharpe P. The cutting-edge of mammalian development; how the embryo makes teeth. Nat Rev Genet. 2004; 5(7): 499-508.

12. Sonoyama W, Liu Y, Yamaza T, Tuan RS, Wang S, Shi S, et al. Characterization of the apical papilla and its residing stem cells from human immature permanent teeth: a pilot study. J Endod. 2008; 34(2): 166-171.

13. Gronthos S, Mankani M, Brahim J, Robey PG, Shi S. Postnatal human dental pulp stem cells (DPSCs) in vitro and in vivo. Proc Natl Acad Sci USA. 2000; 97(25): 13625-13630.

14. Miura M, Gronthos S, Zhao M, Lu B, Fisher LW, Robey PG, et al. SHED: stem cells from human exfoliated deciduous teeth. Proc Natl Acad Sci USA. 2003; 100(10): 5807-5812.

15. Gay IC, Chen S, MacDougall M. Isolation and characterization of multipotent human periodontal ligament stem cells. Orthod Craniofac Res. 2007; 10(3): 149-160.

16. Tachida Y, Sakurai H, Okutsu J, Suda K, Sugita R, Yaginuma Y, et al. Proteomic comparison of the secreted factors of mesenchymal stem cells from bone marrow, adipose tissue and dental pulp. J Proteomics Bioinform. 2015; 8: 266-273.

17. Yu S, Zhao Y, Ma Y, Ge L. Profiling the secretome of human stem cells from dental apical papilla. Stem Cells Dev. 2016; 25(6): 499-508.

18. Yue F, Shirasawa S, Ichikawa H, Yoshie S, Mogi A, Masuda S, et al. Induce differentiation of embryonic stem cells by co-culture system. In: Andrades JA, editor. Regenerative medicine and tissue engineering. IntechOpen; 2013. Available from: https://www.intechopen.com/chapters/44655 (12 Feb 2022).

19. Baharvand H, Ashtiani SK, Taee A, Massumi M, Valojerdi MR, Yazdi PE, et al. Generation of new human embryonic stem cell lines with diploid and triploid karyotypes. Dev Growth Differ. 2006; 48(2): 117-128.

20. Eiraku M, Takata N, Ishibashi H, Kawada M, Sakakura E, Okuda S, et al. Self-organizing optic-cup morphogenesis in three-dimensional culture. Nature. 2011; 472(7341): 51-56.

21. Zuber ME, Gestri G, Viczian AS, Barsacchi G, Harris WA. Specification of the vertebrate eye by a network of eye field transcription factors. Development. 2003; 130(21): 5155-5167.

22. Ruzycki PA, Zhang X, Chen S. CRX directs photoreceptor differentiation by accelerating chromatin remodeling at specific target sites. Epigenetics Chromatin. 2018; 11(1): 42.

23. Gamm DM, Wright LS, Capowski EE, Shearer RL, Meyer JS, Kim HJ, et al. Regulation of prenatal human retinal neurosphere growth and cell fate potential by retinal pigment epithelium and Mash1. Stem Cells. 2008; 26(12): 3182-3193.

24. Ikeda H, Osakada F, Watanabe K, Mizuseki K, Haraguchi T, Miyoshi H, et al. Generation of Rx+/Pax6+ neural retinal precursors from embryonic stem cells. Proc Natl Acad Sci USA. 2005; 102(32): 11331-11336.

25. Nakano T, Ando S, Takata N, Kawada M, Muguruma K, Sekiguchi K, et al. Self-formation of optic cups and storable stratified neural retina from human ESCs. Cell Stem Cell. 2012; 10(6): 771-785.

26. Osakada F, Jin ZB, Hirami Y, Ikeda H, Danjyo T, Watanabe K, et al. In vitro differentiation of retinal cells from human pluripotent stem cells by small-molecule induction. J Cell Sci. 2009; 122(Pt 17): 3169-3179.

27. Reichman S, Terray A, Slembrouck A, Nanteau C, Orieux G, Habeler W, et al. From confluent human iPS cells to self-forming neural retina and retinal pigmented epithelium. Proc Natl Acad Sci USA. 2014; 111(23): 8518-8523.

28. Liu G, Ma S, Zhou Y, Lu Y, Jin L, Wang Z, et al. Signaling pathways in dental stem cells during their maintenance and differentiation. In: Şahin F, Doğan A, Demirci S, editors. Dental stem cells. Stem cell biology and regenerative medicine. Springer; 2016; 69-92.

29. Nelson BR, Gumuscu B, Hartman BH, Reh TA. Notch activity is downregulated just prior to retinal ganglion cell differentiation. Dev Neurosci. 2006; 28(1-2): 128-141.

30. Crawford TQ, Roelink H. The notch response inhibitor DAPT enhances neuronal differentiation in embryonic stem cell-derived embryoid bodies independently of sonic hedgehog signaling. Dev Dyn. 2007; 236(3): 886-892.

31. Völkner M, Zschätzsch M, Rostovskaya M, Overall RW, Busskamp V, Anastassiadis K, et al. Retinal organoids from pluripotent stem cells efficiently recapitulate retinogenesis. Stem Cell Reports. 2016; 6(4): 525-538.

32. Decembrini S, Koch U, Radtke F, Moulin A, Arsenijevic Y. Derivation of traceable and transplantable photoreceptors from mouse embryonic stem cells. Stem Cell Reports. 2014; 2(6): 853-865.

33. Eiraku M, Sasai Y. Mouse embryonic stem cell culture for generation of three-dimensional retinal and cortical tissues. Nat Protoc. 2012; 7(1): 69-79.

34. La Torre A, Lamba DA, Jayabalu A, Reh TA. Production and transplantation of retinal cells from human and mouse embryonic stem cells. Methods Mol Biol. 2012; 884: 229-246.

35. Lamba DA, McUsic A, Hirata RK, Wang PR, Russell D, Reh TA. Generation, purification and transplantation of photoreceptors derived from human induced pluripotent stem cells. PLoS One. 2010; 5(1): e8763.

36. Mellough CB, Sernagor E, Moreno-Gimeno I, Steel DH, Lako M. Efficient stage-specific differentiation of human pluripotent stem cells toward retinal photoreceptor cells. Stem Cells. 2012; 30(4): 673-686.

37. Zhou L, Wang W, Liu Y, Fernandez de Castro J, Ezashi T, Telugu BP, et al. Differentiation of induced pluripotent stem cells of swine into rod photoreceptors and their integration into the retina. Stem Cells. 2011; 29(6): 972-980.

Original Article

Generation of An Induced Pluripotent Stem Cell Line from Human Liver Fibroblasts from A Patient with Combined Hepatocellular-Cholangiocarcinoma

Hyo-Suk Ahn, Ph.D.[1#], Jae-Sung Ryu, Ph.D.[1#], Jaeseo Lee, Ph.D.[1#], Seon Ju Mun, B.Sc.[1, 2], Yeon-Hwa Hong, B.Sc.[1, 2],

Yongbo Shin, M.Sc.[1, 2], Kyung-Sook Chung, Ph.D.[2, 3*], Myung Jin Son, Ph.D.[1, 2*]

1. Stem Cell Convergence Research Center, Korea Research Institute of Bioscience and Biotechnology (KRIBB), 125 Gwahak-ro, Yuseong-gu, Daejeon, Republic of Korea
2. Department of Functional Genomics, Korea University of Science and Technology (UST), 217 Gajungro, Yuseong-gu, Daejeon, Republic of Korea
3. Biomedical Translational Research Center, KRIBB, 125 Gwahak-ro, Yuseong-gu, Daejeon, Republic of Korea

#These authors contributed equally to this work.

*Corresponding Addresses: Department of Functional Genomics, Korea University of Science and Technology (UST), 217 Gajungro, Yuseong-gu, Daejeon, Republic of Korea
Stem Cell Convergence Research Center, Korea Research Institute of Bioscience and Biotechnology (KRIBB), 125 Gwahak-ro, Yuseong-gu, Daejeon, Republic of Korea
Emails: kschung@kribb.re.kr, mjson@kribb.re.kr

Abstract

Objective: Combined hepatocellular-cholangiocarcinoma (cHCC-CC) is a rare type of primary liver cancer with characteristics of both hepatocellular carcinoma (HCC) and cholangiocarcinoma (CC). The pathogenesis of cHCC-CC is poorly understood due to a shortage of suitable *in vitro* models. Due to scarce availability of human liver tissue, induced pluripotent stem cells (iPSCs) are a useful alternative source to produce renewable liver cells. For use in the development of liver pathology models, here we successfully developed and evaluated iPSCs from liver fibroblasts of a patient with cHCC-CC.

Materials and Methods: In this experimental study, human liver fibroblasts (HLFs) were obtained from the liver biopsy of a 69-year-old male patient with cHCC-CC and transduced with a retroviral cocktail that included four factors - OCT4, SOX2, KLF4, and c-MYC (OSKM). Pluripotency of the iPSCs was determined by alkaline phosphatase (AP) staining, quantitative real-time polymerase chain reaction (PCR), and immunofluorescence. We induced *in vitro* embryoid body (EB) formation and performed an *in vivo* teratoma assay to confirm their differentiation capacity into the three germ layers.

Results: HLF iPSCs derived from the cHCC-CC patient displayed typical iPSC-like morphology and pluripotency marker expression. The proficiency of the iPSCs to differentiate into three germ layers was assessed both *in vitro* and *in vivo*. Compared to normal control iPSCs, differentiated HLF iPSCs showed increased expressions of HCC markers alpha-fetoprotein *(AFP)* and Dickkopf-1 *(DKK1)* and the CC marker cytokeratin 7 *(CK7)*, and a decreased expression of the CC tumour suppressor SRY-related HMG-box 17 *(SOX17)*.

Conclusion: We established HLF iPSCs using liver fibroblasts from a patient with cHCC-CC for the first time. The HLF iPSCs maintained marker expression in the patient when differentiated into EBs. Therefore, HLF iPSCs may be a sustainable cell source for modelling cHCC-CC and beneficial for understanding liver cancer pathology and developing therapies for cHCC-CC treatment.

Keywords: Cholangiocarcinoma, Hepatocellular Carcinoma, Induced Pluripotent Stem Cells

Introduction

Combined hepatocellular-cholangiocarcinoma (cHCC-CC) is an uncommon primary liver malignancy with characteristics of both hepatocellular carcinoma (HCC) and cholangiocarcinoma (CC). This mixed carcinoma exhibits a more aggressive behaviour and poorer prognosis than HCC or CC (1, 2). However, the pathogenesis of cHCC-CC is poorly understood, partly due to insufficient information and a shortage of proper *in vitro* models (2). With the scarce availability of human liver tissue, induced pluripotent stem cells (iPSCs) may be a valuable source for various models for rare types of liver cancer as they are capable of unlimited self-renewal and can maintain patient specificity (3). HCC is one of the most frequently

occurring primary liver cancers worldwide. Despite improvements in prevention, diagnostic techniques, and treatment, the incidence and mortality rate are still increasing (4, 5). CC, in which biliary malignancy arises from the bile duct, is the second most frequent primary liver cancer. Based on anatomical location, CC is classified into three subtypes: intrahepatic, perihilar, or distal (6, 7). Long-term survival of CC is low, ranging from 20–40% for patients after curative resection (8).

The diagnosis of liver cancer is usually achieved using biomarkers, which can also help in prognosis prediction. CK19 and PRDM5 are specifically increased in the case of cHCC-CC. HCC-related markers such

as alpha-fetoprotein (AFP), GPC3, and APOE are also highly expressed in cHCC-CC (9). AFP is a major serum glycoprotein produced by the foetal liver during liver development and its expression is elevated in the majority of patients with HCC. It is an important diagnostic marker for HCC (10-12). The glycoprotein Dickkopf-1 (DKK1) is known to promote tumour cell proliferation, migration, and invasion via the Wnt/β-catenin signalling pathway dependent (13) and independent (14) mechanisms. Recently, several studies have indicated that elevated expression of DKK1 is closely associated with HCC progression (13, 15, 16). Additionally, cytokeratin 7 (CK7), an intermediated filament protein expressed by epithelial cells, is another prognostic marker that is upregulated in patients with intrahepatic CC (17, 18). During embryonic development, SRY-related HMG-box 17 (SOX17) is considered essential for the formation of gallbladder and bile duct epithelium and its downregulation promotes CC as a tumour suppressor (19). Hypermethylation of the SOX17 promoter has been reported in patients with CC (20).

Reprogramming technology allows the establishment of patient-specific iPSC lines with self-renewal capacity and the ability to differentiate into various somatic cell types (21, 22). Patient-specific induced pluripotent stem cells (iPSCs) may be an effective source for therapeutic development platforms as they retain specific genetic backgrounds and characteristics associated with a particular disease pathology. Several studies have reported the generation of iPSC lines from patient-specific cell sources such as fibroblasts (23), blood samples (24, 25), and urine samples (26, 27).

Importantly, in rare and unique cases such as cHCC-CC, patient-derived iPSCs can be used as a model for understanding the mechanism of disease pathogenesis and for developing individual therapeutic strategies by simulating complex signalling pathways within disease-specific environments (23, 28, 29). Therefore, we hypothesized that iPSCs derived from a patient with cHCC-CC may contain unique biological characteristics of the disease and investigated the expression of several biomarkers associated with disease pathology. To our knowledge, this is the first study to use iPSCs generated using liver fibroblasts from a patient with cHCC-CC.

Materials and Methods

Cell culture

Human skin fibroblasts (HSFs, CRL-2097) were purchased from the American Type Culture Collection (ATCC) for use as non-malignant control cells. In this experimental study, human liver fibroblasts (HLFs) were isolated from the liver specimen of a 69-year-old male patient with cHCC-CC. All experiments were approved by the Institutional Review Board (IRB) at Chungnam National University Hospital (IRB file no. CNUH 2016-03-018) and at Public Institutional Bioethics Committee designated by the South Korea Ministry of Health and

Welfare (IRB file no. P01-201703-31-010). The patient provided informed consent. The human liver tissues were washed with cold phosphate-buffered saline (PBS, Thermo Fisher, USA), as previously described (30), and minced in a solution that contained 300 units/ml collagenase type IV (Thermo Fisher, USA). The minced tissue was incubated at 37˚C for 30 minutes until they were digested, then filtered through a 70 μm strainer (SPL Life Science, Korea) and washed with a cold solution of 10% foetal bovine serum (FBS, Thermo Fisher, USA) in PBS. The cells were resuspended in minimal essential medium (MEM, Thermo Fisher, USA) containing 10% FBS and 1% penicillin streptomycin (PS, Thermo Fisher, USA).

Generation of induced pluripotent stem cells

iPSCs were generated using previously described protocols (3, 31). Briefly, HSFs and HLFs (1×10^5 cells/well) were plated in 6-well plates and the cells were transduced with OSKM-retrovirus at a multiplicity of infection of 3 on day 2. Before transduction, the cells were pre-incubated with 8 μg/mL of polybrene (Sigma-Aldrich, USA) for one hour. The medium was replaced with fresh fibroblast culture medium every other day, and then the cells were reseeded onto a γ-irradiated mouse embryonic fibroblast (MEFs) feeder layer in a 6-well plate with a cell density of $1\sim2\times10^5$ cells/well on day 7. The next day, the medium was replaced with iPSC medium (DMEM/F12 (Thermo Fisher, USA), 1X GlutaMAX (Thermo Fisher, USA), 1X MEM-nonessential amino acids (Thermo Fisher, USA), 100 μM β-mercaptoethanol (Thermo Fisher, USA), and 1% PS (Thermo Fisher, USA), 20% knockout serum replacement (Thermo Fisher, USA), and 10 ng/ml basic fibroblast growth factor (bFGF, Peprotech, USA), and then replaced daily. When human embryonic stem cell (hESC)-like iPSC colonies were established, the cells were mechanically picked and expanded on γ-MEF feeder layers.

Mycoplasma testing

Mycoplasma contamination of iPSCs was checked via polymerase chain reaction (PCR) using an EZ-PCR Mycoplasma Test Kit (Biological Industries, Israel). Briefly, 1 ml of used iPSC culture supernatant was collected after 24 hours of culture and centrifuged to acquire a pellet. PCR amplification was performed using a primer set provided in the kit.

Alkaline phosphatase staining

Alkaline phosphatase (AP) activity was determined using a commercially available kit (Sigma-Aldrich, USA). Briefly, the iPSCs were treated with a fixation solution for 30 seconds and then incubated with the AP staining solution in the dark for 15 minutes. Images of AP+ iPSC colonies were obtained using an Olympus microscope.

Short tandem repeat and karyotype analyses

Genomic DNA was isolated from HLFs and the

corresponding HLF iPSCs. Short tandem repeat (STR) analysis was performed by HumanPass, Inc. (Korea). A chromosomal GTG banding karyotype analysis was performed at 550 resolution by GenDix, Inc. (Korea).

Immunofluorescence analysis

For immunostaining, the cells were seeded onto a 4-well plate (Thermo Fisher, USA) or Lab-Tek dish (Ibidi, Germany). Samples were washed with PBS and fixed with 4% paraformaldehyde in PBS for 15 minutes at room temperature (RT). The cells were then permeabilised in 0.25% Triton X-100 (Sigma-Aldrich, USA) in PBS for 15 minutes and incubated in blocking buffer (4% bovine serum albumin/PBS) for one hour at RT. The respective primary antibodies and corresponding Alexa Fluor® conjugated secondary antibodies were incubated with in blocking buffer overnight at 4°C and for 40 minutes at RT. The samples were washed three times with washing solution (0.05% Tween-20 [Sigma-Aldrich, USA] in PBS) between each incubation step. Staining of the nuclei was performed using 4',6-diamidino-2-phenylindole (DAPI). Florescence images were visualized with an Olympus microscope (32). The list of antibodies used in this study is presented in Table S1 (See Supplementary Online Information at www.celljournal.org).

Total RNA extraction and polymerase chain reaction

Total RNA was extracted using an RNeasy Mini Kit (Qiagen, Germany) and complementary DNA synthesis was performed by a TOPscript™ RT DryMIX kit (Enzynomics, Korea) according to the manufacturer's protocol. Quantitative real-time PCR (qRT-PCR) was carried out using Fast SYBR® Green Master Mix (Applied Biosystems, USA) and a 7500 Fast Real-Time PCR System (Applied Biosystems, USA). The primer sets used in this study are listed in Table S2 (See Supplementary Online Information at www.celljournal.org).

In vitro and *in vivo* differentiation

iPSCs were detached with Dispase (Thermo Fisher, USA) and transferred into 35-mm petri dishes (SPL Life Science, Korea) for *in vitro* differentiation analysis and cultured in iPSC culture medium without bFGF. After four days of suspension culture, the cell aggregates (embryoid bodies, EBs) were attached to Matrigel (Corning)-coated plates and incubated with iPSC basal culture medium supplemented with 10% FBS for one week. *In vivo* differentiation analysis based on teratoma formation was performed as described previously (8). Briefly, 1×10^6 iPSCs were subcutaneously injected into BALB/c nude mice (CAnN.Cg-*Foxn1^{nu}*/CrljOri) (Orient Bio, Inc., Korea). The animal experiments were approved by the Bioethics Committee of KRIBB (KRIBB-AEC-16139).

Statistical analysis

The graphs represent the mean ± SEM relative to mRNA expression levels of triplicate samples used for the PCR analysis. All data analyses were performed on Microsoft Office Excel (version 2019). The student's t test was conducted to evaluate inter-group comparisons, and P<0.05 indicated statistical significance.

Results

Generation of human liver fibroblast induced pluripotent stem cells from a patient with combined hepatocellular-cholangiocarcinoma

The HLFs were isolated from the patient with cHCC-CC, who showed mixed histopathology of both HCC and CC and were mainly charged by CC in the liver biopsy sample. The HLFs were reprogrammed into iPSCs (HLF iPSCs) using retroviral transduction of OSKM (Fig.1A). HSFs were also reprogrammed into iPSCs for use as a normal control (Con iPSCs). Both Con iPSC and HLF iPSC colonies expanded well with a typical hESC-like morphology (Fig.1B). The HLF iPSCs were negative for mycoplasma contamination (Fig.1C). Both types of iPSCs retained the undifferentiated characteristics of strong AP activity (Fig.1D). The established HLF iPSCs STR profile matched that of the original fibroblasts (Fig.1E).

Locus/Clone	HLFs		HLF iPSCs	
Gender	XY		XY	
D3S1358	15	17	15	17
TH01	6	8	6	8
D21S11	30	30	30	30
D18S51	14	18	14	18
D5S818	10	11	10	11
D13S317	11	12	11	12
D7S820	8	11	8	11
D16S539	10	11	10	11
CSF1PO	11	12	11	12
vWA	14	14	14	14
D8S1179	11	13	11	13
TPOX	8	11	8	11
FGA	22	22	22	22
D19S433	15.2	15.2	15.2	15.2
D2S1338	23	24	23	24
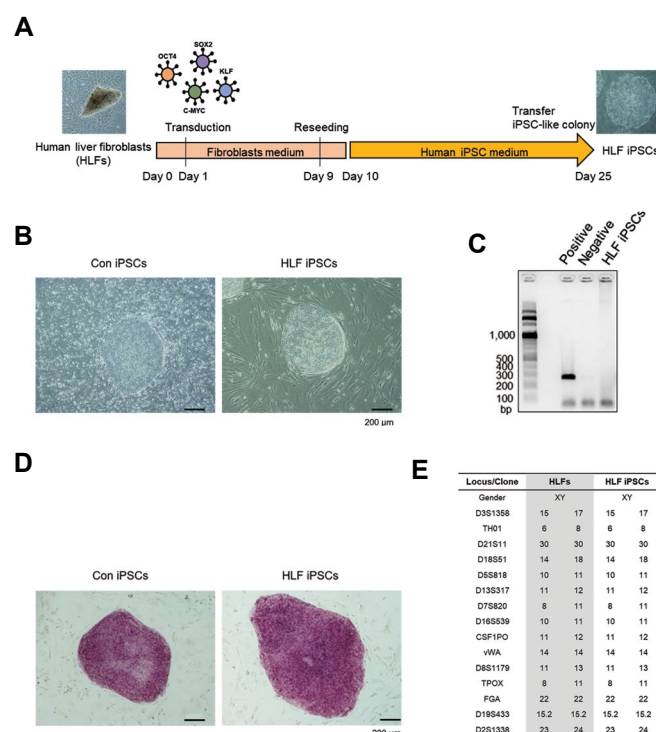
Fig.1: Generation of human liver fibroblast induced pluripotent stem cells (HLF iPSCs) from a patient with combined hepatocellular-cholangiocarcinoma (cHCC-CC). **A.** Experimental schematic for the generation of human iPSCs. HLFs derived from a patient with cHCC-CC and human skin fibroblasts (HSFs) from a healthy individual were reprogrammed into iPSCs using retroviral transduction of OSKM. **B.** Representative morphology of HSFs-derived control iPSCs (Con iPSCs) and cHCC-CC patient-derived iPSCs (HLF iPSCs). **C.** Confirmation of lack of mycoplasma contamination of the HLF iPSCs. **D.** Representative alkaline phosphatase (AP) activity of Con iPSCs and HLF iPSCs. **E.** Short tandem repeat (STR) profiles of HLFs and HLF-derived iPSCs (scale bar: 200 µm).

Pluripotency characterisation of human liver fibroblast induced pluripotent stem cells

Based on real-time PCR analysis, we observed higher mRNA expressions of pluripotent stem cell markers such as *OCT4*, *SOX2*, *NANOG*, and *REX1* in the Con iPSCs and HLF iPSCs than in the corresponding fibroblasts (Fig.2A). High expression of pluripotent markers such as OCT4, TRA-1-60, NANOG, and SSEA4 proteins were observed in both Con iPSCs and HLF iPSCs, as determined by immunostaining (Fig.2B). Total and endogenous pluripotency markers were well-expressed, but exogenous expressions similar to those of an hESC line, H9, were not detected by PCR (Fig.S1A, See Supplementary Online Information at www.celljournal. org). Karyotype analysis showed that no genetic abnormality had occurred during the reprogramming process of the iPSCs (Fig.S1B, See Supplementary Online Information at www. celljournal.org).

carried out (Fig.3). The formation of EBs allowed the spontaneous differentiation of iPSCs into the embryonic three germ layers *in vitro* (Fig.3A). Both Con iPSCs and HLF iPSCs, which differentiated *in vitro*, expressed representative markers for ectoderm (TUJ1), mesoderm (alpha smooth muscle actin, α-SMA), and endoderm (FOXA2), as shown in Figure 3A. Teratoma induced *in vivo* by subcutaneous injection of iPSCs contained representative tissues of each particular layer, including ectoderm (pigment epithelium containing melanocytes or neural rosettes), mesoderm (cartilage), and endoderm (gut-like epithelium), as revealed by haematoxylin and eosin staining (Fig.3B). These results demonstrated that the established HLF iPSC line retained pluripotency *in vitro* and *in vivo*, which was indistinguishable from that of Con iPSCs.
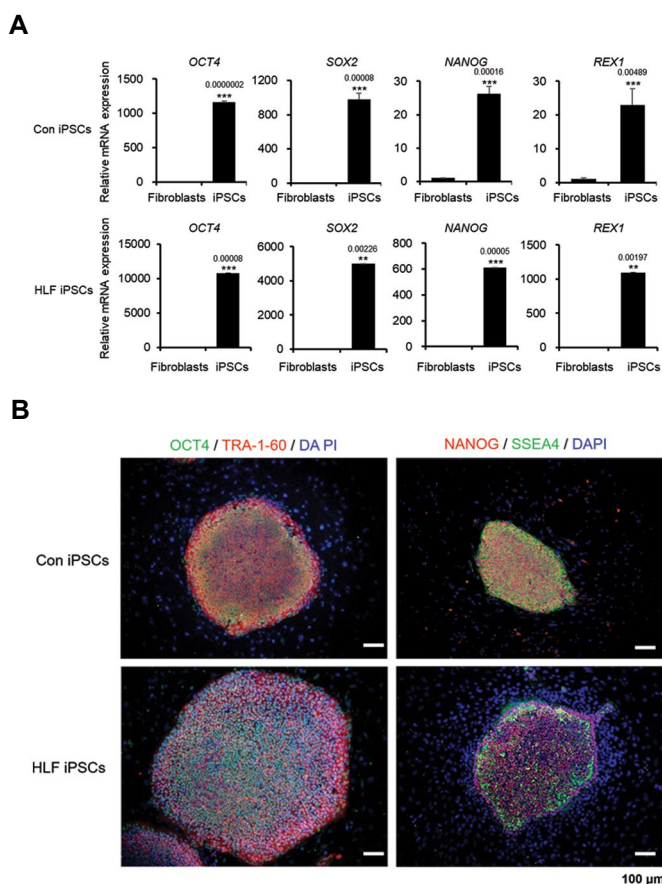

A

B

Fig.2: Pluripotency marker expressions in combined hepatocellular-cholangiocarcinoma (cHCC-CC)-derived human liver fibroblast induced pluripotent stem cells (HLF iPSCs). **A.** mRNA expression levels of pluripotency markers *OCT4*, *SOX2*, *NANOG*, and *REX-1* in fibroblasts and iPSCs from normal control (upper) and cHCC-CC patient (lower). **B.** Representative immunostaining images of HSFs-derived control iPSCs (Con iPSCs) (upper) and cHCC-CC patient-derived iPSCs (HLF iPSCs) (lower) stained for pluripotency markers using the indicated antibodies. Data are expressed as the mean ± SEM (n=3) and were analysed using the student's t test, **; P<0.01 and ***; P<0.001 (scale bar: 100 µm).

To further determine the full pluripotency potential of the iPSCs, *in vitro* and *in vivo* differentiation analyses were

A

B

Fig.3: *In vitro* and *in vivo* differentiation potential of combined hepatocellular-cholangiocarcinoma (cHCC-CC)-derived human liver fibroblast induced pluripotent stem cells (HLF iPSCs). **A.** *In vitro* differentiation of the iPSCs determined through embryoid body (EB) formation. Representative immunofluorescence images of ectodermal, mesodermal, and endodermal markers in differentiated cells from HSFs-derived control iPSCs (Con iPSCs) (upper) and cHCC-CC patient-derived iPSCs (HLF iPSCs) (lower) (scale bar: 100 µm) **B.** *In vivo* differentiation of Con iPSCs (upper) and HLF iPSCs (lower) determined through teratoma formation. Representative histology of teratomas, including the three germ layers, stained with haematoxylin and eosin (scale bar: 200 µm).

Hepatocellular carcinoma and cholangiocarcinoma marker expression in human liver fibroblast induced pluripotent stem cells during differentiation

We evaluated the expressions of various makers during *in vitro* differentiation to determine if HLF iPSCs could maintain the characteristics of the patient (Fig.4). The expressions of pluripotency markers *OCT4* and *NANOG*

136

Fig.4: Expression of markers for hepatocellular carcinoma (HCC) and cholangiocarcinoma (CC) in combined hepatocellular-cholangiocarcinoma (cHCC-CC)-derived human liver fibroblast induced pluripotent stem cells (HLF iPSCs) during differentiation. **A.** mRNA expression levels of stem cell markers *OCT4* and *NANOG* on days 0, 2, and 6 after embryoid body (EB) formation of HSF-derived control iPSCs (Con iPSCs) and HCC-CC patient-derived iPSCs (HLF iPSCs). **B.** mRNA expression levels of definitive endoderm markers *FOXA2* and *CXCR4* on days 0, 2, and 6 after EB formation of Con iPSCs and HLF iPSCs. **C.** mRNA expression levels of HCC markers *AFP* and *DKK1* on days 0, 2, and 6 after EB formation of Con iPSCs and HLF iPSCs. **D.** mRNA expression levels of CC marker *CK7* and CC tumour suppressor marker *SOX17* on days 0, 2, and 6 after EB formation of Con iPSCs and HLF iPSCs. Data are shown as the mean ± SEM (n=3) and were analysed by the student's t test, *; P<0.05, **; P<0.01, and ***; P<0.001.

gradually decreased upon differentiation and the levels did not differ significantly between Con iPSCs and HLF iPSCs (Fig.4A). In contrast, the expressions of definitive endoderm markers *FOXA2* and *CXCR4* (Fig.4B), ectoderm markers *NESTIN* and *OTX2*, and mesoderm markers *VIMENTIN* and *BRACHYURY* (Fig.S1C, See Supplementary Online Information at www.celljournal. org) increased during differentiation in both Con iPSCs and HLF iPSCs. These results were consistent with the data shown in Figure 3A and confirmed that the *in vitro* differentiation potential of the HLF iPSCs was not different from that of the normal Con iPSCs. However, expression levels of HCC markers *AFP* and *DKK1* substantially increased by 25-fold and 40-fold, respectively, compared to undifferentiated HLF iPSCs. In contrast, the expression levels of *AFP* and *DKK1* were similar in undifferentiated and differentiated cells from Con iPSCs (Fig.4C). We also examined the expressions of CC markers, *CK7* and *SOX17*. *CK7* expression increased aberrantly in the differentiated EBs from HLF iPSCs compared to the undifferentiated HLF iPSCs (by 56.2-fold); it was more than 10 times higher than the difference between undifferentiated and differentiated normal Con iPSCs. Furthermore, *SOX17*, which is known to have tumour suppressive roles in CC patients (21, 22), did not increase during differentiation of HLF iPSCs. However, its expression continually increased in Con iPSCs during differentiation (Fig.4D). Overall, these results demonstrated that patient-derived HLF iPSCs exhibited the expression of pluripotency markers, general differentiation potential, and HCC and CC patient-specific marker expression. Therefore, HLF iPSCs may provide a renewable cell source for modelling cHCC-CC.
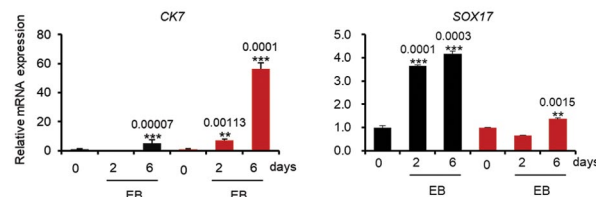
Discussion

While cHCC-CC is a rare type of primary hepatic cancer, there are limited therapeutic options due to an incomplete understanding of its pathogenesis. One of the biggest challenges in developing therapeutics for liver diseases is the lack of accessibility to human liver tissue, which results in difficulty for *in vitro* modelling of disease progression (2, 33). For uncommon cases of liver cancer such as cHCC-CC, patient-specific models are crucial to understand novel mechanisms of disease pathology and to develop personalized therapies. Patient-derived iPSCs that retain individual characteristics and exhibit unlimited self-renewal and differentiation potential into various cell types (34) can be a valuable source for modelling rare diseases, including liver cancer.

In this study, we isolated HLFs from a cHCC-CC specimen and reprogrammed them into indefinitely proliferative iPSCs. These patient-derived HLF iPSCs demonstrated prominent pluripotency and differentiation potential similar to that of normal Con iPSCs. Notably, when the HLF iPSCs were differentiated *in vitro* via EB formation, unique marker expression of the patient was clearly observed. For example, AFP is considered a gold standard in liver cancer diagnosis and DKK1 has been implicated in tumourigenesis in many tissues, including HCC. Both are involved in embryonic liver development (13, 15, 16). The combined expression of AFP and DKK1 demonstrates a more precise diagnosis of HCC than AFP or DKK1 alone (35). The biliary marker CK7 is highly expressed in intrahepatic CC and thus has been studied as a prognostic marker in this type of cancer (17, 36). SOX17 is also necessary for the normal formation of the biliary epithelium, and its epigenetic downregulation by aberrant hypermethylation of the *SOX17* promoter is observed in CC patients (19). The expressions of these markers was clearly distinguishable in the cHCC-CC-derived HLF iPSCs.

Here, we demonstrated the spontaneous differentiation of the HLF iPSCs into three germ layers via EB formation; however, further direct differentiation of iPSCs into specific endodermal cell types such as hepatocytes (37) or cholangiocytes (38) is also possible. Recent developments in organoid technology (39) make it possible to differentiate iPSCs to recapitulate three-dimensional (3D) miniature livers that maintain cell composition and organ function (40). Our group has also generated expandable and functional 3D human liver organoids from iPSCs and demonstrated that iPSC-derived liver organoids can be used for toxicity prediction and drug screening in conditions with long-term maintenance of individual characteristics (30, 32) . Therefore, we aim to generate liver organoids in future using the cHCC-CC -derived HLF iPSCs established in the current study. Patient-derived liver organoids may provide a personalized disease modelling platform for revealing the molecular mechanisms of individual pathogenesis, developing therapeutics, and identifying hepatotoxic responses against targeted anti-cancer drugs. Moreover, patient-derived iPSCs may also provide various types of organoid models for the brain, lung, kidney, and gut in addition to the liver and may prove to be a valuable resource for modelling rare diseases.

Conclusion

We generated iPSCs using liver tissue-derived fibroblasts from a patient with rare cHCC-CC. The HLF iPSCs exhibited prognostic marker expression of cHCC-CC upon differentiation. Therefore, the HLF iPSC line may be used as a practical and renewable cell source for personalized disease modelling, uncovering the molecular mechanisms of individual pathogenesis, and developing therapeutics.

Acknowledgments

Authors' Contributions

H.-S.A., J-S.R, S.J.M., K.-S.C., M.J.S.; Study conception and design. H.-S.A., J-S.R, J.L., S.J.M., Y.-H.H.; Acquisition of data. H.-S.A., J-S.R, J.L., S.J.M., K.-S.C., M.J.S.; Analysis and interpretation of data. H.-S.A., J-S.R, J.L., Y.S., K.-S.C., M.J.S.; Drafting of manuscript. All authors read and approved the final manuscript.

References

1. Maximin S, Ganeshan DM, Shanbhogue AK, Dighe MK, Yeh MM, Kolokythas O, et al. Current update on combined hepatocellular-cholangiocarcinoma. Eur J Radiol Open. 2014; 1: 40-48.
2. Stavraka C, Rush H, Ross P. Combined hepatocellular cholangio-carcinoma (cHCC-CC): an update of genetics, molecular biology, and therapeutic interventions. J Hepatocell Carcinoma. 2019; 6: 11-21.
3. Takahashi K, Tanabe K, Ohnuki M, Narita M, Ichisaka T, Tomoda K, Yamanaka S. Induction of pluripotent stem cells from adult human fibroblasts by defined factors. Cell. 2007; 131(5): 861-872.
4. Balogh J, Victor D 3rd, Asham EH, Burroughs SG, Boktour M, Saharia A, et al. Hepatocellular carcinoma: a review. J Hepatocell Carcinoma. 2016; 3: 41-53.
5. Villanueva A. Hepatocellular carcinoma. N Engl J Med. 2019; 380(15): 1450-1462.
6. Massironi S, Pilla L, Elvevi A, Longarini R, Rossi RE, Bidoli P, et al. New and emerging systemic therapeutic options for advanced cholangiocarcinoma. Cells. 2020; 9(3): 688.
7. Rizvi S, Khan SA, Hallemeier CL, Kelley RK, Gores GJ. Cholangiocarcinoma - evolving concepts and therapeutic strategies. Nat Rev Clin Oncol. 2018; 15(2): 95-111.
8. Son MJ, Son MY, Seol B, Kim MJ, Yoo CH, Han MK, et al. Nicotinamide overcomes pluripotency deficits and reprogramming barriers. Stem Cells. 2013; 31(6): 1121-1135.
9. Leoni S, Sansone V, Lorenzo S, Ielasi L, Tovoli F, Renzulli M, et al. Treatment of combined hepatocellular and cholangiocarcinoma. Cancers (Basel). 2020; 12(4): 794.
10. Murugavel KG, Mathews S, Jayanthi V, Shankar EM, Hari R, Surendran R, et al. Alpha-fetoprotein as a tumor marker in hepatocellular carcinoma: investigations in south Indian subjects with hepatotropic virus and aflatoxin etiologies. Int J Infect Dis. 2008; 12(6): e71-76.
11. Galle PR, Foerster F, Kudo M, Chan SL, Llovet JM, Qin S, et al. Biology and significance of alpha-fetoprotein in hepatocellular carcinoma. Liver Int. 2019; 39(12): 2214-2229.
12. Lou J, Zhang L, Lv S, Zhang C, Jiang S. Biomarkers for hepatocellular carcinoma. Biomark Cancer. 2017; 9: 1-9.
13. Chen L, Li M, Li Q, Wang CJ, Xie SQ. DKK1 promotes hepatocellular carcinoma cell migration and invasion through β-catenin/MMP7 signaling pathway. Mol Cancer. 2013; 12: 157.
14. Bhavanasi D, Speer KF, Klein PS. CKAP4 is identified as a receptor for Dickkopf in cancer cells. J Clin Invest. 2016; 126(7): 2419-2421.
15. Watany M, Badawi R, Elkhalawany W, Abd-Elsalam S. Study of dickkopf-1 (DKK-1) gene expression in hepatocellular carcinoma patients. J Clin Diagn Res. 2017; 11(2): OC32-OC34.
16. Awad AE, Ebrahim MA, Eissa LA, El-Shishtawy MM. Dickkopf-1 and amphiregulin as novel biomarkers and potential therapeutic targets in hepatocellular carcinoma. Int J Hematol Oncol Stem Cell Res. 2019; 13(3): 153-163.
17. Liu LZ, Yang LX, Zheng BH, Dong PP, Liu XY, Wang ZC, et al. CK7/CK19 index: a potential prognostic factor for postoperative intrahepatic cholangiocarcinoma patients. J Surg Oncol. 2018; 117(7): 1531-1539.
18. Zhang H, Yu X, Xu J, Li J, Zhou Y. Combined hepatocellular-cholangiocarcinoma: An analysis of clinicopathological characteristics after surgery. Medicine (Baltimore). 2019; 98(38): e17102.
19. Merino-Azpitarte M, Lozano E, Perugorria MJ, Esparza-Baquer A, Erice O, Santos-Laso Á, et al. SOX17 regulates cholangiocyte differentiation and acts as a tumor suppressor in cholangiocarcinoma. J Hepatol. 2017; 67(1): 72-83.
20. Goeppert B, Konermann C, Schmidt CR, Bogatyrova O, Geiselhart L, Ernst C, et al. Global alterations of DNA methylation in cholangiocarcinoma target the Wnt signaling pathway. Hepatology. 2014; 59(2): 544-554.
21. Singh VK, Kalsan M, Kumar N, Saini A, Chandra R. Induced pluripotent stem cells: applications in regenerative medicine, disease modeling, and drug discovery. Front Cell Dev Biol. 2015; 3: 2.
22. Soldner F, Jaenisch R. Medicine. iPSC disease modeling. Science. 2012; 338(6111): 1155-1156.
23. Cayo MA, Mallanna SK, Di Furio F, Jing R, Tolliver LB, Bures M, et al. A drug screen using human ipsc-derived hepatocyte-like cells reveals cardiac glycosides as a potential treatment for hypercholesterolemia. Cell Stem Cell. 2017; 20(4): 478-489 e5.
24. Ye Z, Zhan H, Mali P, Dowey S, Williams DM, Jang YY, et al. Human-induced pluripotent stem cells from blood cells of healthy donors and patients with acquired blood disorders. Blood. 2009; 114(27): 5473-5480.
25. DeRosa BA, Van Baaren JM, Dubey GK, Lee JM, Cuccaro ML, Vance JM, et al. Derivation of autism spectrum disorder-specific induced pluripotent stem cells from peripheral blood mononuclear cells. Neurosci Lett. 2012; 516(1): 9-14.
26. Zhou J, Wang X, Zhang S, Gu Y, Yu L, Wu J, et al. Generation and

138

characterization of human cryptorchid-specific induced pluripotent stem cells from urine. Stem Cells Dev. 2013; 22(5): 717-725.

27. Zhang SZ, Li HF, Ma LX, Qian WJ, Wang ZF, Wu ZY. Urine-derived induced pluripotent stem cells as a modeling tool for paroxysmal kinesigenic dyskinesia. Biol Open. 2015; 4(12): 1744-1752.

28. Chun YS, Chaudhari P, Jang YY. Applications of patient-specific induced pluripotent stem cells; focused on disease modeling, drug screening and therapeutic potentials for liver disease. Int J Biol Sci. 2010; 6(7): 796-805.

29. Moriguchi H, Chung RT, Sato C. An identification of novel therapy for human hepatocellular carcinoma by using human induced pluripotent stem cells. Hepatology. 2010; 51(3): 1090-1091.

30. Mun SJ, Ryu JS, Lee MO, Son YS, Oh SJ, Cho HS, et al. Generation of expandable human pluripotent stem cell-derived hepatocyte-like liver organoids. J Hepatol. 2019; 71(5): 970-985.

31. Son MJ, Jeong JK, Kwon Y, Ryu JS, Mun SJ, Kim HJ, et al. A novel and safe small molecule enhances hair follicle regeneration by facilitating metabolic reprogramming. Exp Mol Med. 2018; 50(12): 1-15.

32. Mun SJ, Hong YH, Ahn HS, Ryu JS, Chung KS, Son MJ. Long-term expansion of functional human pluripotent stem cell-derived hepatic organoids. Int J Stem Cells. 2020; 13(2): 279-286.

33. Schizas D, Mastoraki A, Routsi E, Papapanou M, Tsapralis D, Vassiliu P, et al. Combined hepatocellular-cholangiocarcinoma: an update on epidemiology, classification, diagnosis and management. Hepatobiliary Pancreat Dis Int. 2020; 19(6): 515-523.

34. Aquina CT, Pawlik TM, Ejaz A. Cholangiocarcinoma: three different entities based on location. Ann Transl Med. 2020; 8(12): 738.

35. Erdal H, Gül Utku Ö, Karatay E, Çelik B, Elbeg Ş, Doğan İ. Combination of DKK1 and AFP improves diagnostic accuracy of hepatocellular carcinoma compared with either marker alone. Turk J Gastroenterol. 2016; 27(4): 375-381.

36. Ye J, Zhang J, Lv Y, Wei J, Shen X, Huang J, et al. Integrated analysis of a competing endogenous RNA network reveals key long noncoding RNAs as potential prognostic biomarkers for hepatocellular carcinoma. J Cell Biochem. 2019; 120(8): 13810-13825.

37. Si-Tayeb K, Noto FK, Nagaoka M, Li J, Battle MA, Duris C, et al. Highly efficient generation of human hepatocyte-like cells from induced pluripotent stem cells. Hepatology. 2010; 51(1): 297-305.

38. Ogawa M, Ogawa S, Bear CE, Ahmadi S, Chin S, Li B, et al. Directed differentiation of cholangiocytes from human pluripotent stem cells. Nat Biotechnol. 2015; 33(8): 853-861.

39. Huch M, Gehart H, van Boxtel R, Hamer K, Blokzijl F, Verstegen MM, et al. Long-term culture of genome-stable bipotent stem cells from adult human liver. Cell. 2015; 160(1-2):299-312.

40. Takebe T, Sekine K, Enomura M, Koike H, Kimura M, Ogaeri T, et al. Vascularized and functional human liver from an iPSC-derived organ bud transplant. Nature. 2013; 499(7459): 481-484.

Original Article

LINC00174 Suppresses Non-Small Cell Lung Cancer Progression by Up-Regulating LATS2 via Sponging miR-31-5p

Xueling Cheng, B.D.[1#], Mali Sha, B.D.[2#], Wenjin Jiang, M.D.[3#], Linjing Chen, B.D.[1], Meihua Song, B.D.[2*]

1. Department of Operation, Yantai Yuhuangding Hospital, Qingdao University, Yantai, Shandong, China
2. Department of Thoracic Surgery, Yantai Yuhuangding Hospital, Qingdao University, Yantai, Shandong, China
3. Department of Interventional Radiology, Yantai Yuhuangding Hospital, Qingdao University, Yantai, Shandong, China

#These authors contributed equally to this work.

*Corresponding Address: Department of Thoracic Surgery, Yantai Yuhuangding Hospital, Qingdao University, Yantai, Shandong, China
Email: cypw283913@163.com*

Abstract

Objective: Dysregulation of long non-coding RNAs (lncRNAs) is associated with the progression of non-small cell lung cancer (NSCLC). This study aimed to investigate the role of long intergenic non-protein coding RNA 174 (LINC00174) in NSCLC.

Materials and Methods: In this experimental study, LINC00174 expression in NSCLC tissues and cell lines was investigated by reverse transcription-quantitative polymerase chain reaction (RT-qPCR). Besides, cell counting kit-8 (CCK-8), 5-bromo-2'-deoxyuridine (BrdU). Transwell and Flow Cytometry assays were applied to detect the regulatory function of LINC00174 on the growth, migration and apoptosis of NSCLC cells. Bioinformatics analysis, dual luciferase reporter gene assay and RNA immunoprecipitation (RIP) assay predicted and verified the targeting relationship between LINC00174 and miR-31-5p, and between miR-31-5p and the 3′-untranslated region (3′UTR) of large tumor suppressor kinase 2 (LATS2), respectively. Western blotting was performed to detect the regulatory function of LINC00174 and miR-31-5p on LATS2 protein expression.

Results: Compared with that in normal lung tissues, LINC00174 expression in NSCLC tissues and cell lines was reduced. LINC00174 expression was negatively associated with the TNM stage of the patients. Functional experiments showed that LINC00174 overexpression inhibited NSCLC cell multiplication and migration, and induced apoptosis. Furthermore, LINC00174 targeted miR-31-5p and repressed its expression. Additionally, LINC00174 upregulated LATS2 expression through competitively binding to miR-31-5p.

Conclusion: LINC00174, as a competitive endogenous RNA, elevates LATS2 expression by adsorbing miR-31-5p, thereby inhibiting the viability and migration of NSCLC cells, and promoting apoptosis.

Keywords: Human, LATS2 Protein, Long Noncoding, Non-Small-Cell Lung Cancer, RNA

Introduction

Non-small cell lung cancer (NSCLC) accounts for 85% of all lung cancer cases (1). Despite important progresses have been made in the treatment of NSCLC in recent years, the prognosis of patients with NSCLC is still not satisfactory, with a 5-year overall survival rate of <20% (2). Thus, clarifying the molecular mechanism of NSCLC progression is of great importance to further improve the prognosis of the patients.

Long non-coding RNA (lncRNA) is pivotal in the progression of tumors by regulating cancer cell viability, metastasis and resistance to treatment (3). For example, lncRNA NEAT1 is abnormally upregulated in colorectal cancer, and activates the Wnt/β-catenin signaling pathway via binding with DEAD-box helicase 5, thereby promoting colorectal cancer metastasis (4). The dysregulation of lncRNAs is also a common biological event in NSCLC (5). For instance, lncRNAs such as BRAF-activated non-protein coding RNA, growth arrest specific 6-antisense RNA 1 and maternally expressed 4 have been shown

to inhibit the progression of NSCLC, while metastasis associated lung adenocarcinoma transcript 1 (MALAT1), colon cancer associated transcript 2 and HOX transcript antisense RNA function as oncogenes in NSCLC (6). Long intergenic non-protein coding RNA 174 (LINC00174) is abnormally expressed in glioma, hepatocellular carcinoma and colorectal cancer (7). However, the expression, function and mechanism of LINC00174 in NSCLC are not-well clarified.

In recent years, the interaction between lncRNA and microRNA (miRNA/miR) has attracted great attention in the field of cancer research. LncRNA can sponge miRNA to inhibit the expression and activity of miRNA, leading to upregulation of downstream target genes (8). This study is aimed to probe the molecular mechanism of LINC00174 modulating the progression of NSCLC. Here we report that LINC00174 expression is down-regulated in NSCLC, while miR-31-5p expression is increased. Functionally and mechanistically, LINC00174 represses the malignant phenotype of NSCLC cells, and the

suppressive effect of LINC00174 on the multiplication and migration of NSCLC cells depends on the miR-31-5p/large tumor suppressor kinase 2 (LATS2) axis.

Materials and Methods

Tissue samples

In this experimental study, all the patients involved in the present study were >18 years old (57.3 ± 8.4 years old). A total of 38 pairs of NSCLC tissues and adjacent tissues were collected from patients (23 males and 15 females) with NSCLC who attended Yantai Yuhuangding Hospital from 2018 May to 2019 March. Among the 38 cases of NSCLC, 21 cases were adenocarcinoma, and 17 cases were squamous carcinoma. None of the patients received anti-cancer therapies before the surgery. All specimens obtained during surgery were immediately stored in liquid nitrogen for subsequent experiments. The present study, with informed consent, was approved by the Ethics Committee of Yantai Yuhuangding Hospital (YHD20180146).

Cell culture

The Shanghai Cell Bank of Chinese Academy of Sciences provided the human NSCLC cell lines (95-D, H1299 and A549) and the normal bronchial epithelial cell line (HBE), which were used in the present study. All cells were cultured in Roswell Park Memorial Institute (RPMI)-1640 medium (Gibco, Thermo Fisher Scientific, Inc., USA) with 10% fetal bovine serum (FBS, Gibco, Thermo Fisher Scientific, Inc., USA), 100 U/ml penicillin and 100 μg/ml streptomycin (Gibco, Thermo Fisher Scientific, Inc., USA) at 37˚C in 5% CO_2.

Cell transfection

pcDNA3.1 vectors containing the LINC00174 sequence (pcDNA3.1-LINC00174), empty vector, small interfering RNA (siRNA) targeting LATS2 (si-LATS2), scramble siRNA negative control (si-NC), miR-31-5p mimic (5′-CUUUUUGCGGUCUGGGCUUGC-3′), miR-31-5p inhibitor (5′-CGUUCGGGUCUGGCGUUUUC-3′) and the control miRNA (5′-UCACAACCUCCUAGAAAGAGUAGA-3′) were purchased from Shanghai GenePharma Co., Ltd. A549 and H1299 cells were respectively transfected with Lipofectamine® 2000 (Invitrogen, Thermo Fisher Scientific, Inc., USA) as instructions.

Reverse transcription-quantitative polymerase chain reaction

Total RNA was extracted from tissues or cells using TRIzol® reagent (Vazyme, Biotech Co., Ltd., Nanjing, China). cDNA was prepared by reverse transcription with a PrimeScript™ RT Reagent kit (Takara Biotechnology Co., Ltd., Shiga, Japan). Next, using cDNA as a template, RT-qPCR was performed with SYBR Premix Ex Taq™ II (Takara Biotechnology Co., Ltd., Shiga, Japan), with housekeeping genes *U6* and *GAPDH* as the endogenous control. The relative expression of the genes was quantified

with $2^{-\Delta\Delta Ct}$ method. The sequences of the primers are shown in Table 1.

Table 1: Sequences used for reverse transcription-quantitative polymerase chain reaction

Name	Primer sequences (5′-3′)
LINC00174	F: GGCCCAACACTTCCCTCAAA
	R: CAGGGAGAAACGACCTGGAG
miR-31-5p	F: GGAGAGGCAAGATGCTGGCA
	R: GTGCAGGGTCCGAGGT
LATS2	F: ACCCCAAAGTTCGGACCTTAT
	R: CATTTGCCGGTTCACTTCTGC
U6	F: GCTTCGGCAGCACATATACTAAAAT
	R: CGCTTCACGAATTTGCGTGTCAT
GAPDH	F: AAATCCCATCACCATCTTCCAG
	R: TGATGACCCTTTTGGCTCCC

Cell counting kit-8 assay

Transfected A549 and H1299 cells in logarithmic phase were trypsinized with 0.25% trypsin (Thermo Fisher Scientific, Wilmington, DE, USA), and the cell density was accordingly adjusted to 2×10^4 cells/ml with medium. Next, the cells were seeded in 96-well plates (100 μl of cell suspension/well). The following day, 10 μl of CCK-8 solution (Biosharp Life Sciences, Biosharp, China) was added into each well. After incubation for 1 hour, the absorbance of each well at 450 nm was recorded with a microplate reader (Thermo Fisher Scientific, Wilmington, DE, USA). With the same method, the absorbance of the cells was measured every 24 hours for 3 days.

5-bromo-2′-deoxyuridine proliferation assay

A total of 1×10^5 cells/ml cells were inoculated in a 35-mm-diameter petri dish containing a glass cover slip, cultured for 1 day and synchronized with medium containing 0.4% FBS for 3 days so that the majority of cells were in G_0 phase. Subsequently, 1.0 mg/ml 5-bromo-2'-deoxyuridine (BrdU) reagent (BD Pharmingen, BD Biosciences, USA) was added, and the cells were cultured in complete medium at 37˚C for 2 hours. Next, the culture solution was removed; besides, the cover slips were washed in phosphate-buffered saline (PBS) three times; and the cells were accordingly fixed with methanol for 10 minutes. The dried slides were subsequently blocked with 5% normal rabbit serum (Beyotime, China), and nucleic acids were denatured with formamide (Sigma-Aldrich, China). Subsequently, the cover slips were rinsed with PBS and then incubated with the primary antibody anti-BrdU (Beyotime, China, 1: 500) at room temperature for 1 hour, while the control group was incubated with PBS. Next, the nuclei of the cells were stained with DAPI staining solution (Beyotime, China) for 2 hours at room

temperature, and finally, the number of BrdU-positive cells in 10 visual fields were observed and counted under a fluorescence microscope (Olympus, Japan), and the average number of the BrdU positive cells was calculated.

Transwell assay

Cell migration was detected with a Transwell system (Corning Inc., Corning, NY, USA). The transfected NSCLC cells were trypsinized with 0.25% trypsin (Gibco, Thermo Fisher Scientific, Inc., USA), and 1×10^5 cells/ml cell suspension was subsequently prepared with serum-free medium. Next, 200 µl of cell suspension was loaded into the upper chamber of the Transwell system, while the lower chamber was added with 600 µl of medium containing 20% FBS. Subsequently, the cells were cultured for 24 hours, and then the cells on the upper surface of the membrane were removed by a cotton swab. Notably, the cells remaining on the below surface of the membrane were then subjected to formaldehyde fixation for 15 minutes and crystal violet staining for 30 minutes. Next, five visual fields were randomly selected under a microscope (Olympus, Japan) for cell counting, and the average was accordingly recorded to represent the migration ability of NSCLC cells.

Western blot analysis

Western blot assay was conducted to measure LATS2 protein expression. Cells in different groups were respectively lysed with 1 ml of RIPA lysis buffer (Biosharp Life Sciences, China) on ice for 20 minutes, and the mixture was centrifuged (1000 g, 4°C) for 10 minutes and the supernatant was accordingly collected, with the the protein concentration of the samples detected with a BCA Protein Assay kit (Beyotimes, China). Subsequently, the protein sample was mixed with loading buffer (Biosharp Life Sciences, China) and then denatured in boiling water. Next, the samples (10 µg/lane) were dissolved by sulfate-polyacrylamide gel electrophoresis (SDS-PAGE) (4% stacking gel and a 12% separation gel). After electrophoresis, the proteins were transferred to polyvinylidene fluoride (PVDF) membranes (EMD Millipore, Billerica, MA, USA), which were blocked with 5% skimmed milk for 30 minutes at room temperature and firstly incubated with rabbit anti-LATS2 antibody (1:1,000; ab110780, Abcam, Cambridge, UK) or anti-GAPDH antibody (1:3000, Beyotime, China) at 4°C overnight, and secondly incubated with a horseradish peroxidase-conjugated secondary antibody (1:2,000; ab205718; Abcam, Cambridge, UK) at room temperature for 1 hour. Finally, the protein bands were developed with enhanced chemiluminescent (ECL) reagent (EMD Millipore, Billerica, MA, USA). Signal quantification was achieved with Quantity One software version 4.6.6 (Bio-Rad Laboratories, Inc., Hercules, CA, USA), with

GAPDH as the loading control.

Luciferase reporter assay

The binding sites of miR-31-5p on LINC00174 and the 3′-untransalted region (UTR) of LATS2 were predicted by bioinformatics analysis with StarBase database, and the sequences containing the binding sites were amplified by PCR. The amplified products were inserted into the pGL3-promoter plasmid vector to construct the LINC00174 and LATS2 wild-type (WT) reporter plasmids, while mutant (MUT) plasmids were constructed by site-directed mutagenesis. The above recombinant reporter plasmids were co-transfected into 293T cells with miR-31-5p (or miR-NC). 48 hours later, the cells were collected, and a dual luciferase reporter gene assay system (Promega Corporation, Madison, WI, USA) was conducted to detect the value of luciferase activity.

RNA immunoprecipitation

Cells lysates from different groups were respectively incubated with RIP buffer containing magnetic beads conjugated with anti-human argonaute 2 (Ago2) antibody (EMD Millipore, Billerica, MA, USA), with normal mouse IgG (EMD Millipore, Billerica, MA, USA) as normal controls (NCs). The samples were subsequently incubated with Proteinase K, and then immunoprecipitated RNAs were isolated. The RNA concentration was measured by a spectrophotometer, and the RNA quality was assessed by a bioanalyzer. Purified RNAs were accordingly extracted and qPCR was performed to detect the enrichment of LINC00174.

Bioinformatics analysis

StarBase database was used to predict the binding sites among lncRNA, miRNA and the 3′UTR of mRNA, and Gene Expression Profiling Interactive Analysis (GEPIA) database was used to investigate the expression characteristics of genes in NSCLC tissues.

Flow cytometry

Annexin V-FITC/propidium iodide (PI) double staining was used to detect cell apoptosis. Cells were collected 48 hours after transfection, and the density of cell suspension was adjusted to 1×10^6 cells/mL. The cells were fixed in pre-cooled 70% ethanol and incubated overnight at 4°C. Subsequently, 100 µL of cell suspension were centrifuged and resuspended in 200 µL of binding buffer. The resuspended cells were immediately stained with 10 µL of Annexin V-FITC staining solution and 5 µL of PI staining solution at ambient temperature for 15 minutes in the dark. Cell apoptosis was then detected with a flow cytometer (Attune NxT, Thermo Fisher, USA) at an excitation wavelength of 488 nm.

Immunohistochemistry

Immunohistochemistry (IHC) was performed to determine LATS2 protein expression in the NSCLC

samples. The NSCLC tissue samples were fixed in 10% formaldehyde and then embedded in paraffin. Subsequently, tissues sections were prepared, and the sections were dewaxed, rehydrated, and next antigen retrieval was conducted. Then the tissues were immersed in 2% H_2O_2 for 10 minutes to inactivate peroxidase, and immersed in 5% bovine serum albumin for 30 minutes to block the non-specific antigens. Then anti-LATS2 antibody (1: 200; ab110780; Abcam, Cambridge, UK) was used to incubate the tissues at 4°C overnight in a wet box. Next, the tissues were washed with PBS and then incubated with a biotin-linked antiserum for 1 hour at room temperature in a wet box. Next, the tissues were washed by PBS again and stained with 3,3-diaminobenzidine hydrochloride. Eventually, the tissue staining was observed and scored under a microscope by two independent pathologists.

Statistical analysis

All the experiments were performed in triplicate. The data were presented as the "mean ± standard deviation", and GraphPad Prism 8 (GraphPad Software, Inc., La Jolla, CA, USA) was adopted for statistical analysis. Whether the data are normally distributed or not was examined by the Kolmogorov-Smirnov test. Notably, for normally distributed data, an unpaired or paired Student's t test was executed to compare the data between two groups. Besides, comparisons among ≥3 groups were made with one-way ANOVA. If the data exhibited significant differences, Tukey's post-hoc test was then performed to compare the data between groups. For data that were not normally distributed, comparisons between two groups were made by paired-sample Wilcoxon signed-rank test. Additionally, Pearson's correlation coefficient was utilized to examine the correlation between the genes' expressions in the NSCLC samples. Statistically, $P < 0.05$ is meaningful.

Results

LINC00174 expression is reduced in human NSCLC tissues

First, RT-qPCR was employed to probe *LINC00174* expression in paired NSCLC tissues and paracancerous tissues. As against that in normal tissues, *LINC00174* expression in cancer tissues was markedly downregulated (Fig.1A). *LINC00174* expression in NSCLC cell lines was also dramatically lower than that in a normal bronchial epithelial cell line HBE (Fig.1B). *LINC00174* expression in lung squamous cell carcinoma and lung adenocarcinoma was respectively analyzed by searching GEPIA database, and the results showed that *LINC00174* expression in both lung squamous cell carcinoma and lung adenocarcinoma was downregulated relative to that in normal tissues

(Fig.1C). Additionally, *LINC00174* expression was negatively correlated to the TNM stage of NSCLC patients (Fig.1D), suggesting that the low expression of *LINC00174* could probably be relevant to the progression of NSCLC.
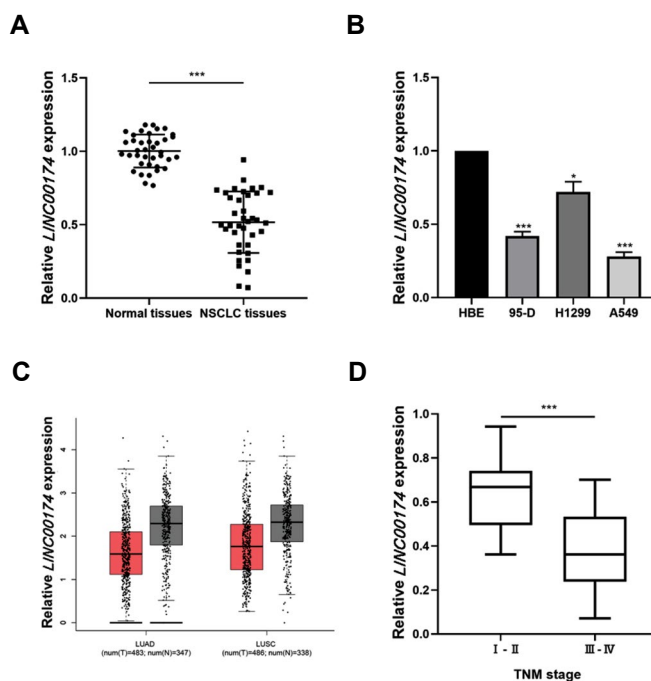

Fig.1: *LINC00174* is expressed at low level in NSCLC. **A.** RT-qPCR was used to detect the expression of *LINC00174* in NSCLC tissues (n=38) and adjacent normal tissues (n=38), and the results indicated that *LINC00174* was down-regulated in NSCLC. **B.** RT-qPCR was employed to detect the expression of *LINC00174* in normal bronchial epithelial cells and NSCLC cell lines, and the results indicated that *LINC00174* was down-regulated in NSCLC cell lines. **C.** Gene Expression Profiling Interactive Analysis (GEPIA) database was applied to analyze the expression of *LINC00174* in normal tissues and NSCLC (lung adenocarcinoma and lung squamous cell carcinoma) tissues, and the results indicated that *LINC00174* was down-regulated in NSCLC. **D.** The correlation between the expression levels of *LINC00174* and the patient's TNM stage (I-II, n=21; III-IV, n=17) was analyzed with Student's t test. *; P<0.05, ***; P<0.001, NSCLC; Non-small cell lung cancer, RT-qPCR; Reverse transcription-quantitative polymerase chain reaction, and TNM; Tumor node metastasis.

Effect of *LINC00174* on the growth and migration of NSCLC cells

We then explored the possible biological functions of *LINC00174* in tumor progression. A549 and H1299 cells were transfected with pcDNA3.1-*LINC00174* and si-*LINC00174*, respectively (Fig.2A, B). CCK-8 and BrdU assays highlighted that, as against that of the control group, the growth of A549 cells transfected with pcDNA3.1-*LINC00174* was greatly inhibited, while the growth of H1299 cells transfected with si-*LINC00174* was demonstrably enhanced (Fig.2C, D). In addition, the results of the Transwell assay revealed that *LINC00174* overexpression inhibited the migration of A549 cells relative to the control, while knocking down *LINC00174* promoted the migration of H1299 cells (Fig.2E). Additionally, *LINC00174* overexpression induced the apoptosis of NSCLC cells, while its knockdown

inhibited the apoptosis of NSCLC cells (Fig.2F). These data uncovered that *LINC00174* repressed the malignant biological behaviors of NSCLC cells.
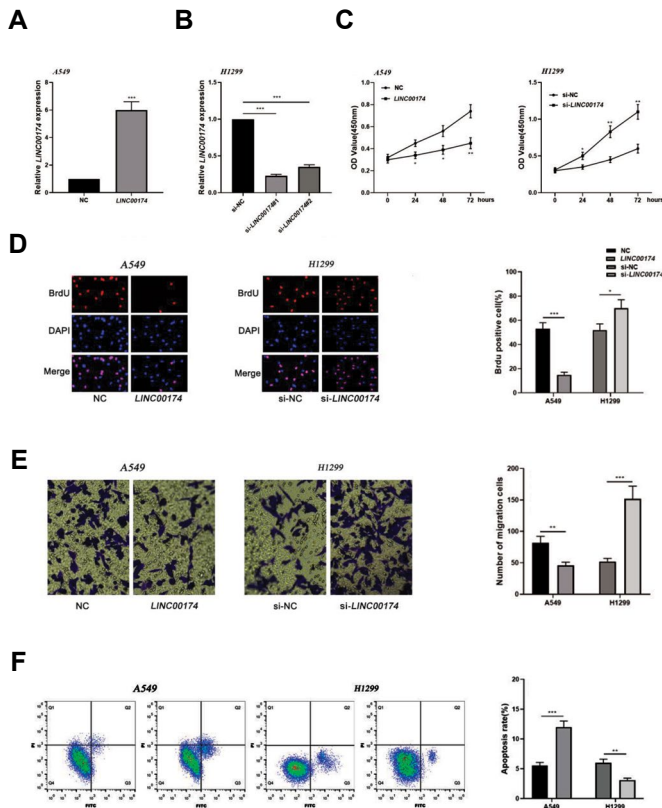

Fig.2: *LINC00174* inhibits NSCLC cell proliferation and migration. **A, B.** RT-qPCR confirmed that the *LINC00174* overexpression and knockdown cell models were successfully constructed. **C.** CCK-8 assay and **D.** BrdU assay were used to detect the proliferation of NSCLC cells, the results of which indicated that *LINC00174* negatively regulated the proliferation of NSCLC cells. **E.** Transwell assay was used to detect the migration of NSCLC cells, the results of which indicated that *LINC00174* negatively regulated the migration of NSCLC cells. **F.** Flow cytometry was used to detect the apoptosis of NSCLC cells, the results of which indicated that *LINC00174* positively regulated the apoptosis of NSCLC cells. *; P<0.05, **; P<0.01, ***; P<0.001, NSCLC; Non-small cell lung cancer, and RT-qPCR; Reverse transcription-quantitative polymerase chain reaction.

miR-31-5p is a target of *LINC00174*

Bioinformatics analysis with StarBase suggested that there was a potential binding site between *LINC00174* and miR-31-5p (Fig.3A). Dual luciferase reporter gene assay was performed to verify the above prediction, and the findings indicated that miR-31-5p greatly decreased *LINC00174*-WT luciferase activity but had no effect on that of *LINC00174*-MUT (Fig.3B). RIP assay was conducted to verify the interaction between *LINC00174* and miR-31-5p. The results indicated that compared with the non-specific IgG group, *LINC00174* and miR-31-5p were specifically enriched by anti-Ago2 antibodies, indicating that *LINC00174* could directly bind with miR-31-5p (Fig.3C). Furthermore, the

effects of *LINC00174* overexpression and knockdown on miR-31-5p expression were examined, and it was found that *LINC00174* overexpression remarkably inhibited miR-31-5p expression as against that of the control, while knocking down *LINC00174* led to a higher expression of miR-31-5p (Fig.3D). The present study also analyzed miR-31-5p expression in NSCLC tissues using bioinformatics tools (StarBase database) and RT-qPCR. The results demonstrated that miR-31-5p expression in cancer tissues was higher than that in paracancerous tissues (Fig.3E, F). In addition, RT-qPCR revealed that *LINC00174* negatively regulated miR-31-5p expression (Fig.3G). The above results indicated that miR-31-5p was the downstream target of *LINC00174*, and miR-31-5p was negatively regulated by it.
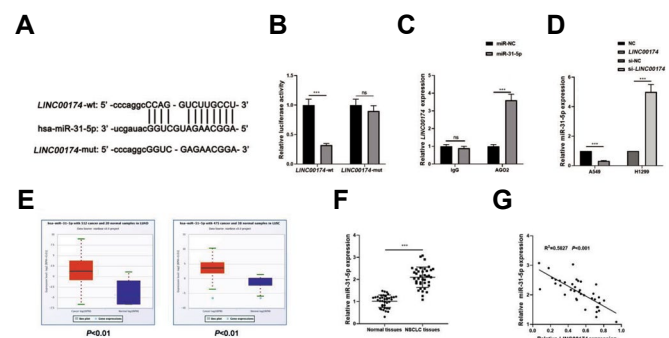

Fig.3: miR-31-5p is the target of *LINC00174*. **A.** StarBase (http://starbase.sysu.edu.cn/index.php) predicted the binding site between *LINC00174* and miR-31-5p. **B.** Dual luciferase reporter gene assay validated the binding association between *LINC00174* and miR-31-5p. **C.** RIP assay was conducted to verify the interaction between *LINC00174* and miR-31-5p. **D.** RT-qPCR was applied to detect the effect of overexpression or knockdown of *LINC00174* on miR-31-5p expression, and the results indicated that *LINC00174* negatively regulated the expression of miR-31-5p in NSCLC cells. **E.** StarBase database and **F.** RT-qPCR were employed to analyze the expression of *miR-31-5p* in NSCLC tissues (n=38) and normal lung tissues (n=38), and the results showed that *miR-31-5p* was up-regulated in NSCLC tissues. **G.** *LINC00174* was negatively correlated with the expression of miR-31-5p in NSCLC samples (n=38). ***; P<0.001, ns; No statistical significance, NSCLC; Non-small cell lung cancer, RT-qPCR; Reverse transcription-quantitative polymerase chain reaction, and miR; microRNA.

LINC00174 functions by inhibiting miR-31-5p

To clarify whether *LINC00174* inhibits the malignancy of NSCLC cells by suppressing miR-31-5p expression, miR-31-5p mimics were transfected into A549 cells with *LINC00174* overexpression, and miR-31-5p inhibitors were subsequently transfected into H1299 cells with *LINC00174* knockdown (Fig.4A, B). The findings revealed that the transfection of miR-31-5p mimics partially reversed the effects of *LINC00174* overexpression on the multiplication, migration and apoptosis of A549 cells, while miR-31-5p inhibitors partially counteracted the effect of knocking down *LINC00174* on the malignant biological behaviors of H1299 cells (Fig.4C-F).
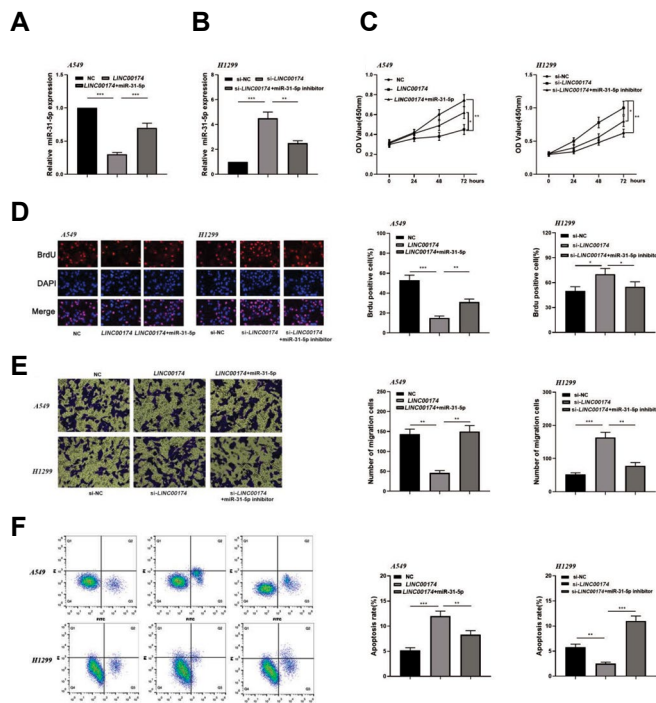
Fig.4: miR-31-5p partially reverses the inhibitory effect of *LINC00174* on NSCLC. NSCLC cells with *LINC00174* overexpression or knockdown were transfected with **A.** miR-31-5p mimics or **B.** miR-31-5p inhibitor, respectively, and the miR-31-5p expression levels in NSCLC cells were detected by RT-qPCR. **C.** CCK-8 and **D.** BrdU assay were used to detect the proliferation of NSCLC cells after transfection, the results of which showed that miR-31-5p counteracted the biological function of *LINC00174*. **E.** Transwell assay was used to detect the migration of NSCLC cells after transfection, the results of which showed that miR-31-5p counteracted the biological function of *LINC00174*. **F.** Flow cytometry was used to detect the apoptosis of NSCLC cells after transfection, the results of which showed that miR-31-5p counteracted the biological function of *LINC00174*. *; P<0.05, **; P<0.01, ***; P<0.001, NSCLC; Non-small cell lung cancer, RT-qPCR; Reverse transcription-quantitative polymerase chain reaction, and miR; MicroRNA.

LINC00174 upregulates LATS2 by inhibiting miR-31-5p

StarBase database predicted that LATS2 mRNA is a hidden target of miR-31-5p (Fig.5A). Luciferase reporter gene assay suggested that miR-31-5p greatly decreased LATS2-WT luciferase but that of LATS2-MUT was not significantly affected (Fig.5B). GEPIA database was used to analyze LATS2 expression in NSCLC. It was found that, relative to that in normal tissues, LATS2 expression in NSCLC was markedly downregulated (Fig.5C). Furthermore, miR-31-5p restrained LATS2 expression at the mRNA and protein level in NSCLC cells, while miR-31-5p inhibitors had opposite effects (Fig.5D). These data confirmed that LATS2 mRNA was a target of miR-31-5p, and that miR-31-5p inhibited its expression and translation via binding to the 3′UTR of LATS2 mRNA.

Considering that miR-31-5p is targeted by *LINC00174*, the present study also examined the effect of the *LINC00174*/miR-31-5p axis on LATS2 expression in NSCLC cells. Western blotting showed that *LINC00174* overexpression promoted LATS2 expression, and that

the effect of *LINC00174* was partially reversed by miR-31-5p (Fig.5E). Furthermore, RT-qPCR uncovered that LAST2 expression was positively correlated with that of *LINC00174* and negatively correlated with that of miR-31-5p in NSCLC samples (Fig.5F, G). LATS2 expression in cancer tissues and adjacent tissues of 38 patients with NSCLC was also detected by IHC. It showed that the expression of LAST2 protein was markedly reduced in NSCLC tissues (Fig.5H, I). These data implied that *LINC00174* could upregulate LATS2 expression in NSCLC via repressing miR-31a-5p.
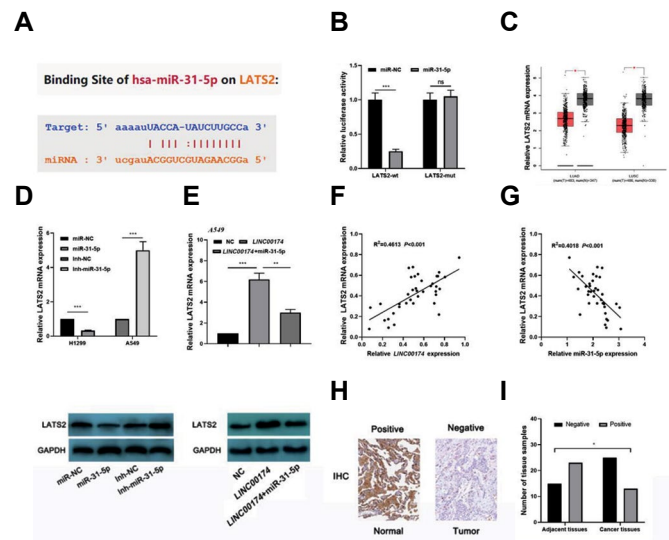

Fig.5: *LINC00174* upregulates LATS2 mRNA by decoying miR-31-5p. **A.** StarBase database was used to predict the binding site between miR-31-5p and LATS2 mRNA. **B.** Dual luciferase reporter gene assay was adopted to verify the targeted binding relationship between miR-31-5p and LATS2 mRNA. **C.** The Gene Expression Profiling Interactive Analysis (GEPIA) database was used to analyze the mRNA expression of LATS2 in normal tissues and NSCLC (lung adenocarcinoma and lung squamous cell carcinoma) tissues, which suggested that LATS2 was underexpressed in NSCLC tissues. **D, E.** The mRNA (upper) and protein (below) expression levels of LATS2 were detected by RT-qPCR and western blot. **F, G.** The correlations between *LINC00174* and LATS2 mRNA, and between miR-31-5p and LATS2 mRNA were analyzed. **H, I.** IHC was used to detect the expression of LATS2 expression in NSCLC samples, which showed that LATS2 expression was reduced in NSCLC tissues. *; P<0.05, **; P<0.01, ***; P<0.001, ns; No statistical significance, NSCLC; Non-small cell lung cancer, RT-qPCR; Reverse transcription-quantitative polymerase chain reaction, and miR; microRNA.

Discussion

LncRNAs play crucial roles in cancer biology through diverse mechanisms. In the nuclei, lncRNAs can regulate gene expression by directly interacting with DNA or chromatin-regulatory factors, transcription factors and RNA-binding proteins, functioning as enhancers, baits or scaffolds; in the cytoplasm, lncRNAs interact with mRNA and regulate the stability or translation of mRNAs; furthermore, lncRNAs serve as competitive endogenous RNAs (ceRNAs), reducing the inhibitory effect of miRNA on mRNA (5, 9). For example, in colorectal cancer, small nucleolar RNA host gene 1 is induced by Sp1 transcription factor (SP1), and, as the ceRNA of miR-154-5p, it reduces the ability of miR-154-5p to inhibit

cyclin D2 expression, thus promoting cell multiplication (10). Since lncRNAs can be detected in body fluids such as blood, urine and saliva, they also have the potential to act as biomarkers. It has been reported that lncRNA MALAT1 expression in the serum of patients with NSCLC is greatly higher than that in healthy controls (11). The levels of nuclear paraspeckle assembly transcript 1, CDKN2B-AS1 and sprouty RTk signaling antagonist 4-IT1 levels are increased in the plasma of patients with NSCLC (12). LINC00174 adsorbs miR-320 to increase oncogene S100A10 expression in hepatocellular carcinoma, thereby promoting the growth and metastasis of hepatocellular carcinoma cells while inhibiting apoptosis (13). In glioma, LINC00174 acceletrates the multiplication and metastasis of cancer cells, and inhibits apoptosis via modulating the miR-152-3p/solute carrier family 2 member 1 axis (7). The present study demonstrated that LINC00174 expression in NSCLC tissues and cell lines was evidently lower than that in normal tissues and cell lines, and that LINC00174 expression was negatively correlated with the TNM stage of patients with NSCLC. In addition, *in vitro* functional experiments confirmed that LINC00174 inhibited the viability and migration of NSCLC cells. Our data indicated that LINC00174 acted as a tumor suppressor in NSCLC.

Reportedly, miRNAs targets and inhibits the translation of mRNA or reduces the stability of mRNA, thus playing a regulatory role in the development of cancer (1, 14). For example, miR-449b-3p inhibits the epithelial-mesenchymal transformation of NSCLC cells via targeting IL-6 and modulating the JAK2/STAT3 signaling pathway (15). miR-128-3p promotes the growth and migration of NSCLC cells via activating the Wnt/β-catenin and TGF-β pathways (16). miR-31-5p plays different roles in different tumors, either promoting or inhibiting cancer progression. For example, miR-31-5p facilitates the growth, migration and invasion of colorectal cancer cells by targeting NUMB endocytic adaptor protein (17). In hepatocellular carcinoma, miR-31-5p inhibits the malignant biological behaviors via modulation of SP1 transcription factors (18). Some previous studies report that miR-31-5p expression in NSCLC is elevated, and its overexpression is dramatically correlated with the unfavorable prognosis of patients with NSCLC (19-22). The present study confirmed that miR-31-5p expression in NSCLC tissues was markedly higher than that in the normal tissues, suggesting that miR-31-5p works as an oncomiR in NSCLC.

ceRNA is a vital regulatory mechanism in cancer biology. The ceRNA network links the function of protein coding mRNA with that of non-coding RNA (23). For example, HOXD-AS1, as the ceRNA of miR-147a, upregulates pRB expression, thus promoting the multiplication and cell cycle progression of NSCLC cells, and inhibiting cell apoptosis (24). MALAT1 competitively sponges miR-124 to upregulate STAT3 expression, thus accelerating the malignant progression of NSCLC (25). MiR-31-5p is also modulated by ceRNA mechanisms. For example, in bladder cancer, circular-bromodomain PHD finger transcription factor expedites the multiplication

and metastasis of bladder cancer cells by regulating the the miR-31-5p/RAB27A axis (26). MiR-31-5p, which is decoyed by long intergenic non-protein coding RNA 1234, inhibits the expression of MAGE family member A3 in hepatocellular carcinoma, thus reducing the multiplication, invasion and drug resistance of hepatocellular carcinoma cells (27). The present study revealed that LINC00174 functioned as the ceRNA of miR-31-5p and negatively regulates its expression. In addition, it was found that miR-31-5p could reverse the inhibitory effect of LINC00174 on the multiplication and migration of NSCLC cells.

LATS2 has been reported to be a tumor suppressor, and it is vital in regulating the cell cycle, mitosis and genomic stability (28). LATS2 forms a positive feedback loop with p53: it promotes the tumor-suppressive effect of p53 by binding or inactivating MDM2; in turn, p53 directly regulates the transcription of LATS2 (29). In addition, LATS2 is the key regulator of the Hippo signaling pathway, which is closely relevant to the occurrence and progression of multiple types of cancers. It has been reported that low expression of LATS2 in NSCLC is associated with poor prognosis (30, 31). In NSCLC, LATS2 blocks the growth, migration and invasion of NSCLC cells: LATS2 overexpression leads to the phosphorylation of the oncoprotein YY1 associated protein 1, which is a downstream effector of Hippo signaling, resulting in increased expression of E-cadherin, and downregulation of vimentin and matrix metalloproteinase 9 (32). Previous studies report that miR-31-5p can target peroxisomal biogenesis factor 5, tensin 1, CDK1 and other genes involved in the regulation of hepatocellular carcinoma, colon adenocarcinoma and renal cell carcinoma (33-35). In addition, miR-31-5p modulates the drug sensitivity of colorectal cancer cells by targeting LATS2 (36). Here we demonstrated that LATS2 was expressed at low level in NSCLC and negatively modulated by miR-31-5p, but positively regulated by LINC00174. Our data provide a novel mechanism explaining the dysregulation of LAST2 in NSCLC.

Conclusion

On all accounts, LINC00174 is lowly expressed in NSCLC tissues and cell lines, and that LINC00174 functions as a ceRNA to inhibit the multiplication and migration of NSCLC cells via the miR-31-5p/LATS2 axis. To our best knowledge, this is the first study on the role of LINC00174 in lung cancer, and our data extend the understanding of the mechanism of NSCLC progression. In the following studies, *in vivo* experiments are necessary to further validate our demonstrations, and more patients should be enrolled to verify the potential of LINC00174 as a prognostic marker.

Acknowledgements

in this study.

Authors' Contributions

Me.S.; Designed this study. X.C., Ma.S., W.J., L.C.; Performed the experiments. X.C., Ma.S.; Analyzed and interpreted the experimental data. X.C., W.J., Ma.S.; Wrote the draft. X.C., W.J.; Performed the revision. Me.S.; Confirmed the authenticity of all the raw data. All authors read and approved the final manuscript.

References

1. Lee SS, Cheah YK. The interplay between micrornas and cellular components of tumour microenvironment (TME) on non-small-cell lung cancer (NSCLC) progression. J Immunol Res. 2019; 2019: 3046379.
2. Dercle L, Fronheiser M, Lu L, Du S, Hayes W, Leung DK, et al. Identification of non-small cell lung cancer sensitive to systemic cancer therapies using radiomics. Clin Cancer Res. 2020; 26(9): 2151-2162.
3. Sun W, Zu Y, Fu X, Deng Y. Knockdown of lncRNA-XIST enhances the chemosensitivity of NSCLC cells via suppression of autophagy. Oncol Rep. 2017; 38(6): 3347-3354.
4. Zhang M, Weng W, Zhang Q, Wu Y, Ni S, Tan C, et al. The lncRNA NEAT1 activates Wnt/β-catenin signaling and promotes colorectal cancer progression via interacting with DDX5. J Hematol Oncol. 2018; 11(1): 113.
5. Wei MM, Zhou GB. Long non-coding RNAs and their roles in non-small-cell lung cancer. Genomics Proteomics Bioinformatics. 2016; 14(5): 280-288.
6. Lu W, Zhang H, Niu Y, Wu Y, Sun W, Li H, et al. Long non-coding RNA linc00673 regulated non-small cell lung cancer proliferation, migration, invasion and epithelial mesenchymal transition by sponging miR-150-5p. Mol Cancer. 2017; 16(1): 118.
7. Shi J, Zhang Y, Qin B, Wang Y, Zhu X. Long non-coding RNA LINC00174 promotes glycolysis and tumor progression by regulating miR-152-3p/SLC2A1 axis in glioma. J Exp Clin Cancer Res. 2019; 38(1): 395.
8. An J, Lv W, Zhang Y. LncRNA NEAT1 contributes to paclitaxel resistance of ovarian cancer cells by regulating ZEB1 expression via miR-194. Onco Targets Ther. 2017; 10: 5377-5390.
9. Lin W, Zhou Q, Wang CQ, Zhu L, Bi C, Zhang S, et al. LncRNAs regulate metabolism in cancer. Int J Biol Sci. 2020; 16(7): 1194-1206.
10. Xu M, Chen X, Lin K, Zeng K, Liu X, Pan B, et al. The long noncoding RNA SNHG1 regulates colorectal cancer cell growth through interactions with EZH2 and miR-154-5p. Mol Cancer. 2018; 17(1): 141.
11. Zhang R, Xia Y, Wang Z, Zheng J, Chen Y, Li X, et al. Serum long non coding RNA MALAT-1 protected by exosomes is up-regulated and promotes cell proliferation and migration in non-small cell lung cancer. Biochem Biophys Res Commun. 2017; 490(2): 406-414.
12. Lu T, Wang Y, Chen D, Liu J, Jiao W. Potential clinical application of lncRNAs in non-small cell lung cancer. Onco Targets Ther. 2018; 11: 8045-8052.
13. Zhao JT, Chi BJ, Sun Y, Chi NN, Zhang XM, Sun JB, et al. LINC00174 is an oncogenic lncRNA of hepatocellular carcinoma and regulates miR-320/S100A10 axis. Cell Biochem Funct. 2020; 38(7): 859-869.
14. Syed SN, Brüne B. MicroRNAs as emerging regulators of signaling in the tumor microenvironment. Cancers (Basel). 2020; 12(4): 911.
15. Cai K, Li HX, Li PP, Guo ZJ, Yang Y. MicroRNA-449b-3p inhibits epithelial-mesenchymal transition by targeting IL-6 and through the JAK2/STAT3 signaling pathway in non-small cell lung cancer. Exp Ther Med. 2020; 19(4): 2527-2534.
16. Cai J, Fang L, Huang Y, Li R, Xu X, Hu Z, et al. Simultaneous overactivation of Wnt/β-catenin and TGFβ signalling by miR-128-3p confers chemoresistance-associated metastasis in NSCLC. Nat Commun. 2017; 8: 15870.
17. Peng H, Wang L, Su Q, Yi K, Du J, Wang Z. MiR-31-5p promotes the cell growth, migration and invasion of colorectal cancer cells by targeting NUMB. Biomed Pharmacother. 2019; 109: 208-216.
18. Zhao G, Han C, Zhang Z, Wang L, Xu J. Increased expression of microRNA-31-5p inhibits cell proliferation, migration, and invasion via regulating Sp1 transcription factor in HepG2 hepatocellular carcinoma cell line. Biochem Biophys Res Commun. 2017; 490(2): 371-377.
19. Zhang J, Li D, Zhang Y, Ding Z, Zheng Y, Chen S, et al. Integrative analysis of mRNA and miRNA expression profiles reveals seven potential diagnostic biomarkers for non-small cell lung cancer. Oncol Rep. 2020; 43(1): 99-112.
20. Song F, Xuan Z, Yang X, Ye X, Pan Z, Fang Q. Identification of key microRNAs and hub genes in non-small-cell lung cancer using integrative bioinformatics and functional analyses. J Cell Biochem. 2020; 121(3): 2690-2703.
21. Jin X, Guan Y, Zhang Z, Wang H. Microarray data analysis on gene and miRNA expression to identify biomarkers in non-small cell lung cancer. BMC Cancer. 2020; 20(1): 329.
22. Li C, Yin Y, Liu X, Xi X, Xue W, Qu Y. Non-small cell lung cancer associated microRNA expression signature: integrated bioinformatics analysis, validation and clinical significance. Oncotarget. 2017; 8(15): 24564-24578.
23. Qi X, Zhang DH, Wu N, Xiao JH, Wang X, Ma W. ceRNA in cancer: possible functions and clinical implications. J Med Genet. 2015; 52(10): 710-718.
24. Wang Q, Jiang S, Song A, Hou S, Wu Q, Qi L, et al. HOXD-AS1 functions as an oncogenic ceRNA to promote NSCLC cell progression by sequestering miR-147a. Onco Targets Ther. 2017; 10: 4753-4763.
25. Li S, Mei Z, Hu HB, Zhang X. The lncRNA MALAT1 contributes to non-small cell lung cancer development via modulating miR-124/STAT3 axis. J Cell Physiol. 2018; 233(9): 6679-6688.
26. Bi J, Liu H, Cai Z, Dong W, Jiang N, Yang M, et al. Circ-BPTF promotes bladder cancer progression and recurrence through the miR-31-5p/RAB27A axis. Aging (Albany NY). 2018; 10(8): 1964-1976.
27. Chen Y, Zhao H, Li H, Feng X, Tang H, Qiu C, et al. LINC01234/MicroRNA-31-5p/MAGEA3 axis mediates the proliferation and chemoresistance of hepatocellular carcinoma cells. Mol Ther Nucleic Acids. 2020; 19: 168-178.
28. Furth N, Aylon Y. The LATS1 and LATS2 tumor suppressors: beyond the Hippo pathway. Cell Death Differ. 2017; 24(9): 1488-1501.
29. Furth N, Bossel Ben-Moshe N, Pozniak Y, Porat Z, Geiger T, Domany E, et al. Down-regulation of LATS kinases alters p53 to promote cell migration. Genes Dev. 2015; 29(22): 2325-2330.
30. Zhang H, Lang TY, Zou DL, Zhou L, Lou M, Liu JS, et al. miR-520b promotes breast cancer stemness through Hippo/YAP signaling pathway. Onco Targets Ther. 2019; 12: 11691-11700.
31. He C, Lv X, Huang C, Hua G, Ma B, Chen X, et al. YAP1-LATS2 feedback loop dictates senescent or malignant cell fate to maintain tissue homeostasis. EMBO Rep. 2019; 20(3): e44948.
32. Wu T, Hu H, Zhang T, Jiang L, Li X, Liu S, et al. miR-25 promotes cell proliferation, migration, and invasion of non-small-cell lung cancer by targeting the LATS2/YAP signaling pathway. Oxid Med Cell Longev. 2019; 2019: 9719723.
33. Wen J, Xiong K, Aili A, Wang H, Zhu Y, Yu Z, et al. PEX5, a novel target of microRNA-31-5p, increases radioresistance in hepatocellular carcinoma by activating Wnt/β-catenin signaling and homologous recombination. Theranostics. 2020; 10(12): 5322-5340.
34. Mi B, Li Q, Li T, Liu G, Sai J. High miR-31-5p expression promotes colon adenocarcinoma progression by targeting TNS1. Aging (Albany NY). 2020; 12(8): 7480-7490.
35. Li Y, Quan J, Chen F, Pan X, Zhuang C, Xiong T, et al. MiR-31-5p acts as a tumor suppressor in renal cell carcinoma by targeting cyclin-dependent kinase 1 (CDK1). Biomed Pharmacother. 2019; 111: 517-526.
36. Hsu HH, Kuo WW, Shih HN, Cheng SF, Yang CK, Chen MC, et al. FOXC1 regulation of miR-31-5p confers oxaliplatin resistance by targeting LATS2 in colorectal cancer. Cancers (Basel). 2019; 11(10): 1576.

Original Article

Hypothyroidism and Fertility: An Animal Model follows up in The Second-Generation

Faezeh Panahandeh, M.Sc.[1], Farideh Feizi, Ph.D.[1, 2]*, Mohsen Pourghasem, Ph.D.[1, 2], Sorya Khafri, Ph.D.[3], Zeinab

Abedian, Ph.D.[2, 4], Kaveh Pourghasem, B.Sc.[5], Zohre Esmaeili, M.Sc.[1]

1. Department of Anatomy, Embryology and Histology, Faculty of Medicine, Babol University of Medical Sciences, Babol, Iran
2. Cellular and Molecular Biology Research Center, Health Research Institute, Babol University of Medical Sciences, Babol, Iran
3. Department of Epidemiology and Biostatistics, School of Public Health, Infertility and Reproductive Health Research Center, Health Research Institute, Babol University of Medical Sciences, Babol, Iran
4. Dental Materials Research Center, Health Research Institute, Babol University of Medical Sciences, Babol, Iran
5. Department of Medical Sciences, Macquarie University, Sydney, NSW, Australia

Corresponding Address: P.O.Box: 47745-47176, Department of Anatomy, Embryology and Histology, Faculty of Medicine, Babol University of Medical Sciences, Babol, Iran
Email: faridehfeizi@yahoo.com

Abstract

Objective: Hypothyroidism is known as the most common endocrine disorder. The prevalence of hypothyroidism in the female and male population is 2% and 0.2%, respectively. Maternal hypothyroidism is a defect in the thyroid hormones transition from the mother to the fetus. The present study was conducted to find whether maternal hypothyroidism affects the fertility of the second generation.

Materials and Methods: In this experimental study, twelve adult female rats weighting 180-220 g were randomly divided into case and control groups. Hypothyroidism was induced by dissolving 0.1 g/L of 6-n-propyl-2-thiouracil in drinking water toward the end of pregnancy and lactation. At the end of the breastfeeding period, the blood samples of female children were collected. Six healthy, mature, female rats were selected and kept until they reached maturity, and were then mated with male rats. After observing the female rats' delivery, blood samples were collected from their male and female newborns and the healthy rats were selected.

Results: There was a significant difference in the volume and size of ovarian as well as in the number of secondary follicles in comparison with the control group (P=0.025). However, there were no significant changes in the other parameters including the number of primary follicles, the number of Graafian follicles and sperm parameters. There was no significant decrease in the testicular volume and size, number of Leydig cells and seminiferous tubules diameter.

Conclusion: Maternal hypothyroidism has no significant effects on testicular tissue function, and sperm parameters in the second generation, but can significantly reduce the rate of secondary follicles in the second generation female rats.

Keywords: Congenital Hypothyroidism, Fertilization, Ovary, Propylthiouracil, Testis

Introduction

The presence of thyroid hormones is essential for the development, differentiation, metabolism and control of various types of physiological processes in the body (1). Although their exact mechanism and consequences during pregnancy and lactation are yet to be fully determined, thyroid gland disorders can lead to a wide range of abnormalities. Among these disorders, hypothyroidism can be associated with reproductive disorders, including menstrual disorders, ovulation disorder, hyperprolactinemia, infertility, amenorrhea and spontaneous abortion that are common features in both humans and animals. The clinical manifestations of hypothyroidism are very diverse and dependent on age, duration of disease and severity of thyroid hormone reduction in humans. The prevalence rate of hypothyroidism is 2% of female and 0.2% for male (2). This disorder is also reportedly more prevalent in women with a smaller figure at the birth and during childhood.

Congenital hypothyroidism, one of the most common types of hypothyroidism, is classified into transient and permanent types. Transient type can arise due to maternal abnormalities during pregnancy, such as transplacental passage of maternal thyroid stimulating hormone (TSH) receptor blocking antibodies, while permanent type can occur due to primary or secondary causes such as thyroid dysgenesis (3).

Maternal hypothyroidism during pregnancy is associated with a wide range of disorders, including pregnancy hypertension, placental contractions, preterm delivery, stillbirth (4), impaired brain and nervous system development in the fetus (5-8), fetal genital system developmental disorders (9), congenital hypothyroidism, intrauterine growth restriction (10). Thyroid gland hormones are involved in the body growth regulating during fetal development and after birth alongside stimulating the growth factors production (11). Clinical studies conducted on the hypothyroidism in the pregnant

women have shown that thyroid hormones deficiency during pregnancy can affect the children's emotional functional capacity (12). During pregnancy, the fetus receives thyroid hormones from the mother through the placenta (13). An embryo's thyroid gland is not fully functional until mid-pregnancy, and in the first trimester, it is completely dependent on the thyroxine produced by the mother (14). During pregnancy, the T4 transmitted from the mother to the fetus is present in the amniotic fluid for up to four weeks and protects the fetal brain. Free T4 (FT4) increases rapidly in the fetal fluids, and its concentration is determined by the FT4 from the mother's serum. When the secretion of thyroid hormones begins in the fetus, the mother's T4 transmission continues to play the main role in the T4 concentrations in the fetal serum (12, 15). The metabolism disease will have severe consequences if left untreated.

Here, we conducted an animal model study to investigate the embryonic genital and reproductive systems development in the second generation in infants born from mothers with and without hypothyroidism.

Materials and Methods

Ethical consideration

This research was carried out in accordance with the Animal Ethics Committee guidelines at the Babol Medical Sciences University, Mazandaran, Iran (MUBABOL. REC.1395.38).

Animals

In this experimental study, twelve adult female Wistar rats (weighing 220-280 g, 14 weeks old) were randomly divided into case and control groups. The rats were housed under standard conditions in terms of humidity, temperature, light and access to water and food. Two female rats were allocated to one male rat in the both groups. After confirming the vaginal plaque, the case group received a daily dose of 0.1 g/L of 6-n-propyl-2-thiouracil (PTU) (Iran hormone, Iran) dissolved in their drinking water until the end of their pregnancy and lactation (16). Three days after the administration of PTU, the levels of T4, triiodothyronine (T3), and TSH were measured with an ELISA kit (30K-E30615-17, East Biopharm, China) to confirm hypothyroidism. An approximately threefold increase in the TSH and a nearly twofold reduction in the T4 and T3 compared to the control group were taken as the criteria for hypothyroidism (16, 17). After confirming the mothers' hypothyroidism in the case group, blood samples were taken from their newborn female rats. After puberty, six healthy female rats were randomly selected and kept alongside the male rats for 60 days. Upon detecting pregnancy and delivery, blood samples were taken from infants. Then, 24 healthy rats of both sexes (equal sex ratio; 60 days old) were divided into two equal groups as the second generation. Throughout all the stages of this study, the number of rats in the case group was equal to that of the control.

Hormonal assay

The blood Samples were left for 15 minutes at room temperature for clotting and centrifuged at 2000 (rpm) for 15 minutes. Then, the separated serum was kept frozen at - 20ºC till the analysis of the thyroid function test. The levels of T3, T4 and TSH hormones were measured by using an ELISA kit specific for rats)   (30K-E30615-17, East Biopharm, China).

The testicular and ovarian weight and volume

A scale with an accuracy of 0.001 was used to measure each testicle and ovary weight. A 100 ml glass measuring cylinder was used to measure volume. Initially, 20 ml of distilled water was poured into a cylinder, then the tissue was placed inside the cylinder. The difference between the initial volume of water and the new volume was considered as the tissue volume.

Sperm collection and count

The caudal epididymis of each rat was minced with an insulin needle in a petri dish containing 10 ml of Ham's F_{10} (Albuminated) medium (01131, Bioidea, Iran). And allow the sperms to swim up under an incubation at 37ºC for 30 minutes. Then, 10 μl of sperm suspension were placed on a glass slide and counted under a light microscope at 40X magnification at room temperature in triplicate for each sample.

Sperm morphology

For the morphological evaluation of sperm, one drop of the sperm suspension was spread on the slide and after fixation with ethanol alcohol 96% (Hamon Teb, Iran) dried at room temperature. The sperm smear was prepared in accordance with the Papanicolaou staining protocol with five repetitions for each sample. In brief, after rehydration by alcohol, the slides were stained with Hematoxylin (0B14695802, Merck, Germany) for 5 minutes and washed with distilled water. After dipping in acid alcohol for 5 seconds, washed with running water for 3 minutes and soaked in the chambers of 96% alcohol twice, 15 seconds for each chamber. Afterwards, the slides were stained with orange G6 dye (OG6, Asiapajohesh, Iran) for 5 minutes and then with 96% alcohols I and II for 15 seconds. After staining with Eosin Azure 50 (EA 50, Asiapajohesh, Iran) for 5 minutes, the slides were dipping in the chambers, two times of 96% alcohol (Hamon Teb, Iran) for 15 seconds and the chamber of 100% alcohol (Merck, Germany) for 1 minute. Finally, the slides were cleared with Xylene and mounted with Entallan. Ultimately, 50-100 sperms were seen under a light microscope at 100X magnification.

Histological assessment

Using 10% neutral buffered formalin (131328.1212 Panreac AppliChem, Germany), the testis and ovary tissues were fixed. The tissues were dehydrated in a series

of graded alcohols (70, 80, 90, 96 and 100), cleared in the Xylene (Asiapajohesh, Iran) and embedded in the paraffin (Asiapajohesh, Iran). The blocks were serially sectioned at 5 micrometers, and every 10 consecutive sections were on one slide, and stained with the Hematoxylin and Eosin (H&E) (0B14695802,Merck, Germany) (18). For the tissues study, using an Olympus optical microscope (BX41TF, Japan) equipped with a Canon camera (PC1587, Japan), pictures were captured at many random locations of slides at 10X and 40X magnification. Using of Motic Image Plus2.0ML (Micro - optic industrial group Co. LTD), we calculated diameter, surface area of the seminiferous tubules cross-sections and number of Leydig cells. For the evaluation of the ovary, after the preparation of the tissue, 10 random sections of each rat were selected randomly and primary, secondary and Graafian follicles were counted.

Statistical analysis

All data were encoded and analyzed using the Statistical Package for the Social Sciences Windows, version 22.0 (SPSS, Chicago, IL, USA). The normality of the variables was estimated by the Shapiro-Wilk test. The t test was used to compare the two groups in terms of the quantitative variables. $P \leq 0.05$ was considered statistically significant.
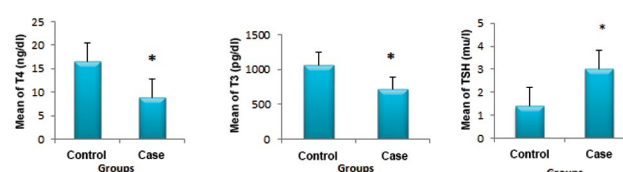
Results

Hormonal assay

The concentrations of T3, T4, and TSH in the pregnant female rats of both groups showed a significant difference. The mean concentration of T3 was 1098.67 ± 104.2 pg/dl in the control group and 686.67 ± 131.9 pg/dl in the case group (P=0.00). The mean concentration of T4 was 16.58 ± 1.8 ng/dl in the control group and 8.00 ± 2.1 in the case group (P=0.00). The mean concentration of TSH was 1.4 ± 0.46 mU/l in the control group and 3.1 ± 0.47 mU/l in the case group (P=0.00, Fig.1A).

Our results showed no significant variation among the mean concentrations of T3, T4, and TSH in the blood samples of second generation infants in the control and case groups (P=0.723). The mean concentration of T3 in the healthy male infants of the second generation of hypothyroid mothers was 1079.33 ± 71.35 pg/dl, in the healthy female infants was 1064.30 ± 80.7 pg/dl and in the both male and female control group, the mean concentration was 1064.90 ± 78.29 pg/dl (P=0.64). The mean concentration of T4 in the healthy infants of the second generation of hypothyroid mothers was 13.3750 ± 1.29 ng/dl for males, and 15.88 ± 1.5 ng/dl for females. Also, in the both control group, the mean concentration was 13.2083 ± 1.35 ng/dl (P=0.76). The concentration of TSH in the healthy male and female infants of the second generation of hypothyroid mothers were 1.65 ± 0.27 mU/l, 1.0.57 ± 7 mU/l respectively, and was 1.75 ± 0.24 mU/l in the both control groups (P=0.33, Fig.1B).
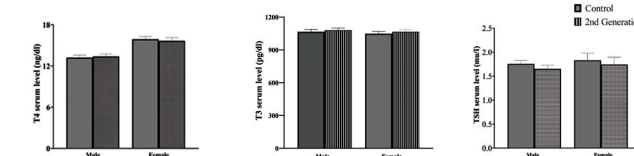

Fig.1: The concentration of T3, T4 and TSH hormones (mean ± SD). **A.** Case (PTU treated mothers) and controls and **B.** Second generation female and male. TSH; Thyroid stimulating hormone.

Comparing the number of pups in the case and control groups

Examining the number of pups in the second-generation rats born from hypothyroid mothers using the t test showed a reduction in the number of pups in the case group compared to the control group, but this difference was not significant for both male and female (P=0.633, Table 1).

Table 1: A glance on the second-generation male rats of hypothyroid mothers

Parameter	Control group	Case group	P value
Number of live births	8.83 ± 1.169	8.20 ± 2.588	0.633
Testicular weight (g)	1.5183 ± 0.04489	1.4867 ± 0.05087	0.12
Testicular volume (cm³)	2.7008 ± 0.04602	2.6767 ± 0.04793	0.221
Maximum diameter of testicles (mm)	20.9167 ± 0.514	20.6667 ± 0.4923	0.237
Minimum diameter of testicles (mm)	11.50 ± 0.522	11.25 ± 0.452	0.223
Number of Leydig cells (per microscopic field 40X)	44.752 ± 2.265	45.959 ± 1.623	0.148
Seminal tube diameter (μm)	1110.46 ± 27.51	1096.04 ± 28.42	0.220
Area of the seminal tube (μm²)	3700.19 ± 14.34	3692.34 ± 16.59	0.229
Motility (%)	56.00 ± 9.74	53.42 ± 8.73	0.501
Morphology (%)	58.92 ± 6.73	56.92 ± 6.77	0.476
Sperm concentration($\times 10^6$/ml)	44.83 ± 9.32	40.91 ± 8.27	0.288

All data are shown in mean ± SD.

Comparing the testicular and ovarian weight and volume of the second-generation rats in the case and control groups

Examining the testicular weight of the second-generation male rats born from hypothyroid mothers showed weight loss in the case group, but this difference was not significant (P=0.120, Table 1). However, a significant decrease in the weight of ovaries for the second-generation female rats born from hypothyroid mothers was seen (P≤0.001).

Also, a decrease in the testicular volume of the second-generation male rats born from hypothyroid mothers was seen, but this difference was not significant (P=0.221, Table 1). Examining the ovarian volume for the second-generation female rats showed a significant decrease in comparison with the control rats (P≤0.001).

Evaluating male reproductive system

The Leydig cells count, the diameters of the seminal tubes and cross-sectional area of the seminiferous tubules in the case group compared to the control group was the same with no significant differences between the two groups (Table 1).

Sperm parameters (morphology, count, motility)

Examining the number, motility and morphology of the sperms in the second-generation male rats using the t test showed a reduction in the second-generation male rats born from hypothyroid mothers, but this reduction was not notable from the control group (P>0.05, Table 1, Fig.2).

Examining the testicular tissue in the second-generation male rats born from hypothyroid mothers found one infertile case with azoospermia (Fig.3).
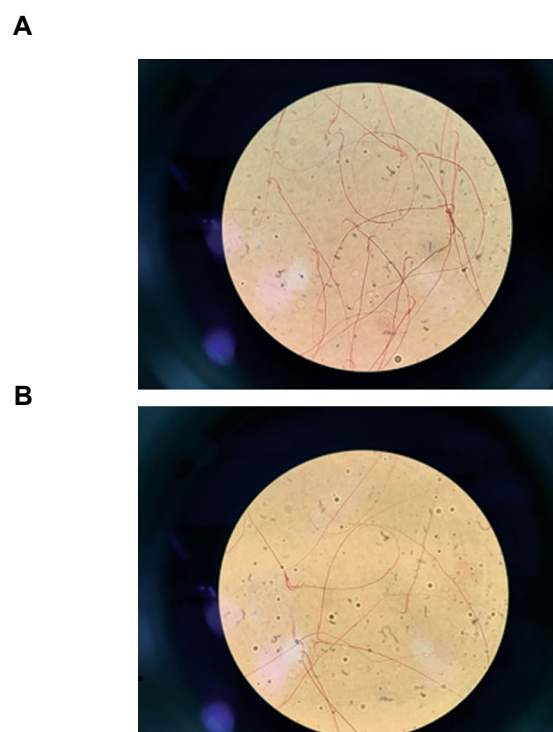

A

B

Fig.2: Papanicolaou staining of semen smear. **A.** Control group and **B.** Case group (magnification: 100X).
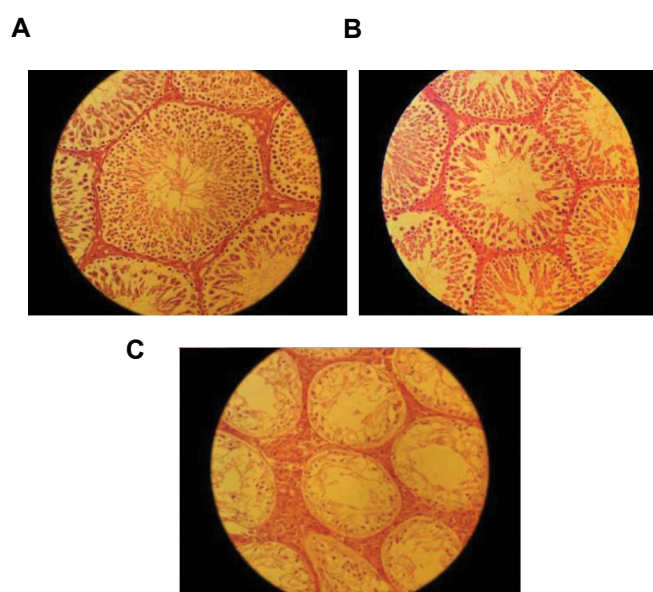
Fig.3: Hematoxylin-Eosin (H&E) Staining of testicular tissue. **A.** Control group, **B.** Case group, and **C.** Azoospermia case (magnification: 40X).
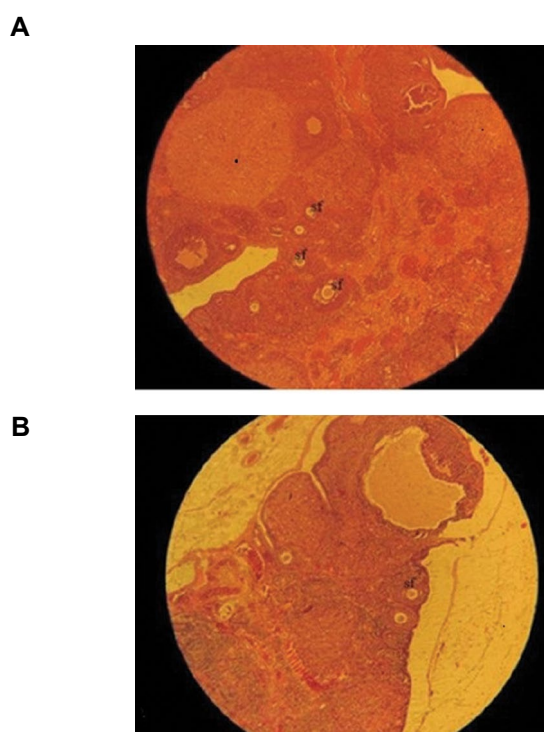
Fig.4: Hematoxylin-Eosin (H&E) staining of ovarian tissue. **A.** Control group and **B.** Case group. (magnification: 10X).

Evaluating the female reproductive system by checking the number of different follicles

Three types of follicles (primary, secondary and Graafian) were counted. The t test analysis showed no significant differences between groups in primary and Graafian follicles count, but the number of secondary follicles was significantly decreased in the case group in comparison with the control group (P≤0.05, Table 2, Fig.4).

Table 2: A glance on the second-generation female rats of hypothyroid mothers

Parameters	Control group	Case group	P value
Number of live births	9.17 ± 1.329	6.00 ± 3.464	0.13
ovarian weight (g)	0.3350 ± 0.019	0.2400 ± 0.013	0.001
ovarian volume (cm³)	0.2843 ± 0.013	0.2479 ± 0.011	0.001
Number of primary follicles	16.60 ± 3.738	14.53 ± 4.503	0.197
Number of secondary follicles	6.09 ± 740	5.48 ± 612	0.025
Number of graafian follicles	0.414 ± 0.140	0.342 ± 0.122	0.163

All data are shown in mean ± SD.

Discussion

The lifestyle of pregnant women may have long-term effects on their children's health. Smoking, alcohol abuse and hypothyroidism diseases are their samples that may affect fetal development and health. Although, genetic factors are an important factor of fetal growth environmental factors. In the present study, examining fertility in the male and female rats showed that the case group had reproductive abilities, but the number of children born from the rats in the case group was insignificantly less than the control group.

A study by Dijkstra et al. (19) showed a decrease in the number of antral follicles, minor non-atretic antral follicles and an increase in the number of atretic follicles in the PTU treated rats and concluded that the folliculogenesis disturb is because of thyroid hormone supply deficiency.

Also, Zertashia et al. (20) reported a significant weight reduction in the ovarian tissue of offspring in the postnatal PTU treatment group in comparison with the control group. They didn't see any notable changes in the ovaries diameters, although, observed a significant increase in the diameters of Graafian follicles. The present study showed a decline in the ovarian volume in the case group. Hypothyroidism inhibits the basal luteinizing hormone (LH) release and could cause ovarian atrophy (21). Decreasing of secondary follicles which seen in our study lead to ovarian hypotrophy.

Thyroid hormone deficiency is associated with changes in the menstrual patterns and associates with menstrual cycle frequency decrease and an increase in menses volume. Thyroid hormones and their transporters, and nuclear thyroid hormone receptors have been discovered in ovarian follicles and in oocyte (22). Thyroid hormone receptors are located in the primordial, primary and secondary follicles with minimal expression in the secondary follicles. This could explain why the number of secondary follicles decreased significantly while this change was not significant in the primary follicles. This means that more of the secondary follicles were destroyed in the response to minimal decreasing changes of thyroid hormones in comparison with the primary and graafian follicles (23).

Hapon et al. reported that hypothyroidism induces various alterations in the hormone profiles of virgin and pregnant rats and induces pseudopregnancy and mammary development in the virgin rats. According Sarkar and Singh (24) study, thyroid hormones play an important role in testicular steroidogenesis and spermatogenesis regulation. In the present study, examining the diameter and the area of the seminiferous tubules indicates no significant differences between the two groups. In a study by Al-Awdan et al. (25) on the testicular tissues of 21-60-day-old rats born from hypothyroid mothers, the diameters of the seminal tubes decreased in the case group, in which the ancestral cells were irregular and the tubes had many degenerated cells. Also, Francavilla et al. (26) study on the structure and function of testicles in the matured rats born from hypothyroid mothers during prenatal and postnatal period showed that they had no effect on their testicular development and morphological changes in adulthood, and the diameter of the tubules was not significantly different between the case and control groups. These researchers also stated that hypothyroidism in the 60-day-old male rats reduces the diameter of the seminal tubes, reduces the number of interstitial cells, and delays spermatogenesis; they also found delayed testicle maturation in the rats who had transient hypothyroidism at birth. In the present study, there was no significant change in the number of Leydig cells between two groups. Opposite to our result, Canale et al. (27) concluded that hypothyroidism in the first generation increases the testicle size without increasing the number of androgens, which is due to the inactivation of the Leydig cells. Valle et al. (28) examined the Leydig cells in the 40-day-old male rats and concluded that hypothyroidism in the young male rats reduces the number of LH receptors on the Leydig cells during puberty. Mendis-Handagama and Ariyaratne (29) also found that hypothyroidism delays the onset of the differentiation of mesenchymal progenitor cells into Leydig cells. In the present study, sperm parameters exhibited a reduction in the case group in comparison with the control rats, but this difference was not significant. Epigenetic information of the male

germ lines will be changed by the alteration in the thyroid hormone level. This information changes can transmit to future generations. This could be applicable for follicles of the ovary (27).

La Vignera et al. (30) study showed thyrotoxicosis and thyroid hormone deficiency are associated with changes that affect the sexual behavior, or reproductive functions. Particularly, the concentration of free and bioavailable testosterone of hyperthyroid patients was lower than the control group. The increasing rate of astheno-zoospermia, oligo-zoospermia, and terato-zoospermia, and high prevalence of sexual disturbances, such as premature ejaculation (PE) was seen in the hypothyroidism group in comparison with the control group. Dick et al. (31) indicated that hyperthyroidism is associated with PE and delaying ejaculation (DE) which can cause fertility issues. A study on the seminal tubes of male rats born from hypothyroid mothers found no sperm in the tubes (25) that has harmony with our study which showed a rat with azospermia in the second generation. Amer's et al. (32) study showed that defective thyroid function was associated with an increased risk of infertility. Koyyada and Orsu (33) mentioned that the occurrence of preterm delivery and abortion is associated with untreated hypothyroidism in pregnant mothers. Nonetheless, there was no study on the effect of maternal hypothyroidism on testicular and ovarian tissue and sperm parameters in second-generation male rats.

Conclusion

It can be concluded that the second-generation offspring of the hypothyroid mothers experienced a reduction in the number of sperm cells, sperm morphology and motility in male rats and reduction in the number of secondary follicles in female rats compared to the control group. This could indicate that these differences in first generation rats due to maternal hypothyroidism could show themselves in the second-generation rats, but with a lesser impact, or in other word, they could be corrected in the following generation.

Acknowledgements

Authors' Contributions

F.P., F.F., M.P.; Involved in study plan, data collection, assessment and drafting. S.Kh.; Determined the size of the statistical population, performed statistical analysis and prepared the graphs. F.P., Z.A., Z.E.; Performed all experimental, histological work and hormonal assay data. F.P.; Performed editting. K.P.; Prepared the scientific resources required for study, performed editing. All authors read and approved the final manuscript.

References

1. El-Sayed MS, El Badawy A, Abdelmoneim RO, Mansour AE, Khalil MEM, Darwish K. Relationship between serum sialic acid concentration and diabetic retinopathy in Egyptian patients with type 2 diabetes mellitus. Benha Med J. 2018; 35(2): 257.
2. Poppe K, Velkeniers B, Glinoer D. Thyroid disease and female reproduction. Clin Endocrinol (Oxf). 2007; 66(3): 309-321.
3. Rastogi MV, LaFranchi SH. Congenital hypothyroidism. Orphanet J Rare Dis. 2010; 5: 17.
4. Hou J, Yu P, Zhu H, Pan H, Li N, Yang H, et al. The impact of maternal hypothyroidism during pregnancy on neonatal outcomes: a systematic review and meta-analysis. Gynecol Endocrinol. 2016; 32(1): 9-13.
5. Pop VJ, Kuijpens JL, van Baar AL, Verkerk G, van Son MM, de Vijlder JJ, et al. Low maternal free thyroxine concentrations during early pregnancy are associated with impaired psychomotor development in infancy. Clin Endocrinol (Oxf). 1999; 50(2): 149-155.
6. Morreale de Escobar G, Obregón MJ, Escobar del Rey F. Is neuropsychological development related to maternal hypothyroidism or to maternal hypothyroxinemia? J Clin Endocrinol Metab. 2000; 85(11): 3975-3987.
7. Klein RZ, Sargent JD, Larsen PR, Waisbren SE, Haddow JE, Mitchell ML. Relation of severity of maternal hypothyroidism to cognitive development of offspring. J Med Screen. 2001; 8(1): 18-20.
8. Pop VJ, Brouwers EP, Vader HL, Vulsma T, van Baar AL, de Vijlder JJ. Maternal hypothyroxinaemia during early pregnancy and subsequent child development: a 3-year follow-up study. Clin Endocrinol (Oxf). 2003; 59(3): 282-288.
9. Hamouli-Said Z, Tahari F, Hamoudi F, Hadj-Bekkouche F. Comparative study of the effects of pre and post natal administration of a thyroid drug on testicular activity in adult rat. Folia Histochem Cytobiol. 2007; 45 Suppl 1: S51-57.
10. Saki F, Dabbaghmanesh MH, Ghaemi SZ, Forouhari S, Ranjbar Omrani G, Bakhshayeshkaram M. Thyroid function in pregnancy and its influences on maternal and fetal outcomes. Int J Endocrinol Metab. 2014; 12(4): e19378.
11. Cabello G, Wrutniak C. Thyroid hormone and growth: relationships with growth hormone effects and regulation. Reprod Nutr Dev. 1989; 29(4): 387-402.
12. Patel J, Landers K, Li H, Mortimer RH, Richard K. Delivery of maternal thyroid hormones to the fetus. Trends Endocrinol Metab. 2011; 22(5): 164-170.
13. Blazer S, Moreh-Waterman Y, Miller-Lotan R, Tamir A, Hochberg Z. Maternal hypothyroidism may affect fetal growth and neonatal thyroid function. Obstet Gynecol. 2003; 102(2): 232-241.
14. Mitchell ML, Klein RZ. The sequelae of untreated maternal hypothyroidism. Eur J Endocrinol. 2004; 151 Suppl 3: U45-48.
15. Obregon MJ, Calvo RM, Escobar Del Rey F, Morreale de Escobar G. Ontogenesis of thyroid function and interactions with maternal function. Endocr Dev. 2007; 10: 86-98.
16. Hapon MB, Gamarra-Luques C, Jahn GA. Short term hypothyroidism affects ovarian function in the cycling rat. Reprod Biol Endocrinol. 2010; 8: 14.
17. Pirahanchi Y, Tariq MA, Jialal I. Physiology, thyroid. StatPearls. 2020. Available from: https://www.ncbi.nlm.nih.gov/books/NBK519566/ (25 Apr 2021).
18. Safarpour S, Zabihi E, Ghasemi-Kasman M, Nosratiyan N, Feizi F. Prenatal and breastfeeding exposure to low dose of diethylhexyl phthalate induces behavioral deficits and exacerbates oxidative stress in rat hippocampus. Food Chem Toxicol. 2021; 154: 112322.
19. Dijkstra G, de Rooij DG, de Jong FH, van den Hurk R. Effect of hypothyroidism on ovarian follicular development, granulosa cell proliferation and peripheral hormone levels in the prepubertal rat. Eur J Endocrinol. 1996; 134(5): 649-654.
20. Zertashia A, Jalali S, Ahmad L, Mirza A. Effect of hypothyroidism induced by propylthiouracil on ovarian function and structure in offspring from treated mothers (Rats). J Exp Zool. 2002; 293(4): 407-413.
21. Ortega E, Rodriguez E, Ruiz E, Osorio C. Activity of the hypothalamo-pituitary ovarian axis in hypothyroid rats with or without triiodothyronine replacement. Life Sci. 1990; 46(6): 391-395.

22. Colella M, Cuomo D, Giacco A, Mallardo M, De Felice M, Ambrosino C. Thyroid hormones and functional ovarian reserve: systemic vs. peripheral dysfunctions. J Clin Med. 2020; 9(6): 1679.

23. Aghajanova L, Stavreus-Evers A, Lindeberg M, Landgren BM, Sparre LS, Hovatta O. Thyroid-stimulating hormone receptor and thyroid hormone receptors are involved in human endometrial physiology. Fertil Steril. 2011; 95(1): 230-237.

24. Sarkar D, Singh SK. Effect of neonatal hypothyroidism on prepubertal mouse testis in relation to thyroid hormone receptor alpha 1 (THRα1). Gen Comp Endocrinol. 2017; 251: 109-120.

25. Al-Awdan AE-WA, Idrees SE, Shalaby SA, Mehlab EM, Mannawy SM. Prenatal and postnatal effects of hypothyroidism and thyroxin replacement on the development of rat testis. Am J Sci. 2014; 10(9).

26. Francavilla S, Cordeschi G, Properzi G, Di Cicco L, Jannini EA, Palmero S, et al. Effect of thyroid hormone on the pre- and post-natal development of the rat testis. J Endocrinol. 1991; 129(1): 35-42.

27. Canale D, Agostini M, Giorgilli G, Caglieresi C, Scartabelli G, Nardini V, et al. Thyroid hormone receptors in neonatal, prepubertal, and adult rat testis. J Androl. 2001; 22(2): 284-288.

28. Valle LB, Oliveira-Filho RM, Romaldini JH, Lara PF. Pituitary-testicular axis abnormalities in immature male hypothyroid rats. J Steroid Biochem. 1985; 23(3): 253-257.

29. Mendis-Handagama SM, Ariyaratne HB. Differentiation of the adult Leydig cell population in the postnatal testis. Biol Reprod. 2001; 65(3): 660-671.

30. La Vignera S, Vita R, Condorelli RA, Mongioì LM, Presti S, Benvenga S, et al. Impact of thyroid disease on testicular function. Endocrine. 2017; 58(3): 397-407.

31. Dick B, Koller C, Herzog B, Greenberg J, Hellstrom WJ. The role of hormones in male sexual function. Curr Sex Health Rep. 2020: 1-12.

32. Amer MH, Thuwain MM, AL-Snafi A. Investigation of thyroids dysfunction among infertile women in Nasiriyah city. Int J Curr Pharm Res. 2020; 12(5): 31-34.

33. Koyyada A, Orsu P. Role of hypothyroidism and associated pathways in pregnancy and infertility: Clinical insights. Tzu Chi Med J. 2020; 32(4): 312-317.

Original Article

The Impact of Different Cell Culture Mediums on CD8⁺ T Cells Expansion: A Bioinformatics Study

Arsalan Jalili, M.Sc.[1, 2], Abbas Hajifathali, M.D.[3], Ahmad Bereimipour, M.Sc.[2, 4], Elham Roshandel, Ph.D.[3]*,

Nasser Aghdami, M.D., Ph.D.[5]*

1. Department of Applied Cell Sciences, Faculty of Basic Sciences and Advanced Medical Technologies, Royan Institute, ACECR, Tehran, Iran
2. Department of Stem Cells and Developmental Biology, Cell Science Research Center, Royan Institute for Stem Cell Biology and Technology, ACECR, Tehran, Iran
3. Hematopoeitic Stem Cell Research Center, Shahid Beheshti University of Medical Sciences, Tehran, Iran
4. Faculty of Sciences and Advanced Technologies in Biology, University of Science and Culture, Tehran, Iran
5. Department of Regenerative Medicine, Cell Science Research Center, Royan Institute for Stem Cell Biology and Technology, ACECR, Tehran, Iran

Corresponding Address: P.O.Box: 1985711151, Hematopoeitic Stem Cell Research Center, Shahid Beheshti University of Medical Sciences, Tehran, Iran
P.O.Box: 16635-148, Department of Regenerative Medicine, Cell Science Research Center, Royan Institute for Stem Cell Biology and Technology, ACECR, Tehran, Iran
Emails: elham.roshandel@gmail.com, nasser.aghdami@royaninstitute.org

Abstract

Objective: Different Cell Culture medias can affect the expansion of T cells. The aim of this study is to assess signaling pathways, protein interactions and genes in T cells cultured in different common T cell expansion medias to select the best candidate.

Materials and Methods: In this in silico observational study, with the use of bioinformatics analysis and the use of enrichment databases, gene expression profiles were investigated using microarray analysis.

Results: The results of this study were the joint selection of 26 upregulated genes and 59 downregulated genes that were involved in SREBP control of lipid synthesis, co-stimulatory signal during T-cell activation mitosis and chromosome dynamics, telomeres, telomerase, and cellular aging signal pathways.

Conclusion: Using bioinformatics analyzes, integrated and regular genes were selected as common genes *CD80, LST1, ATM* and *ITM2B in 4-1BBL, Akt* inhibitor, interleukin 7 and 15 expansion media.

Keywords: Expansion, Microarray, TCD8⁺ Cells

Introduction

T cell immunotherapy is a well-known treatment method for many infectious diseases and cancers. Over the years, extensive studies and research have been done to solve this treatment method's problems and improve the quality of treatment (1). One of the subtypes of T cells, called CD8⁺ T cells, have a lethal property against abnormal cells and by destroying them, can restore the balanced condition in immune system. This feature has made these cells as a great therapeutic tool for many clinical complications, such as post bone marrow transplantation infections with high mortality annually (2). So far, a lot of research has been done to make the best use of these cells for treatment, which unfortunately was either very expensive or they could not produce a cost effective high quality product with adequate quantity (3). Due to the importance of T-cell therapy in immunocompromised patients and the crucial role of these cells in thymus regeneration, providing the appropriate number of proliferating cells can be really vital.

Therefore, increasing the division of CD8⁺ cells and their optimal growth quality is very important. To do this, finding precise molecular pathways and effective mechanisms of cell culture media affecting CD8⁺ cells can improve CD8⁺ cells expansion. By combining different culture media a better effect on CD8⁺ cell quality can be achieved. Various studies have been done on CD8⁺ cells expansion in the last few years. Each of them had their own unique theories. However, the study of several culture media's molecular mechanisms on CD8⁺ cells expansion has not yet been elucidated (4).

Due do all the aforementioned reasons, bioinformatics is a very good way to accurately identify molecular pathways, the genes involved in them, and the function and relationship between their protein products. Over the past decade, bioinformatics, particularly gene expression profile, has played a significant role in the discovery of signaling pathways which can be used to identify the relationship between CD8⁺ cells expansion condition media and pathways affected by these media more accurately (5).

Accordingly, this study aimed to investigate the datasets correlated with T cell expansion media with each other, classification of genes and common signaling pathways between them, and finally the genes and pathways

involved in cell division, cytoskeletal dynamics, activation and stimulation of CD8+ cells.

Methods and Materials

Gene expression profile datasets

This original study was performed based on bioinformatics analysis by Hematopoietic Stem Cell Research Center of Shahid Beheshti University of Medical Sciences and Department of Stem Cells and Developmental Biology of Royan institute. For this study, 3 datasets from the GEO database (https://www.ncbi.nlm.nih.gov/geo) were selected according to the purpose of this study. GSE86284 examines CD8+ lymphocyte cell expansion using 4-1BBL medium. GSE41909, using interleukin 7 and 15 medium, examines lymphocyte cells in the central memory and naive cells, and GSE98078 deals with Akt inhibitor media. Figure 1 shows the schematic pathway of bioinformatics analysis.

Preparing gene expression profile data for additional analysis

We extracted each of these data separately from GEO database and categorized the upregulated and downregulated genes in an Excel file. At this stage, P<0.05 was selected to isolate the genes. Then, upregulated and downregulated genes were separately plotted in the venny diagram, and the intersection genes were isolated and prepared for further analysis.

Signaling pathways analysis

We entered the common genes from the four desired modes in question separately to examine the signaling pathways in the Enrichr database (https://amp.pharm.mssm.edu/Enrichr). Then, through Biocarta database, we categorized the signaling pathways corresponding to the genes with high and low expression. In this section, P<0.05 was selected.

Investigating the genes ontology

To examine the three important components, namely molecular functions, biological processes, and cellular components, we again performed the necessary evaluations from the Enrichr database in the GO subset.

Studying the correlation between proteins

In the first part of the study, we used STRING database (https://string-db.org) to investigate the relationship between the protein products derived from common genes, and separately examined the upregulated and downregulated genes.

Results

Cell division, cytoskeletal dynamics, and pathways associated with activation and stimulation of T cells were more pronounced in shared expansion media.

Gene expression profile analysis of GSE86284, GSE41909 and GSE98078 datasets showed that 26 genes upregulated and 59 genes downregulated in four groups of CD8+ lymphocytes in the expansion culture medium. SREBP control of lipid synthesis, RNA polymerase III transcription, co-stimulatory signal during T-cell activation, PKC-catalyzed phosphorylation, mTOR, Rho cell motility and Rac 1 cell motility signaling pathways for upregulated genes and protein kinase A at the centrosome, T cell receptor signaling, cdc25 and chk1 regulatory, TSP-1 induced apoptosis in microvascular endothelial cell, AKAP95 role in mitosis and chromosome dynamics, telomeres, telomerase, cellular aging and immortality, and IL-7 signal transduction signaling pathways for downregulated genes were identified. Figure 2 shows the selection of genes with up/downregulated genes and that were common in culture media obtained by venny diagram and investigation of signaling pathways between common genes identified based on P value and also, Table 1 shows the most important involved and intersection genes between expansion culture media based on their expression.
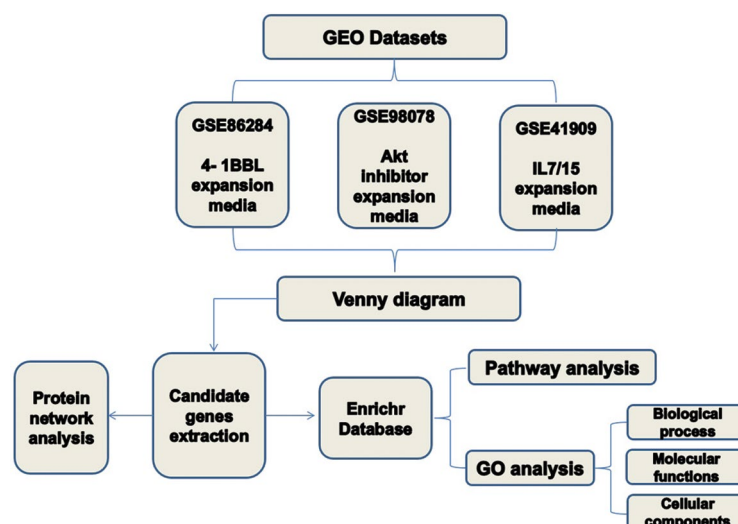

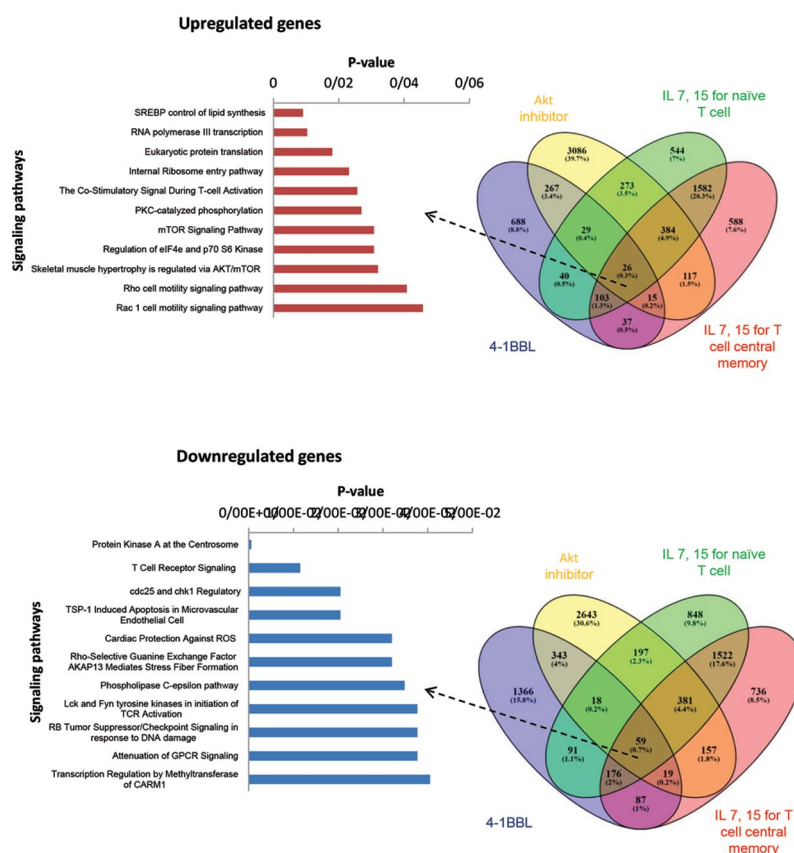**Fig.1:** Schematic pathway of bioinformatics analysis.

Fig.2: Selection of genes with up/downregulated genes and that were common in culture media obtained by venny diagram (right). Investigation of signaling pathways between common genes identified based on P value (left).

Table 1: The most important involved and intersection genes between expansion culture media based on their expression

Gene symbol	Expansion media Log FC			
Upregulated genes				
	Akt inhibitor	4-1BBL	IL 7, 15 for naïve CD8 [+] cells	IL 7, 15 for CD8 [+] central memory
MBTPS2	0.212	0.8626975	0.49437857	0.41288571
GTF3C4	0.364	0.5169238	0.55612475	0.44324705
EIF4E	0.195	2.0968478	0.314085	0.31697059
CD80	2.13	1.1257803	2.49266806	2.04126263
ARHGEF5	0.499	1.4043171	0.3970478	0.52683412
LST1	0.306	1.1870456	2.53155006	2.35809529
PALLD	1.12	0.853437	1.47607414	2.20898005
ATP2C1	0.654	0.5136197	0.48385932	0.22093148
Downregulated genes				
FYN	-0.341	-0.4571853	-1.23132161	-1.42432493
ATM	-0.203	-0.6682416	-1.9654061	-1.50466176
TNKS	-0.144	-1.9316892	-0.60104772	-0.53512023
USP34	-0.175	-0.5955263	-0.53382035	-0.73738285
TBL1X	-0.375	-0.5246813	-0.74522811	-0.75279683
CAPRIN2	-0.269	-0.590714	-1.29518457	-0.80439361
DYRK2	-0.173	-0.6906726	-0.73330931	-0.86589672
CLSTN1	-0.2	-0.5703692	-0.38479256	-0.58479503
ITM2B	-0.384	-0.8688779	-0.71092999	-0.59110175

Gene ontology analysis

This section evaluated up and downregulated genes in three parts: biological processes, molecular functions and cellular components. Negative regulation of lymphocyte proliferation (GO:0050672), negative regulation of cellular response to hypoxia (GO:1900038), release of sequestered calcium ion into cytosol by sarcoplasmic reticulum (GO:0014808), regulation of T-helper 1 cell differentiation (GO:0045625), positive regulation of interleukin-2 biosynthetic process (GO:0045086), positive regulation of T-helper 1 type immune response (GO:0002827), microtubule anchoring (GO:0034453) and positive regulation of granulocyte macrophage colony-stimulating factor production (GO:0032725) biological processes also RNA binding (GO:0003723), hydrogen-exporting ATPase activity, phosphorylative mechanism (GO:0008553), inositol trisphosphate phosphatase activity (GO:0046030), calcium-transporting ATPase activity (GO:0005388) and alpha-actinin binding (GO:0051393) molecular functions were identified in intersection of upregulated genes. On the other hand, positive regulation of canonical Wnt signaling pathway (GO:0090263), intracellular protein transport (GO:0090316), telomere maintenance (GO:0032206) and fibroblast migration (GO:0010763), as well as biological processes and also NAD+ ADP-ribosyltransferase activity (GO:0003950), protein serine/threonine kinase activity (GO:0004674), transferase activity, transferring pentosyl groups (GO:0016763) and cAMP-dependent protein kinase activity (GO:0004691) molecular functions were observed in downregulated genes. Figure 3 shows the common genes selected from the previous step were examined in three different modes of cellular components, biological processes, and molecular functions.

Protein- protein interactions network analysis

Examination of the protein-protein relationship revealed that there were 61 nodes and 42 edges for downregulated proteins and 125 nodes and 72 edges for upregulated proteins participated in network. Figure 4 shows the association between the upregulated proteins.
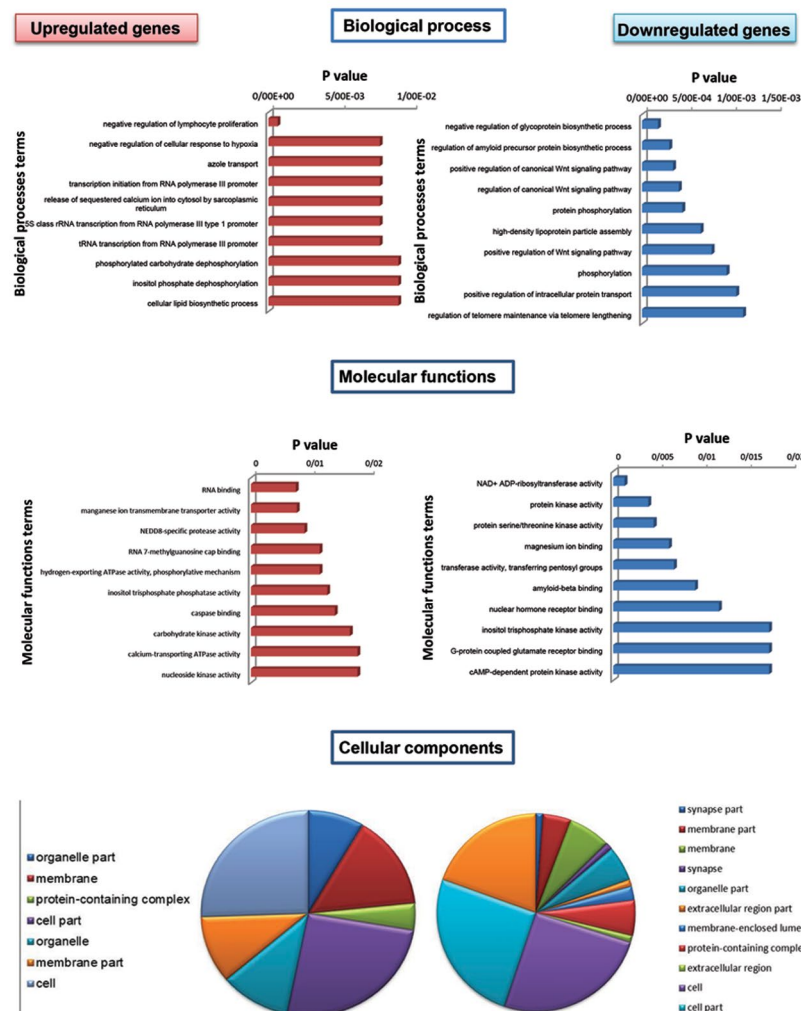

Fig.3: Common genes selected from the previous step were examined in three different modes of cellular components, biological processes, and molecular functions.
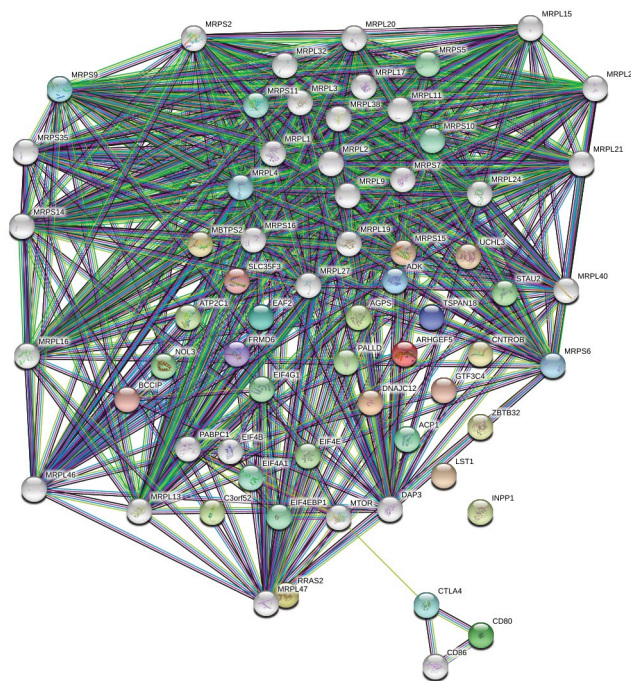
158

Fig.4: In this image, the association between the upregulated proteins was examined.

Discussion

T cell expansion, especially CD8, division, proper and timely differentiation, and a large amount of cell memory, are of importance in various diseases related to the immune system. Finding necessary and involved regulatory elements and their role in T cell expansion can provide suitable solutions for further studies. Therefore, in this study, different pathways related to division, differentiation, cytoskeletal dynamics, and activation and stimulation of T cells, were selected more prominently.

In the first part, we examined the effect of expansion media on T cells. 4-1BBL is involved as a vital culture medium in T cell expansion. In HIV-specific T cells study, it was found that 4-1BBL, by acting on a TNF receptor factor dependent on the BIM pro-apoptotic molecule, could reduce cell apoptosis and crucial molecules. Other markers such as CD70, increased the efficiency of T cells (6). Another study proved that 4-1BBL, by increasing the transcription factors of Cyclin D2/D3, naturally increases the expression of these molecules. In turn, increased expression of these two molecules increases the expression of Cyclin E. On the other hand, the presence of 4-1BBL in the environment of T cells reduces the expression of P27^{kip1} inhibitor and as a result of this activity, division of T cells is facilitated (7). Dealing with tumor cells is also one of the problems of today's research. A study showed that the presence of CD80 and 4-1BBL can betterly activate and stimulate cells and make them perform better against tumors (8). The production of cytokines is significant for increasing the function of T cells. In one study, production of cytokines in T cells was increased and a synergistic effect with interleukin-2 was achieved (9).

Another dataset examined in this study was the expansion medium mediated by Akt inhibitor. One of the critical roles in T cell expansion is to regulate the memory of these cells. The inhibition of Akt activates MAPK and FOXO1, which is an essential regulator of T cell memory and can play an important role in the discussion of immune compatibility. It is found in the differentiation of cells in two types of cell populations. One is useful cells with a short-lived effector cell (SLECs), and the other is memory precursor cells (MPECs). The study showed that inhibition of PI3K/Akt could play an active role in cell expansion by stimulating and strengthening their memory (10). A different study on leukemia cancer mouse model showed that inhibition of Akt in CD19CAR cells could increase the immune compatibility and memory formation in these cells, which also had significant antitumor properties (11). An almost similar study was performed to evaluate T cells' final differentiation and the formation of immune compatibility in the face of tumors on suspicious stem cells in an environment with Akt inhibitors, which showed acceptable efficacy (12).

Another dataset examined in this study is related to interleukins 15 and 7. Interleukins are important cytokines that can affect the activity of other lymphocytes.

One of the studies showed that, when IL-7 affects EBV-specific T cells, cause cell division, survival and cytotoxicity in them (13). Numerous other studies have also shown the role of restoration and induction of homeostasis in T cells by interleukin-7 (14). Another fascinating study in human immunodeficiency virus (HIV) patients showed that interleukin 7 had a significant therapeutic and recovery effect on T lymphocytes and played an important role in cell division and homeostasis (15). The relationship between expansion and CD19 CART cells was investigated using interleukins 15 and 7 in lymphoids. The results showed that these two interleukins' affect reduces apoptosis of T cells and increase memory in their stem cells (16). Various other studies have been performed on interleukin-15. Zeng et al. (17) study showed that in melanoma-mouse model, interleukin 15 had a strong synergistic effect with interleukin-21 and played a vital role in enhancing memory and expansion and division of T cells.

In another study with *mouse models* with selective deficiency in *NK cells, it was shown that,* the addition of interleukin-15 to the existing body could play an effective role in regenerating the development and memory of T cells and NK (18). In HIV infection, interleukin 15 has been shown to play a significant role in the activation and expansion of T cells at high levels (19). Another study proved that there is a correlation between dendritic cells and NK in lymphoid organs. The presence of interleukin-15 in dendritic cells increases the viability, division, and maturation of NK cells (20). Another study showed that interleukin-15 increased the homeostasis and the division of CD8 nasal cells and played an important role in expanding these cells (21).

In the next step, we shared the datasets and obtained multiple genes in different paths. Based on the literature, we selected the most relevant signaling pathways with T cell expansion and their characteristics, and based on this, we selected some of them. In contrast, we examined common genes for GO and finally isolated important genes.

Wnt signal pathway is one of the pathways identified in this study which plays a wide variety of cell roles. This pathway plays a significant role in development, cell division, and differentiation of activity. But in T cells, high and low expression of genes involved in this pathway play attractive roles in expansion. Low expression of genes in Wnt pathway accelerates the differentiation of T cells. On the other hand, low expression of genes in this pathway increases cell division and is also effective in increasing T cells' memory. Therefore, it can act as a secondary stimulant of T cells and perform better during vaccination (22). In naive T cells, the issue is different, and activation of Wnt/B catenin pathway inhibits differentiation in naive T cells. Further investigation of this pathway and its regulation can be a good option for the function of naive T cells (23). Another study showed that modulation of Wnt pathway had an acceptable effect on T cells' production with a better memory to increase immune adaptation efficiency (24).

T cells' fate depends on several pathways, such as growth factors, cytokines, cell division, and various metabolic pathways. mTOR is one of the most important pathways involved in controlling many cellular processes. When mTOR is inhibited, it can increase the tolerance of competent Th1 cells. mTOR activation is necessary for the differentiation of Th1 / 2/17 cells, and its inhibition is required for differentiation into Foxp3 regulatory T cells (25). Another study showed that temporal inhibition of leptin/mTOR pathway in the absence of interleukin-2 resulted in better differentiation of regulatory T cells, which could play a significant role in immune adaptation and autoimmune diseases (26). The hemostatic division is one of the important mechanisms in T cells to deal with different tumors. One study found that interleukin-7 and interleukin-15 indirectly affected mTOR pathway activity. Accordingly, naive T cells are involved in two important transcription factors for hemostatic division, T. bet, and eomesoderm. CD122 is included in the development of eomezodermine expression. When mTOR pathway is inhibited, T.bet and CD122 are also inhibited, but eomezodermin can act indirectly by adding interleukin-15 to the medium, ultimately increasing the memory of T cells to fight tumor cells (27). Binding proteins of sterol regulatory elements are important pathways in the production of lipids and fatty acids involved in many T cellular processes such as growth, division, post-translational mechanisms, cell motility, and tectonic activity. mTOR is directly related to SERBP and mTOR activity in the Golgi membrane and endoplasmic reticulum effectively facilitates lipid production process (28).

Cell motility is one of the most important pathways in developing and differentiation of cells from an early population. Rho and Rac1 are two vital proteins involved in cytoskeletal dynamics as well as actin filaments activity. Various studies have highlighted the importance of these two proteins with hematopoietic cells as well as lymphocytes. One of these studies showed that Rac1/2 was necessary for the initial expansion of hematopoietic cells in the bone marrow, but when they go to the spleen and the cells reach maturity, this group's protein expression decreases. One of the critical factors for clustering T cells together is the binding of T cell receptor antigen (29). NF-KB transcription factor also increases when the coupling between antigen and T cells occurs. The inhibition of PI3K activity inhibits the NF-KB pathway and reduces the clustering of T cells. Thus, increasing Rho pathway activity helps regenerate NF-KB pathway and the aggregation of T cells together, which is involved as a different pathway (30). PYGM is one of the glycogen phosphorylation isoforms with a high enzymatic role in muscle and is useful in cell division. One study showed that stimulation of T cells with interleukin-2 induced PYGM activity, which also affected Rac1. Finally, this study showed that in the presence of interleukin 2 pathways, PYGM/Rac1 has a high activity for T cell division (31). MEKK3 is a member of the MAPK family and is a serine/threonine protein, which has been continuously seen in T cells. A study showed that in a MEKK3 deficient mouse model, the immune system's response to bacterial infections is greatly reduced, and interferon-gamma, derived from interleukins 12 and 18, is not produced or is produced in minimal amounts. Besides, defects in MEKK3 cause weakness in ERK1/2, JNK, and P38 pathways. However, activation of Rac1/2 activates MEKK3 and produces cytokines (32).

One of the important data in this study was the sharing of CD80 with significant expression in each expansion culture media. CD80 is also an important co-stimulantory molecule in the immune system and response to various pathogens. Extensive studies have examined the association of CD80 with the immune system and its various pathways. CD80, 86, and 28 have high stimulatory activity in T cells and are effective in the immune response and production of interleukin-2 (33). Another study on a mouse model of lymphocytic choriomeningitis virus infection showed that the presence of CD80 and 86 were effective in boosting T cell memory and fighting a viral infection (34). An exciting study in rheumatoid arthritis showed that CD80 and 86 molecules' activity affects the differentiation and activity of B cells and the integration of blood vessels and causes the autocrine effect on T cells, which helps the strengthen of the immune system (35). Another study on HIV infection showed that the activity and presence of CD80 causes a more robust response of T cells to the virus (36). Programmed death-ligand is one of the most critical proteins on the surface of cancer cells that acts as a protector against these cells, and T cells are unable to respond to them. Therefore, if

present, CD80 molecule causes repression, and T cells can respond to these cells more effectively (37). Also, the activity of interleukin 12 and CD80 has increased the antitumor property of T cells in breast and ovarian cancer (38). A study showed that CD80 and 86 with autocrine effect for the long time, can have an acceptable effect for T cells. CD80 also has a positive impact on repairing T cell tolerance (39).

Conclusion

Finally, it can be said that this study examines the expansion environments used on T cells, and the signaling pathways, genes, and proteins shared between these pathways play a significant role in improving the function of T cells with the approach of increasing the cell division. They had memory, immune compatibility, and, ultimately, stimulation and activation of T cells. Among these, CD80 genes were selected as essential genes in these pathways.

Acknowledgments

Authors' Contributions

A.J., A.B.; Participated in study design, data collection and evaluation, drafting, and statistical analysis. A.H., E.R., N.A.; Designing the project and corresponding. All authors performed editing and approving the final version of this manuscript.

References

1. Ottaviano G, Chiesa R, Feuchtinger T, Vickers MA, Dickinson A, Gennery AR, et al. Adoptive T cell therapy strategies for viral infections in patients receiving haematopoietic stem cell transplantation. Cells. 2019; 8(1): 47.
2. Wang W, Green M, Choi JE, Gijón M, Kennedy PD, Johnson JK, et al. CD8+ T cells regulate tumour ferroptosis during cancer immunotherapy. Nature. 2019; 569(7755): 270-274.
3. Shrestha B, Zhang Y, Yu B, Li G, Boucher JC, Beatty NJ, et al. Generation of antitumor T cells for adoptive cell therapy with artificial antigen presenting cells. J Immunother. 2020; 43(3): 79-88.
4. Weiss L, Letimier FA, Carriere M, Maiella S, Donkova-Petrini V, Targat B, et al. In vivo expansion of naive and activated CD4+CD25+FOXP3+ regulatory T cell populations in interleukin-2-treated HIV patients. Proc Natl Acad Sci USA. 2010; 107(23): 10632-10637.
5. Wu D, Rice CM, Wang X. Cancer bioinformatics: a new approach to systems clinical medicine. BMC Bioinformatics. 2012; 13: 71.
6. Wang C, Wen T, Routy JP, Bernard NF, Sekaly RP, Watts TH. 4-1BBL induces TNF receptor-associated factor 1-dependent Bim modulation in human T cells and is a critical component in the costimulation-dependent rescue of functionally impaired HIV-specific CD8 T cells. J Immunol. 2007; 179(12): 8252-8263.
7. Lee HW, Nam KO, Park SJ, Kwon BS. 4-1BB enhances CD8+ T cell expansion by regulating cell cycle progression through changes in expression of cyclins D and E and cyclin-dependent kinase inhibitor p27kip1. Eur J Immunol. 2003; 33(8): 2133-2141.
8. Stephan MT, Ponomarev V, Brentjens RJ, Chang AH, Dobrenkov KV, Heller G, et al. T cell-encoded CD80 and 4-1BBL induce auto- and transcostimulation, resulting in potent tumor rejection. Nat Med. 2007; 13(12): 1440-1449.
9. Wen T, Bukczynski J, Watts TH. 4-1BB ligand-mediated costimulation of human T cells induces CD4 and CD8 T cell expansion, cytokine production, and the development of cytolytic effector function. J Immunol. 2002; 168(10): 4897-4906.
10. Klebanoff CA, Crompton JG, Leonardi AJ, Yamamoto TN, Chandran SS, Eil RL, et al. Inhibition of AKT signaling uncouples T cell differentiation from expansion for receptor-engineered adoptive immunotherapy. JCI Insight. 2017; 2(23): e95103.
11. Urak R, Walter M, Lim L, Wong CW, Budde LE, Thomas S, et al. Ex vivo Akt inhibition promotes the generation of potent CD19CAR T cells for adoptive immunotherapy. J Immunother Cancer. 2017; 5: 26.
12. van der Waart AB, van de Weem NM, Maas F, Kramer CS, Kester MG, Falkenburg JH, et al. Inhibition of Akt signaling promotes the generation of superior tumor-reactive T cells for adoptive immunotherapy. Blood. 2014; 124(23): 3490-3500.
13. Perna SK, Pagliara D, Mahendravada A, Liu H, Brenner MK, Savoldo B, et al. Interleukin-7 mediates selective expansion of tumor-redirected cytotoxic T lymphocytes (CTLs) without enhancement of regulatory T-cell inhibition. Clin Cancer Res. 2014; 20(1): 131-139.
14. Boyman O, Ramsey C, Kim DM, Sprent J, Surh CD. IL-7/anti-IL-7 mAb complexes restore T cell development and induce homeostatic T Cell expansion without lymphopenia. J Immunol. 2008; 180(11): 7265-7275.
15. Sereti I, Dunham RM, Spritzler J, Aga E, Proschan MA, Medvik K, et al. IL-7 administration drives T cell-cycle entry and expansion in HIV-1 infection. Blood. 2009; 113(25): 6304-6314.
16. Xu Y, Zhang M, Ramos CA, Durett A, Liu E, Dakhova O, et al. Closely related T-memory stem cells correlate with in vivo expansion of CAR.CD19-T cells and are preserved by IL-7 and IL-15. Blood. 2014; 123(24): 3750-3759.
17. Zeng R, Spolski R, Finkelstein SE, Oh S, Kovanen PE, Hinrichs CS, et al. Synergy of IL-21 and IL-15 in regulating CD8+ T cell expansion and function. J Exp Med. 2005; 201(1): 139-148.
18. Schluns KS, Williams K, Ma A, Zheng XX, Lefrançois L. Cutting edge: requirement for IL-15 in the generation of primary and memory antigen-specific CD8 T cells. J Immunol. 2002; 168(10): 4827-4831.
19. Younes SA, Freeman ML, Mudd JC, Shive CL, Reynaldi A, Panigrahi S, et al. IL-15 promotes activation and expansion of CD8+ T cells in HIV-1 infection. J Clin Invest. 2016; 126(7): 2745-2756.
20. Van den Bergh JMJ, Smits ELJM, Berneman ZN, Hutten TJA, De Reu H, Van Tendeloo VFI, et al. Monocyte-derived dendritic cells with silenced PD-1 ligands and transpresenting interleukin-15 stimulate strong tumor-reactive t-cell expansion. Cancer Immunol Res. 2017; 5(8): 710-715.
21. Alves NL, Arosa FA, van Lier RA. IL-21 sustains CD28 expression on IL-15-activated human naive CD8+ T cells. J Immunol. 2005; 175(2): 755-762.
22. Boudousquié C, Danilo M, Pousse L, Jeevan-Raj B, Angelov GS, Chennupati V, et al. Differences in the transduction of canonical Wnt signals demarcate effector and memory CD8 T cells with distinct recall proliferation capacity. J Immunol. 2014; 193(6): 2784-2791.
23. Gattinoni L, Ji Y, Restifo NP. Wnt/beta-catenin signaling in T-cell immunity and cancer immunotherapy. Clin Cancer Res. 2010; 16(19): 4695-4701.
24. Zhao DM, Yu S, Zhou X, Haring JS, Held W, Badovinac VP, et al. Constitutive activation of Wnt signaling favors generation of memory CD8 T cells. J Immunol. 2010; 184(3): 1191-1199.
25. Delgoffe GM, Kole TP, Zheng Y, Zarek PE, Matthews KL, Xiao B, et al. The mTOR kinase differentially regulates effector and regulatory T cell lineage commitment. Immunity. 2009; 30(6): 832-844.
26. Procaccini C, De Rosa V, Galgani M, Abanni L, Calì G, Porcellini A, et al. An oscillatory switch in mTOR kinase activity sets regulatory T cell responsiveness. Immunity. 2010; 33(6): 929-941.
27. Li Q, Rao RR, Araki K, Pollizzi K, Odunsi K, Powell JD, et al. A central role for mTOR kinase in homeostatic proliferation induced CD8+ T cell memory and tumor immunity. Immunity. 2011; 34(4): 541-553.
28. Pollizzi KN, Powell JD. Regulation of T cells by mTOR: the known knowns and the known unknowns. Trends Immunol. 2015; 36(1): 13-20.
29. Kalfa TA, Pushkaran S, Zhang X, Johnson JF, Pan D, Daria D, et al. Rac1 and Rac2 GTPases are necessary for early erythropoietic expansion in the bone marrow but not in the spleen. Haematologica.

2010; 95(1): 27-35.

30. Herndon TM, Pirone DM, Tsokos GC, Chen CS. T cell-to-T cell clustering enhances NF-kappaB activity by a PI3K signal mediated by Cbl-b and Rho. Biochem Biophys Res Commun. 2005; 332(4): 1133-1139.

31. Arrizabalaga O, Lacerda HM, Zubiaga AM, Zugaza JL. Rac1 protein regulates glycogen phosphorylase activation and controls interleukin (IL)-2-dependent T cell proliferation. J Biol Chem. 2012; 287(15): 11878-11890.

32. Wang X, Zhang F, Chen F, Liu D, Zheng Y, Zhang Y, et al. MEKK3 regulates IFN-gamma production in T cells through the Rac1/2-dependent MAPK cascades. J Immunol. 2011; 186(10): 5791-5800.

33. Fuse S, Zhang W, Usherwood EJ. Control of memory CD8+ T cell differentiation by CD80/CD86-CD28 costimulation and restoration by IL-2 during the recall response. J Immunol. 2008; 180(2): 1148-1157.

34. Grujic M, Bartholdy C, Remy M, Pinschewer DD, Christensen JP, Thomsen AR. The role of CD80/CD86 in generation and maintenance of functional virus-specific CD8+ T cells in mice infected with lymphocytic choriomeningitis virus. J Immunol. 2010; 185(3): 1730-1743.

35. O'Neill SK, Cao Y, Hamel KM, Doodes PD, Hutas G, Finnegan A.

Expression of CD80/86 on B cells is essential for autoreactive T cell activation and the development of arthritis. J Immunol. 2007; 179(8): 5109-5116.

36. Bukczynski J, Wen T, Wang C, Christie N, Routy JP, Boulassel MR, et al. Enhancement of HIV-specific CD8 T cell responses by dual costimulation with CD80 and CD137L. J Immunol. 2005; 175(10): 6378-6389.

37. Haile ST, Bosch JJ, Agu NI, Zeender AM, Somasundaram P, Srivastava MK, et al. Tumor cell programmed death ligand 1-mediated T cell suppression is overcome by coexpression of CD80. J Immunol. 2011; 186(12): 6822-6829.

38. Gückel B, Meyer GC, Rudy W, Batrla R, Meuer SC, Bastert G, et al. Interleukin-12 requires initial CD80-mediated T-cell activation to support immune responses toward human breast and ovarian carcinoma. Cancer Gene Ther. 1999; 6(3): 228-237.

39. Manzotti CN, Liu MK, Burke F, Dussably L, Zheng Y, Sansom DM. Integration of CD28 and CTLA-4 function results in differential responses of T cells to CD80 and CD86. Eur J Immunol. 2006; 36(6): 1413-1422.